Discrete element method simulation of wheat bulk density

by

Marvin Carpena Petingco

B.S., University of the Philippines Los Baños, 2006
M.S., University of the Philippines Los Baños, 2012

AN ABSTRACT OF A DISSERTATION

submitted in partial fulfillment of the requirements for the degree

DOCTOR OF PHILOSOPHY

Carl and Melinda Helwig Department of Biological and Agricultural Engineering
Carl R. Ice College of Engineering

KANSAS STATE UNIVERSITY
Manhattan, Kansas

2020

Abstract

Bulk density indicates how much weight of material can be packed in a bin, truck, or any container used for storage or transportation. Stored grain bulk density is higher than the standard bushel test weight because of the overburden pressure and handling practices. The material and equipment properties, and widely varying interactions between kernels add to the complexity of analyzing bulk density changes in stored grain. The influence of these factors on wheat bulk density was investigated and wheat bulk density was simulated using the discrete element method (DEM). The objectives of this research were to: (1) experimentally investigate the influence of kernel shape and size on packing ratio and compressibility of wheat, (2) determine the influence of particle shape and contact parameters on DEM-simulated bulk density, (3) simulate using DEM the bulk density of wheat as affected by grain drop height and size distribution, and (4) simulate using DEM the bulk density of wheat as affected by overburden pressure. Laboratory experiments showed that packing ratio (compressibility) had strong positive (negative) linear relationship with sphericity and flatness shape factors but strong negative (positive) linear relationship with elongation shape factor. Also, the higher percentage of mass of larger kernel fraction in a mixture contributed to higher packing ratio and lower compressibility. DEM simulation showed that decreasing aspect ratio and geometrical smoothness of particles increased simulated bulk density of wheat. Among the pseudo-ellipsoidal particle models, the five-sphere particle was the best option to represent wheat particles, while among the contact parameters, the wheat-to-wheat coefficient of static friction and wheat-to-wheat rolling friction had the greatest influence on simulated bulk density. Wheat bulk density as affected by drop height and percentage composition of the three kernel fractions can be simulated accurately using either single-sphere or five-sphere pseudo-ellipsoidal particle, provided that the contact

parameters of each particle model representing each size fraction were calibrated individually. DEM simulation of wheat under confined uniaxial compression was implemented to determine the effect of overburden pressure on wheat bulk density. Results showed that the appropriate time step, grid size, and pressure loading rate had to be determined first to avoid instabilities and erroneous results. The DEM simulated bulk densities agreed with the experimental results for overburden pressure below 48kPa and tend to overpredict at higher overburden pressure. This study contributed to better understanding of the influence of particle shape, contact parameters, drop height, overburden pressure, and size distribution on bulk density and provides an approach on how to simulate wheat bulk density using DEM as affected by these factors. These findings can be used in developing accurate models for estimating bulk density and grain packing in bins and other storage structures.

Discrete element method simulation of wheat bulk density

by

Marvin Carpena Petingco

B.S., University of the Philippines Los Banos, 2006
M.S., University of the Philippines Los Banos, 2012

A DISSERTATION

submitted in partial fulfillment of the requirements for the degree

DOCTOR OF PHILOSOPHY

Carl and Melinda Helwig Department of Biological and Agricultural Engineering
Carl R. Ice College of Engineering

KANSAS STATE UNIVERSITY
Manhattan, Kansas

2020

Approved by:

Co-Major Professor
Mark E. Casada, Ph.D., P.E.

Approved by:

Co-Major Professor
Ronaldo G. Maghirang, Ph. D.

Approved by:

Co-Major Professor
Donghai Wang, Ph. D.

Copyright

Abstract

Bulk density indicates how much weight of material can be packed in a bin, truck, or any container used for storage or transportation. Stored grain bulk density is higher than the standard bushel test weight because of the overburden pressure and handling practices. The material and equipment properties, and widely varying interactions between kernels add to the complexity of analyzing bulk density changes in stored grain. The influence of these factors on wheat bulk density was investigated and wheat bulk density was simulated using the discrete element method (DEM). The objectives of this research were to: (1) experimentally investigate the influence of kernel shape and size on packing ratio and compressibility of wheat, (2) determine the influence of particle shape and contact parameters on DEM-simulated bulk density, (3) simulate using DEM the bulk density of wheat as affected by grain drop height and size distribution, and (4) simulate using DEM the bulk density of wheat as affected by overburden pressure. Laboratory experiments showed that packing ratio (compressibility) had strong positive (negative) linear relationship with sphericity and flatness shape factors but strong negative (positive) linear relationship with elongation shape factor. Also, the higher percentage of mass of larger kernel fraction in a mixture contributed to higher packing ratio and lower compressibility. DEM simulation showed that decreasing aspect ratio and geometrical smoothness of particles increased simulated bulk density of wheat. Among the pseudo-ellipsoidal particle models, the five-sphere particle was the best option to represent wheat particles, while among the contact parameters, the wheat-to-wheat coefficient of static friction and wheat-to-wheat rolling friction had the greatest influence on simulated bulk density. Wheat bulk density as affected by drop height and percentage composition of the three kernel fractions can be simulated accurately using either single-sphere or five-sphere pseudo-ellipsoidal particle, provided that the contact

parameters of each particle model representing each size fraction were calibrated individually. DEM simulation of wheat under confined uniaxial compression was implemented to determine the effect of overburden pressure on wheat bulk density. Results showed that the appropriate time step, grid size, and pressure loading rate had to be determined first to avoid instabilities and erroneous results. The DEM simulated bulk densities agreed with the experimental results for overburden pressure below 48kPa and tend to overpredict at higher overburden pressure. This study contributed to better understanding of the influence of particle shape, contact parameters, drop height, overburden pressure, and size distribution on bulk density and provides an approach on how to simulate wheat bulk density using DEM as affected by these factors. These findings can be used in developing accurate models for estimating bulk density and grain packing in bins and other storage structures.

Table of Contents

List of Figures

List of Tables

Acknowledgements

I would like to thank the following people, without whom this dissertation would not have come to fruition.

- To Dr. Mark E. Casada and D. Ronaldo G. Maghirang, two of my co-major professors, for their support, guidance, patience, encouragements, and valuable inputs in my dissertation.
- To Dr. Donghai Wang, my third co-major professor; Dr. Hulya Dogan, and Dr. Joseph P. Harner III, members of my graduate committee; and Dr. Wei-Wen Hsu, outside committee chair, for their guidance, insights, and advice to improve my dissertation.
- The Andersons Research Program, Kansas Agricultural Experiment Station, and the US Department of Agriculture (CRIS No. 5430-43440-008-00D) for funding this research.
- To the Packers group, Dr. Aaron Turner, Dr. Samuel McNeill, Dr. Michael D. Montross, and Dr. Sidney A. Thompson for all the laughter and encouragement during our conference calls.
- To Dr. Oladiran Fasina, Dr. Kingsly Ambrose, Elizabeth Maghirang, Dr. Dan Brabec, Dr. Dennis Tilley, Dr. Floyd Dowell, and Dr. Paul Armstrong for the technical expertise they shared.
- To Dr. Rumela Bhadra, Dr. Josephine M. Boac, Zhengpu Chen, Austin Ebert, Gary Shi, Clayton Van Meter, Clay Thomas, for assisting in my experiments.
- To Alex King, Elizabeth Maghirang, and Dr. Carol Jones for the wheat samples.
- To all faculty members, staff, and graduate students at the Department of Biological and Agricultural Engineering at KSU; and to all my colleagues at USDA-ARS CGAHR, for all their help, advice, and support.

- To all friends, colleagues, members of the Philippine Students Association (PhilSA), Filipino community in Manhattan and beyond, my DnD and board games group, for their encouragements, laughter, and lessons shared.
- To my mother, Mama Necy, and my siblings Marlon, Mark Neslie, Michael Joe, and Venni Lou Michelle, for their unconditional love and support.

Dedication

For my loving father and mother,

Manolito & Necitas Petingco

*I thank God for giving me the best parents. To my **Mama**, I can never repay all your sacrifices for our family. To my **Papa**, I know wherever you are; you will always be my number one fan.*

Chapter 1 - Introduction

1.1 Background

Bulk density is one of the most used properties of grain. It is used by millers in quality grading, by engineers in designing storage and aerations systems, and by federal agencies, insurance companies, and storage managers in inventory measurement and control. However, grain bulk density is an extrinsic property and is affected by several factors in a storage structure.

Grain stored in bins has much higher bulk density than the laboratory measured test weight because of its reduction in volume due to compaction (Figure 1-1). The degree of compaction or packing depends on several factors such as crop type, grain moisture content, laboratory measured (initial) test weight, dockage, bin material, geometry and dimensions, and height of grain (Bhadra et al., 2015; Boac et al., 2015). Because majority of grain inventory and auditing assessments are based on volume measurements, determining accurate pack factors are necessary.

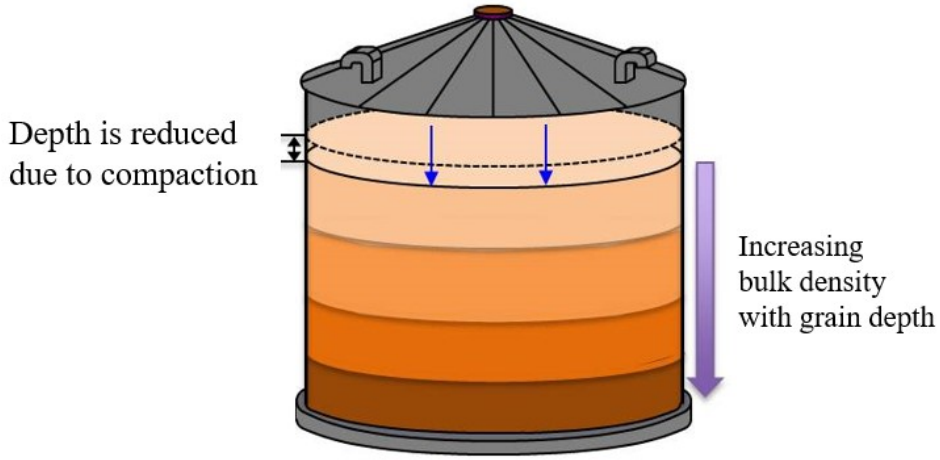

$$Mass = Test\ weight \times pack\ factor \times volume$$

Figure 1-1. Stored grain packing.

1.2 Packing ratio, compaction factor, and pack factor

To avoid confusion with other terminologies, Boac et al. (2015) defined packing ratio, compaction factor, and pack factor. Packing ratio is the ratio of the bulk density after packing in the bin to the initial bulk density (grain test weight) before packing and is defined as:

$$P = \frac{D_A}{D_O} \tag{1-1}$$

where

$$D_A = \frac{\sum_{x=1}^{n} D_x}{n} \tag{1-2}$$

and

$D_A =$ average bulk density of the rain after packing, kg/m^3 (lb/bu)

$D_O =$ initial bulk density, or uncompacted test weight, of the of the grain from the Winchester bushel test, kg/m^3 (lb/bu)

$D_X =$ bulk density of grain in bin at a given depth x, kg/m^3 (lb/bu)

$P =$ average packing ratio of the grain

$n =$ number of layers in the grain depth

$n =$ depth in the grain, m (ft).

The compaction factor is defined as the reduction on volume of stored grain due to compaction. This term is used in ASABE Standard EP413.2 (ASABE, 2010) and defined as:

$$f_C = P - 1 \tag{1-3}$$

where f_C = the average compaction factor of the grain.

The mass of grain in a bin can be calculated from the measured volume of grain using:

$$M = D_O \cdot P \cdot V \tag{1-4}$$

where

M = mass of grain in bin, kg (lb)

V = measured volume of grain in the bin, m^3 (bu).

Pack factor is a common grain industry term used by both RMA and FSA-W. It is also called combined test weight and pack factor by RMA and is defined as:

$$R = P\frac{D_O}{D_S} \tag{1-5}$$

where

R = pack factor including test weight

D_S = standard bulk density (standard test weight) for a given grain type, kg/m^3 (lb/bu).

The mass of grain measured in standard bushels is calculated as:

$$\text{Standard bu} = R \cdot V \tag{1-6}$$

and the mass of grain in pounds (lb) is calculated as:

$$M = D_S \cdot \text{Standard bu} = D_S \cdot R \cdot V. \tag{1-7}$$

Pack factor tables are used in the grain industry for inventory control. According to Boac et al. (2015), the USDA Risk Management Agency, which measures bins for insurance purposes, and the USDA Farm Service Agency – County offices, which measures bins for loan purposes, share empirical pack factor tables for seven types of grain. However, these pack factors are only based on test weight of the crop and the cross-sectional area of the bin.

1.3 Factors affecting grain bulk density and compressibility

Numerous studies have been conducted to study the compressive behavior of granular material. Most of them relate grain packing and bulk density with moisture content (Ross et al., 1979; Thompson and Ross, 1983; Fang and Campbell, 2000; Turner et al., 2016). Some researchers have investigated the effects of foreign materials on grain compressibility such as:

higher chaff percentage on wheat compressibility (Bian et al., 2015); percentage of dockage on wheat bulk density (Bhadra et al., 2016); and broken corn and foreign initial bulk density on packing of corn (McNeil et al., 2004). Others have reported that handling practices might have contributed to increased bulk density of grain such as: higher fall height (Yang and Williams, 1990; Versavel and Britton, 1984) resulted in higher bulk density due to a more packed arrangement of particles; use of mechanical grain spreader over spout filling resulted in higher bulk density caused by greater uniformity of fine material distribution (Chang et al., 1981, 1983); and vibration influenced grain compaction (Hao et al., 1994).

Bulk density indicates how much weight of material can be packed in a bin, truck, or any container used for storage or transportation. It is a result of the interaction of the properties in different scale of structures of a particulate system (Amador and de Juan, 2016). These scales of structure (Figure 1-2) include supramolecular, particle, and mesoscale structures, which we considered in this dissertation as microstructures. For example, the chemical composition affects the true or solid density of the material in the supramolecular scale, particle porosity affects the kernel density at the particle scale, particle shape and size at the particle scale affect the particle arrangement in the mesoscale and directly affect the interparticle porosity. All these micro-properties contribute to the value of loose bulk density. Aside from the microstructure, bulk density is also affected by the macrostructure or the unit operation undergone by the particulate system such as filling method, bin configurations, and presence of vibration. Because of the complexity of the scales of structures, it is very difficult to predict the increase in bulk density of stored grain in bins.

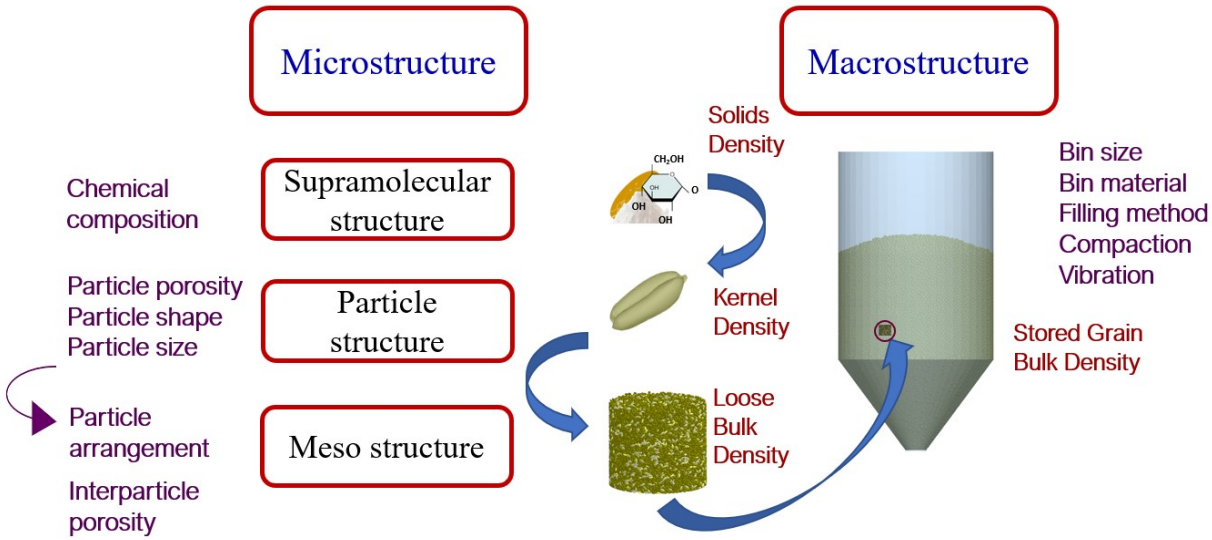

Figure 1-2. Bulk density as affected at the different scales of structure of particulate systems (Amador and de Juan, 2016).

1.4 Discrete element method

The discrete element method (DEM) is an explicit numerical scheme developed by Cundall and Strack (1979) for modeling behavior of granular material. Unlike the finite element method, DEM allows each particle to be represented numerically and to be characterized with its specific properties such as size, shape, material properties, and initial velocity. It also models the overall system behavior of granular material because of individual interactions of a particle to other particles or to a surface. Figure 1-3 shows the process flow for DEM calculation of finite particle displacements and rotations for an assembly of particles; DEM uses contact detection algorithms and suitable contact models to calculate forces acting on particles. Translational and rotational accelerations are calculated using Newton's second law of motion and are numerically integrated over time to determine individual particle velocity and updated individual position. This process is iterated over a set period of time. Unlike the finite or boundary element methods, which treat a particulate system as a continuum, DEM treats a particulate system as a collection

of discrete entities at a microscale level, enabling a better prediction and understanding at the macroscale level of the particulate system, such as stored grain bulk density.

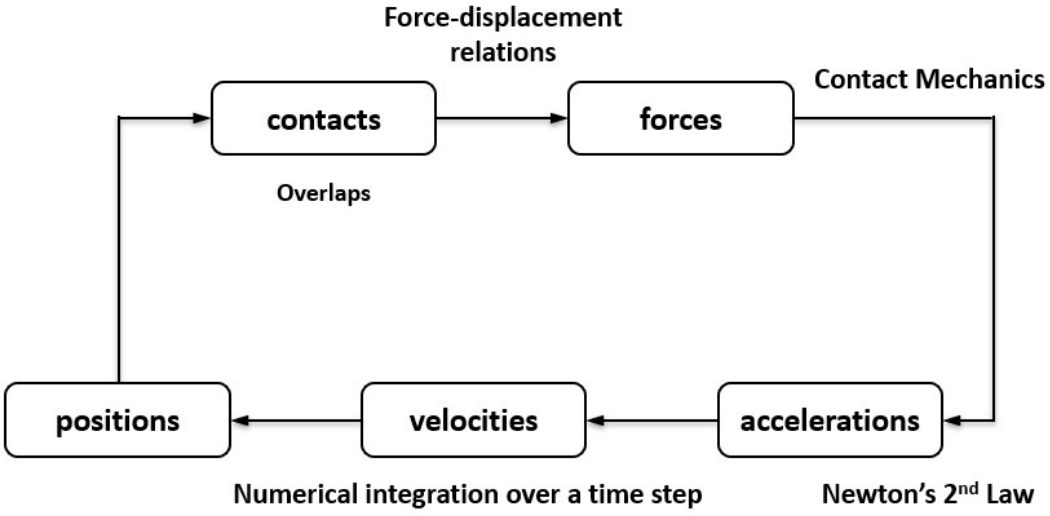

Figure 1-3. Calculation procedure involved in DEM simulation (DEM Solutions, 2017).

1.5 Problem statement

The widely varying details of the interaction between kernels, and between kernel and material surfaces (bin, hoppers, etc.) create a complex problem in analyzing bulk density changes in stored grain. Several studies used empirical methods (Bates, 1925; Malm and Backer, 1985), while others combined experimental and analytical solutions (Thompson et al., 1991; Cheng et al., 2017) to predict grain packing and stored grain bulk density to calculate the amount of grain in bins. Conducting bin experiments are often difficult and expensive, while analytical solutions might not be able to account for all the complexities present in the problem. Numerical methods such as DEM have been proven to be an effective and less expensive alternative in solving complex granular material problems. DEM can provide dynamic information, such as trajectory or forces acting on individual particles, which is difficult to obtain experimentally; moreover, DEM as a Lagrangian model can address the size distribution of individual particles that cannot

be handled in Eulerian models such as finite difference method or finite element method (Zhu et al., 2007). In addition, DEM has the strength of allowing the parametric study to examine the effects of individual particles, process conditions or equipment design on the bulk behavior of cereal grains, oil seeds, and their products (Boac et al., 2014). It can be applied to various simulations of unit operations such as grain cleaning and separation (Sakaguchi et al., 2001; Li et al., 2002), oil expression by compression (Raji and Favier, 2004), and commingling of two types of grain in a bucket-type grain elevator boot system (Boac et al., 2014).

There are very limited studies on how shape and size distribution affect bulk density and compressibility of grain crops, such as wheat. Most compressibility and packing studies (Yu and Standish, 1991; Dodds, 1980; Suzuki et al., 1986; Stovall et al., 1986; Zou et al., 2001) have been done in the chemical and material industries such as glass beads, powders, and plastics, which involved mixture of particles of uniform shapes and sizes, and mostly dealt with fine materials. However, compressibility studies of real particles such as wheat, which come in different shapes and size distributions, are limited. The objective of this research was to develop a DEM model for wheat considering size fraction composition of wheat kernels, and to predict wheat bulk density as affected by grain drop height, size distribution, and overburden pressure.

1.6 Research objectives

This research includes the following specific objectives:

1. experimentally investigate the influence of kernel shape and size on packing ratio and compressibility of wheat;
2. determine the influence of particle shape and contact parameters on DEM-simulated bulk density;

3. simulate with DEM the bulk density of wheat as affected by grain drop height and size distribution; and
4. simulate with DEM the bulk density of wheat as affected by overburden pressure.

1.7 References

Amador, C, & Martin de Juan, L. (2016). Strategies for Structured Particulate Systems Design. In Computer Aided Chemical Engineering (Vol. 39, pp. 509-579).

ASABE. (2010). EP413.2: Procedure for establishing volumetric capacities of cylindrical bins. St. Joseph, Mich.: ASABE.

Bhadra, R., Casada, M. E., Boac, J. M., Turner, A. P., Thompson, S. A., Montross, M. D., Maghirang, R. G., & McNeill, S. G. (2016). Correlating bulk density (with dockage) and test weight (without dockage) for wheat samples. *Appl. Eng. Agric., 32*(6), 925-930. https://doi.org/10.13031/aea.32.11692

Bhadra, R., Turner, A. P., Casada, M. E., Montross, M. D., Thompson, S. A., Boac, J. M., McNeill, S. G., & Maghirang, R. G. (2015). Pack factor measurements for corn in grain storage bins. *Trans. ASABE, 58*(3), 879-890. https://doi.org/10.13031/trans.58.11033

Bates, E. N. (1925). Estimating the quantity of grain in bins with chart reducing and the necessary computations. Misc. Circular No. 41. Washington, D.C.: USDA

Bian, Q., Ambrose, R. P., & Subramanyam, B. (2015). Effect of chaff on bulk flow properties of wheat. *J. Stored Prod. Res., 64*(part A), 21-26. https://doi.org/10.1016/j.jspr.2015.08.004

Boac, J. M., Ambrose, R. P. K., Casada, M. E., Maghirang, R. G., & Maier, D. E. (2014). Applications of discrete element method in modeling of grain postharvest operations. Retrieved from http://krex.ksu.edu

Boac, J. M., Bhadra, R., Casada, M. E., Thompson, S. A., Turner, A. P., Montross, M. D., McNeill, S. G., & Maghirang, R. G. (2015). Stored grain pack factors for wheat:

Comparison of three methods to field measurements. *Trans. ASABE, 58*(4), 1089-1101. https://doi.org/10.13031/trans.58.10898

Cheng, X., Zhang, Q., Shi, C., & Yan, X. (2017). Model for the prediction of grain density and pressure distribution in hopper-bottom silos. *Biosystems Engineering*, 163, 159-166. doi:10.1016/j.biosystemseng.2017.09.006

Cundall, P. A., & Strack, O. D. (1979). A discrete element model for granular assemblies. *Geotechnique, 29*(1), 47-65. https://doi.org/10.1680/geot.1979.29.1.47.

Dodds, J. A. (1980). The porosity and contact points in multicomponent random sphere packings calculated by a simple statistical geometric model. *J. Colloid Interface Sci., 77*(2), 317-327. https://doi.org/10.1016/0021-9797(80)90302-1

Fang, C., & Campbell, G. M. (2000). Effect of measurement method and moisture content on wheat kernel density measurement. *Food Bioprod. Proc., 78*(4), 179-186. https://doi.org/10.1205/09603080051065278

Hao, D., Q. Zhang and M.G. Britton. 1994. Effect of Vibration on Loads in a Corrugated Model Grain Bin. *Canadian Agricultural Engineering*. 36(1): 29-35.

Li, J, Webb, C, Pandiella, S.S, & Campbell, G.M. (2002). A Numerical Simulation of Separation of Crop Seeds by Screening—Effect of Particle Bed Depth. *Food and Bioproducts Processing*, 80(2), 109-117.

Malm, J. K., & Backer, L. F. (1985). Compaction factors for six crops. *Trans. ASAE, 28*(5), 1634-1636. https://doi.org/10.13031/2013.32489

McNeill, S. G., Thompson, S. A., & Montross, M. D. (2004). Effect of moisture content and broken kernels on the bulk density and packing of corn. *Appl. Eng. Agric., 20*(4), 475-480. https://doi.org/10.13031/2013.16477

Raji, A.O, & Favier, J.F. (2004). Model for the deformation in agricultural and food particulate materials under bulk compressive loading using discrete element method. I: Theory, model development and validation. *J. Food Eng*., 64(3), 359-371.

Ross, I. J., Bridges, T. C., Loewer, O. J., & Walker, J. N. (1979). Grain bin loads as affected by grain moisture content and vertical pressure. *Trans. ASAE, 22*(3), 592-597. https://doi.org/10.13031/2013.35068

Sakaguchi E, Suzuki M, Favier JF, Kawakami S (2001) Numerical simulation of the shaking separation of paddy and brown rice using the discrete element method. *J. Agric. Eng. Res.,* 79(3):307–315.

Stovall, T., de Larrard, F., & Buil, M. (1986). Linear packing density model of grain mixtures. *Powder Tech., 48*(1), 1-12. https://doi.org/10.1016/0032-5910(86)80058-4

Suzuki, M., Yagi, A., Watanabe, T., & Oshima, T. (1986). Estimation of the void fraction in a bed randomly packed with particles of three sizes. *Intl. Chem. Eng, 26*(3), 491-497.

Thompson, S. A., & Ross, I. J. (1983). Compressibility and frictional coefficients of wheat. Trans. ASAE, 26(4), 1171-1176, 1180. doi: 10.13031/2013.34099

Thompson, S. A., Schwab, C. V., & Ross, I. J. (1991). Calibration of a model for packing whole grains. *Appl. Eng. Agric., 7*(4), 450-456. https://doi.org/10.13031/2013.26244

Turner, A. P., Montross, M. D., McNeill, S. G., Sama, M. P., Casada, M. E., Boac, J. M., ... Thompson, S. A. (2016). Modeling the compressibility behavior of hard red wheat varieties. *Trans. ASABE, 59*(3), 1029-1038. https://doi.org/10.13031/trans.59.11432

Versavel, P. A., & Britton, M. G. (1986). Interaction of bulk wheat with bin wall configuration in model bins. *Trans. ASAE*, 29(2), 533-537. doi:10.13031/2013.30186

Yang, X., & Williams, D. L. (1990). Airflow resistance of grain sorghum as affected by bulk density. *Trans. ASAE*, 33(6), 1966-1970. doi:10.13031/2013.31565

Yu, A. B., & Standish, N. (1991). Estimation of the porosity of particle mixtures by a linear-mixture packing model. *Ind. Eng. Chem. Res., 30*(6), 1372-1385. https://doi.org/10.1021/ie00054a045

Zou, R. P., Gan, M. L., & Yu, A. B. (2011). Prediction of the porosity of multi-component mixtures of cohesive and non-cohesive particles. *Chemical Engineering Science*, 66(20), 4711-4721. doi:10.1016/j.ces.2011.06.037

Zhu HP, Zhou ZY, Yang RY, Yu AB (2007) Discrete particle simulation of particulate systems: theoretical developments. *Chemical Engineering Science,* 62(13):3378–3396. doi:10.1016/j.ces.2006.12.089

Chapter 2 - Influence of Kernel Shape and Size on the Packing Ratio and Compressibility of Hard Red Winter Wheat[1]

2.1 Introduction

Grain packing has been studied extensively in the past three decades (Malm and Backer, 1985; Thompson et al., 1987, 1991; Thompson and Ross, 1983) because it is important for inventory, government auditing, and loan and insurance purposes. Knowing the degree of packing of different grain crops is necessary to accurately determine the mass of grain in a storage structure and to calculate the storage capacity of grain bins (ASABE, 2010).

Grain packing can be determined from the ratio of the initial bulk density (usually test weight) and the actual average bulk density of the grain confined in a bin. The degree of packing depends on several factors, such as type of crop, grain moisture content, initial test weight of grain, make of bin, bin dimensions, and height of grain (Bhadra et al., 2015; Boac et al., 2015). Other factors include other grain properties, such as particle-to-particle and wall surface-to-particle coefficients of friction and lateral-to-vertical pressure coefficient (Thompson et., 1987). Among these factors, the initial bulk density, moisture content, bin diameter, and grain height have the greatest effect on grain packing in bins (Thompson et al., 1987; Ross et al., 1979).

Most studies relate grain packing and bulk density with moisture content (Ross et al., 1979; Nelson, 1980; Fang and Campbell, 2000; Kalkan and Kara, 2011; Turner et al., 2016). In

---

1 This chapter has been published as a peer-reviewed paper: Petingco, M. C., Casada, M. E., Maghirang, R. G., Thompson, S. A., McNeill, S. G., Montross, M. D., & Turner, A. P. (2018). Influence of kernel shape and size on the packing ratio and compressibility of hard red winter wheat. *Transactions of the ASABE*, 61(4), 1437-1448. doi:10.13031/trans.12648

general, bulk density decreases with increasing moisture content. ASABE Standard D421.4 (ASABE, 2012) predicts the bulk density of different crops as a function of moisture content. Other researchers have investigated the effects of other factors on the bulk density and compressibility of grain. Bian et al. (2015) reported that higher chaff percentage resulted in a decrease in bulk density and an increase in compressibility of wheat. These findings are consistent with those of Bhadra et al. (2016), who reported that increasing the percentage of dockage in wheat decreased bulk density. On the other hand, McNeil et al. (2004) investigated the combined effect of broken corn and foreign material (BCFM) and moisture content on the initial bulk density and packing of corn. They found that moisture content, percentage of broken corn, and particle size significantly affected the initial bulk density. Moreover, an increase in the initial bulk density was observed with an increased concentration of fine broken corn, and a slight decrease or no change in the initial bulk density was observed with an increased concentration of coarse particles. The presence of finer particles resulted in a decrease of bulk density in wheat and an increase in bulk density of corn. This happens because the finer materials in a wheat sample have a lower density than the wheat kernels, while the fines in corn have almost the same density as the corn kernels and tend to fill the voids between kernels.

Bulk density is defined as the ratio of the grain mass to the grain volume. Given the same mass of grain, bulk density can vary depending on the volume it occupies. The more void spaces in a grain mass, the greater the volume it occupies and the lower its bulk density. Hence, grain bulk density depends on both the kernel density and the void volume between kernels. The amount of void space depends on the spatial arrangement, which is dictated by particle properties such as kernel size and shape, and friction coefficients (Meng et al., 2012). It is also affected by the size and shape of the container or bin and the manner of filling the bin (Molenda et al., 1996).

Depending on the initial arrangement of the grain kernels, the void space and bulk density will vary, as well as the compressibility and packing density. Although packing density is a widely used term, in this article we refer it as "packing ratio" to minimize confusion because it does not have units of density.

Numerous studies have been done on the packing ratio of particles in the chemical and material industries. These studies involved the use of linear packing models for spherical and non-spherical particle mixtures (Yu and Standish, 1991, 1993a, 1993b; Yu et al., 1992, 1993, 1996; Zhou and Yu, 1996), binary and ternary mixtures (Yu et al., 1992, 1993; Meng et al., 2012; Suzuki et al., 1986), multi-component spherical particles (Dodds, 1980; Suzuki et al., 1986; Stovall et al., 1986), and coarse and fine particle mixtures (Zou et al., 2011). Most of these studies involved materials such as glass beads, wood, and plastics. Non-spherical particles include cylinders, spherocylinders, ellipsoids, and disks. However, these studies considered particles of uniform shapes and sizes, and mostly dealt with fine materials. Investigations of mixtures of non-spherical particles with different shapes and sizes are limited. Moreover, packing ratio studies of real particles such as grain kernels, which come in different shapes and size distributions, are rare.

This study looked at how the shape, size, and size distribution of wheat kernels affect wheat compressibility and packing ratio. Specifically, the objectives of this study were to (1) determine the relationship between the different shape factors and packing ratio, as well as compressibility, using a single kernel size fraction and (2) determine the effect of different proportions of kernel size fractions in binary and ternary mixtures on wheat packing ratio and compressibility.

2.2 Materials and methods

2.2.1 Basis for variety selection

Seven hard red winter (HRW) wheat varieties were analyzed for kernel size distribution. The wheat samples were cleaned by passing them through a Carter dockage tester (Seedburo Equipment Co., Des Plaines, Ill.) to remove foreign material and through a 1.63 mm × 9.53 mm (0.064 in. × 3/8 in.) oblong sieve to remove shrunken and broken kernels. The kernels were sorted with a mechanical test sieve shaker (Ro-Tap, W.S. Tyler, Mentor, Ohio) using a series of 200 mm (8 in.) diameter sieves. The sieve sizes used were U.S. Tyler sieves #6 (3.36 mm), #7 (2.83 mm), #8 (2.38 mm), and #10 (2.00 mm). Table 2-1 shows the average percentage of kernels retained on each sieve using a 100 g wheat sample and shaking for 120 s. Different varieties had different proportions of kernel size fractions. Everest, Garrison, WinterHawk, and AP503CL2 varieties had 80% to 90% of kernels retained on sieves #7 and #8 and only about 1% of kernels retained on sieve #6. On the other hand, KanMark and 1863 had sufficient kernels in each size fraction needed for this study. These two varieties had similar size distributions and were grown in the same geographic location.

Table 2-1. Kernel size distribution of wheat varieties.

	Percent Retained on Sieve[a]					
Wheat Variety	#6	#7	#8	#10	Pan	Total
Everest (Oklahoma)	0.3	52.2	41.8	5.3	0.3	100.0
Garrison (Oklahoma)	0.2	21.6	60.6	16.0	1.6	100.0
Everest (Kansas)	1.1	62.4	31.6	4.6	0.3	100.0
WinterHawk (Kansas)	0.3	28.1	59.2	12.1	0.3	100.0
AP503CL2 (Kansas)	0.3	21.3	59.2	17.1	2.1	100.0
KanMark (Kansas)	14.2	67.3	15.5	2.8	0.3	100.0
1863 (Kansas)	9.7	64.0	22.0	3.9	0.4	100.0

[a]Values are means of three replications.

2.2.2 Wheat kernel and bulk properties

A bag of wheat (27 kg) of each variety (KanMark and 1863) was used for the study. Wheat samples were analyzed for dockage, moisture content, test weight, and amount of shrunken and broken kernels following the procedures outlined in the FGIS Grain Inspection Handbook (USDA-FGIS, 2013). The kernels were then sorted as discussed above.

Sorted kernels were exposed to room temperature and humidity for two weeks to reach equilibrium moisture content at those conditions. The conditioned samples were placed in sealed bags and inside sealed buckets before they were stored in a refrigerator for a week. ASABE Standard S352.2 (ASABE, 1988) was used to determine the moisture content of each size fraction from the two wheat varieties. One hundred kernels from each size and variety were also pulled from the samples for the determination of kernel length (l), width (w), and thickness (t) using a caliper. These definitions of kernel axial dimensions are like those used by Ponce-Garcia et al. (2017).

2.2.3 Equivalent spherical diameter

Kernels vary in size and shape; thus, comparing two size groups will be facilitated by using the concept of equivalent spherical diameter (d_s). Wheat kernels were assumed to be ellipsoidal in shape, either a prolate spheroid or an oblate spheroid, depending on the ratios of their diameters in the three-dimensional axes. As such, the volume of the kernel (V_k) can be approximated as $V_k = \left(\frac{\pi}{6}\right) \cdot l \cdot w \cdot t$. The equivalent spherical diameter or geometric mean diameter (Mohsenin, 1986) can then be calculated by:

$$d_s = (l \cdot w \cdot t)^{\frac{1}{3}} \quad (2\text{-}1)$$

where d_s is the equivalent spherical diameter of the kernel (mm), and l, w, and t are the kernel length (mm), width (mm), and thickness (mm), respectively.

2.2.4 Shape factors

Particle shape is one of the most important features of particulate assemblies (Podczeck, 1997) and influences packing efficiency. Various methods have been used to describe particle shapes; for this study, sphericity (φ), flatness shape factor (λ), and elongation shape factor (ε) were used. These factors were determined for each size fraction and variety.

Mohsenin (1986) estimated the sphericity of a triaxial ellipsoidal particle as the ratio of the geometric mean diameter to the diameter of the largest inscribed circle of the particle. A sphericity of 1.0 is considered a perfect sphere. Wadell (1935) used another definition of sphericity as the ratio of the surface area of a sphere of the same volume as the particle (A_s) to the actual surface area of the particle (A_p):

$$\Phi_1 = (l * w * t)^{\frac{1}{3}}/l \quad (2\text{-}2)$$

$$\varphi_2 = A_s/A_p \quad (2\text{-}3)$$

where φ_1 and φ_2 are the sphericity based on Mohsenin and Wadell, respectively.

Wadell's sphericity equation can be expressed in terms of kernel dimensions (l, w, and t) by determining A_s and A_p. For a triaxial ellipsoidal particle (with axis lengths given by l, w, and t), A_s can be expressed in terms of the volume of the particle (V_p) as:

$$A_s = (\pi)^{\frac{1}{3}} \cdot \left(6V_p\right)^{\frac{2}{3}} \quad (2\text{-}4)$$

where $Vp = \left(\frac{\pi}{6}\right) \cdot l \cdot w \cdot t$, as given by the volume of an ellipsoid.

However, A_p is not as easy to determine as the surface area of a sphere. A good approximation of the surface area of a triaxial ellipsoid was derived by Klamkin (1971). This equation was refined by Knud Thomsen, as cited by Xu et al. (2009), such that the approximation gave the least relative error of ±1.06% when p = 1.6075. Applying Thomsen's formula for approximating the surface area of an ellipsoid to a wheat particle gives:

$$A_p = 4\pi \left[\frac{\left(\frac{l}{2}\cdot\frac{w}{2}\right)^{1.6075} + \left(\frac{l}{2}\cdot\frac{t}{2}\right)^{1.6075} + \left(\frac{w}{2}\cdot\frac{t}{2}\right)^{1.6075}}{3} \right]^{1.6075} \quad (2\text{-}5)$$

The sphericity of Wadell (1935) can be written as:

$$\varphi_2 = \frac{(l\cdot w\cdot t)^{2/3}}{\left[\frac{(l*w)^{1.6075} + (l*t)^{1.60745} + (w*t)^{1.6075}}{3}\right]^{1/1.6075}} \quad (2\text{-}6)$$

Flatness shape factor is the ratio of the kernel's width to its thickness, while elongation shape factor is the ratio of the kernel's length to its width. These shape factors are given by the following equations:

$$\lambda = w/t \quad (2\text{-}7)$$

$$\epsilon = l/t \quad (2\text{-}8)$$

where λ and ε are the flatness shape factor and elongation shape factor, respectively. A flatness shape factor of 1.0 indicates that the cross-section of the kernel is round. The higher the flatness shape factor, the flatter or more flake-like the kernel is. Similarly, an elongation shape factor of 1.0 indicates that the longitudinal section of the kernel is round. The higher the elongation ratio, the more elongated the kernel is.

2.2.5 Sample preparation

For each variety, kernels from the four size fractions were prepared, and kernel apparent density, loose bulk density, tapped bulk density, and test weight were determined. Approximately 800 g samples were used for each run in the determination of bulk density and test weight. The same amount was used for binary and ternary mixtures.

Six binary mixtures were also produced for each variety by mixing various mass fractions of two different size classes. In each binary mix series, the mass fraction of the smaller size class was increased from 20% to 80% in steps of 20% (at the same time, the mass fraction of the larger size class was decreased from 80% to 20% in steps of 20%). Hence, there were four binary

mixtures in each binary mix series. For each variety, 6 × 4 = 24 binary mixtures were produced for testing. Six ternary mixtures of kernels retained on sieves #7, #8, and #10 were also produced for each variety, with proportions of 0.2-0.6-0.2, 0.4-0.4-0.2, 0.6-0.2-0.2, 0.2-0.4-0.4, 0.4-0.2-0.4, and 0.2-0.2-0.6, respectively.

2.2.6 Density measurements

The kernel apparent density was determined using a helium gas multi-pycnometer. A large cell with a volume of 148.52 cm^3 was filled with a known mass of wheat. The pycnometer measures the volume occupied by the sample. By dividing the known mass of wheat by the volume measured with the pycnometer, the density of the sample can be determined. In this procedure, the measured density is not the kernel apparent density but rather the kernel control density according to Chang (1988). The volume measured in this method excludes the pore spaces inside the individual kernels that are accessible to helium gas. To determine the kernel apparent density, the individual kernels should first be coated with paraffin before volume measurement with the pycnometer, and then computations can determine the volume occupied by the wheat kernels. In the study by Chang (1988), the wheat kernel apparent density was 0.971 times lower than the control density. We used this relationship to calculate kernel apparent density from the pycnometer-measured density.

Carr (1965) discussed four different types of bulk densities that have a direct effect on the compressibility of a substance. Loose bulk density is determined by pouring a quantity of granular material into a container of known volume. It is called loose because the bulk solid has not been subjected to compression or packing. In the grain industry, test weight is the common measure of loose bulk density.

Packed bulk density is the bulk density of the material after it has been compressed. When grain is stored in bins, its bulk density is a packed bulk density. Packed bulk density is always higher than loose bulk density due to a decrease in bulk volume because of displacement of the entrained air in the void spaces between particles. The Canadian Grain Commission (2014) test weight, expressed in kilograms per hectoliter, is a packed bulk density measurement.

All measurements were done in the following order to reduce variation in measurements. First, a sample of approximately 800 g was prepared depending on the required amount of kernel fraction in a mixture. The sample was then passed through a sample divider, and the two parts were combined. This was done five times. Loose bulk density was then determined, followed by tapped bulk density. This sequence was repeated three times using the same 800 g sample.

2.2.6.1 Loose bulk density

A 1000 mL graduated cylinder was used in the determination of loose and tapped (or packed) bulk densities. The cylinder was cut into two parts. The lower half of the cylinder had an internal volume of 400 cm^3 (6.35 cm diameter, 12.63 cm height). The upper half could be replaced and secured on top of the lower half by using a flexible hose connector.

To determine the loose bulk density, only the lower half of the cylinder was used. The test used the same procedure as used for determining the test weight of wheat except that instead of the test kettle, the lower part of the cylinder (Figure 2-1a) was used and the filling funnel was held at a height of 5.70 cm above the cylinder. Dividing the mass of the grain by the cylinder volume gave us the loose bulk density. The cylinder was placed at the same location each time it was filled to limit variability in measured loose bulk density.

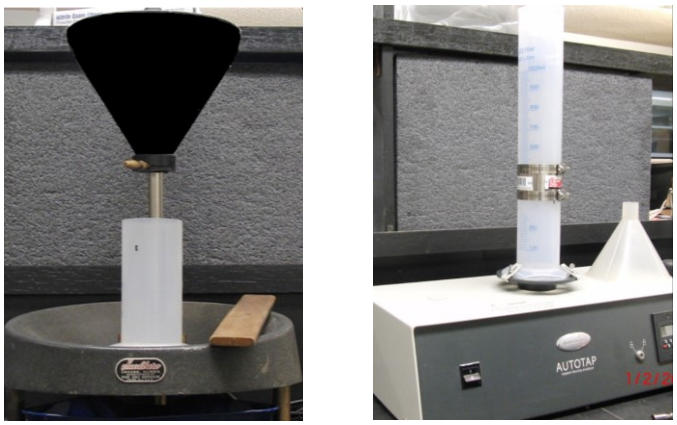

(a) (b)

Figure 2-1. Bulk density measurement: (a) loose and (b) tapped.

2.2.6.2 Tapped bulk density

The packed bulk density was approximated as the tapped bulk density and was obtained by securing the upper half of the cylinder to the lower half of the cylinder that was filled with wheat during the loose bulk density test (Figure 2-1b). This prevented the wheat from spilling during tapping. Tapping was done using a Quantachrome Autotap at a rate of 260 taps per minute (4.33 Hz) and a nominal tapping height of 3 mm. As the grain was tapped, its level decreased, resulting in an increase in bulk density. However, because the change in height was difficult to measure, a fixed volume with varying mass was used for determining tapped bulk density. To achieve a fixed volume, an additional 150 g of wheat was added to the cylinder before mounting it to the Autotap and tapping 500 times. The number of taps was based on results of preliminary tests, which showed no significant change in the tapped bulk density of wheat samples after 500 taps. After tapping, the upper part of the cylinder was carefully removed, the grain was leveled using the strike-off stick, and the remaining grain was weighed. The tapped bulk density was calculated as the grain mass divided by the cylinder volume.

2.2.7 Packing ratio and compressibility

Packing ratio is defined by Stovall et al. (1986) as the volume fraction of the system occupied by solids. When the interstitial fluid is of negligible density, the packing ratio is the bulk density divided by the true density. It can be expressed as one minus the porosity. It is also the reciprocal of the specific volume, which is defined as the apparent volume occupied by a unit volume of solid particles. A high packing ratio indicates a low percentage of interparticle voids. For this study, the tapped bulk density and the kernel apparent density were used in determining the packing ratio of wheat samples. Thus, the packing ratio of wheat particles was defined as:

$$\Phi = \mathrm{BD_t}/\mathrm{AD} \tag{2-9}$$

where Φ is the packing ratio (decimal), BD_t is the tapped bulk density (kg m^{-3}), and AD is the kernel apparent density (kg m^{-3}).

Compressibility indicates the difference between the loose and packed bulk densities of the material (Carr, 1965; Hosokawa Micron Powder Systems, n.d.) and was defined using the measured tapped bulk density for packed bulk density as:

$$\mathrm{C} = (\mathrm{BD_t} - \mathrm{BD_l})/\mathrm{BD_t} \tag{2-10}$$

where C is the compressibility, and BD_l is the loose bulk density.

Low compressibility indicates very good flowability in powder. For free-flowing granular materials such as wheat, compressibility gives a measure of packing from the initial bulk density (loose bulk density) due to outside forces (vibration in this case) that rearrange the kernels and produce a higher final bulk density (tapped bulk density).

2.2.8 Data analysis

Pairwise mean comparison using least significant difference (LSD) was used to determine if there were significant differences in parameter values among the four different size

fractions and between the two varieties. Linear regression was performed, and the coefficient of determination (R^2) was used to determine the relationships between kernel size and shape factors, packing ratio and shape factors, and compressibility and shape factors. Pairwise mean comparison using LSD was also used to determine if there were significant differences among the different binary mixtures of kernel sizes and between the two varieties for the same binary mixture. A stepwise forward selection regression was performed in Minitab to determine the best-fit equations for the packing ratio and compressibility of ternary mixtures for both varieties. MATLAB was used to plot ternary diagrams of the packing ratio and compressibility of the two varieties.

2.3 Results and discussion

2.3.1 Variety comparison

Table 2-2 shows the test weight, moisture content, and percentage composition by mass of dockage, shrunken and broken kernels, and whole kernels for the two varieties. The test weight of wheat can be affected by the amount of shrunken and broken kernels, by the amount of whole kernels, and by the kernel size distribution. How the different particles are arranged can also affect the volume occupied by interparticle voids.

KanMark had a higher average test weight than 1863. The percentages of whole kernels and of shrunken and broken kernels for both varieties were not significantly different ($p > 0.05$). Thus, the significant difference in test weight, which is a measure of bulk density, can be attributed to the difference in kernel apparent density and moisture content. The higher kernel apparent density of 1863 should have resulted in a higher test weight; however, its higher moisture content resulted in a lower test weight than KanMark because wheat kernels tend to swell with moisture and increase in volume (Thompson and Ross, 1983). The moisture content

difference of 0.8% can account for a difference of 8.06 kg m^{-3} (0.5 lb bu^{-1}) in test weight using the equation in ASABE Standard D241.4 (ASABE, 2012). In addition, KanMark had a higher proportion of larger kernel size fractions (retained on sieves #6 and #7) that contributed to a higher test weight than 1863 (Table 2-1). Another possible source of variation in the test weights was the difference in kernel size (Table 2-3) and shape (Table 2-4) for each size fraction between the two varieties.

Table 2-2.Test weight, moisture content, and mass composition of HRW wheat varieties 1863 and KanMark.[a]

			Kernel	Moisture	Mass Composition (%)		
		Test Weight	Apparent Density[b]	Content[c]	Whole	Shrunken	
Wheat Variety	n	(lb bu^{-1})	(kg m^{-3})	(% w.b.)	Kernels	and Broken	Total
1863	5	60.71 (0.20) A	1378 (4) A	12.2 (0.1) A	99.52 (0.08) A	0.48 (0.08) A	100.0
KanMark	5	61.38 (0.15) B	1370 (3) B	11.4 (0.0) B	99.65 (0.05) A	0.35 (0.05) A	100.0

[a]Data are means and standard deviations (in parentheses). In each column, means followed by the same letter are not significantly different at the 5% level of significance.
[b]n = 12 (same as in Table 2-3).
[c]n = 3 for moisture content measurement.

After exposing the two wheat varieties to the same environmental conditions for two weeks, the kernel dimensions were manually determined using a Vernier caliper (Table 2-3). In this article, we use the sieve number to refer to the size of the kernels that were retained on each sieve. For both varieties, the length, width, and thickness of kernels retained on each sieve decreased as the mesh size decreased. The average kernel thickness and width of the two wheat varieties for the same size fraction had very small differences, most likely because kernels were sorted on sieves based on their cross-section. However, the average length of KanMark kernels was always greater than that of 1863 for the same size fraction because of the inherent shape traits of the two wheat varieties. The equivalent spherical diameters followed the same trend (increasing with larger size fraction) because they were derived from the kernel dimensions.

Table 2-3. Kernel dimensions, apparent density, and test weight for different size classes of HRW wheat varieties 1863 and KanMark.[a]

Wheat Variety	Size	n	Length (mm)	Width (mm)	Thickness (mm)	ds (mm)	Apparent Density[b] (kg m^{-3})	Test Weight[b] (lb bu^{-1})	Moisture Content[b] (% w.b.)
1863	#6	90	6.17 (0.23) ^{aA}	3.36 (0.12) ^{aA}	2.95 (0.13) ^{aA}	3.94 (0.12) ^{aA}	1379 (4) ^{aA}	62.88 (0.07) ^{aB}	12.36 (0.03) ^{cA}
	#7	90	5.88 (0.31) ^{bA}	3.01 (0.16) ^{bA}	2.72 (0.14) ^{bA}	3.64 (0.15) ^{bA}	1380 (4) ^{aA}	62.68 (0.07) ^{aA}	12.43 (0.01) ^{bA}
	#8	90	5.45 (0.32) ^{cA}	2.51 (0.21) ^{cA}	2.39 (0.16) ^{cA}	3.19 (0.16) ^{cA}	1375 (4) ^{aA}	60.37 (0.16) ^{bA}	12.58 (0.02) ^{aA}
	#10	90	5.03 (0.43) ^{dA}	2.03 (0.24) ^{dA}	2.00 (0.18) ^{dA}	2.73 (0.18) ^{dA}	1378 (3) ^{aA}	54.65 (0.34) ^{cA}	12.32 (0.03) ^{cA}
KanMark	#6	90	5.81 (0.28) ^{aB}	3.29 (0.22) ^{aB}	2.92 (0.17) ^{aA}	3.82 (0.14) ^{aB}	1370 (5) ^{aA}	63.40 (0.21) ^{aA}	11.40 (0.01) ^{cB}
	#7	90	5.42 (0.28) ^{bB}	2.96 (0.22) ^{bA}	2.65 (0.16) ^{bB}	3.49 (0.16) ^{bB}	1370 (3) ^{aB}	62.69 (0.09) ^{bA}	11.39 (0.00) ^{cB}
	#8	90	5.06 (0.35) ^{cB}	2.46 (0.21) ^{cA}	2.32 (0.15) ^{cB}	3.06 (0.16) ^{cB}	1369 (2) ^{aA}	59.11 (0.10) ^{cB}	11.50 (0.02) ^{bB}
	#10	90	4.86 (0.50) ^{cB}	1.82 (0.30) ^{dB}	1.90 (0.23) ^{dB}	2.55 (0.24) ^{dB}	1370 (3) ^{aB}	54.80 (0.14) ^{dA}	11.75 (0.03) ^{aB}
Combined	#6	180	5.99 (0.31) ^{a}	3.32 (0.18) ^{a}	2.93 (0.15) ^{a}	3.88 (0.14) ^{a}	1374 (7) ^{a}	63.14 (0.31) ^{a}	11.88 (0.53) ^{a}
	#7	180	5.65 (0.38) ^{b}	2.98 (0.19) ^{b}	2.69 (0.15) ^{b}	3.56 (0.17) ^{b}	1375 (6) ^{a}	62.69 (0.07) ^{a}	11.91 (0.57) ^{a}
	#8	180	5.25 (0.39) ^{c}	2.48 (0.21) ^{c}	2.35 (0.16) ^{c}	3.13 (0.17) ^{c}	1372 (4) ^{a}	59.74 (0.70) ^{b}	12.04 (0.59) ^{a}
	#10	180	4.95 (0.47) ^{d}	1.93 (0.29) ^{d}	1.95 (0.21) ^{a}	2.64 (0.23) ^{d}	1374 (5) ^{a}	54.73 (0.25) ^{c}	12.03 (0.32) ^{a}
Average 1863		360	5.64 (0.54) ^{a}	2.73 (0.54) ^{a}	2.51 (0.39) ^{a}	3.37 (0.48) ^{a}	1378 (4) ^{a}	60.15 (3.57) ^{a}	12.42 (0.11) ^{a}
KanMark		360	5.29 (0.51) ^{b}	2.63 (0.60) ^{b}	2.45 (0.42) ^{b}	3.23 (0.51) ^{b}	1370 (3) ^{b}	60.00 (3.47) ^{a}	11.51 (0.15) ^{b}

[a]Data are means and standard deviations (in parentheses). In each column, means followed by the same lowercase letter are not significantly different at the 5% level between size fractions and variety; different uppercase letters indicate significant differences between varieties for the average.

[b]n = 3 for apparent density, test weight and moisture content in each size class, and n = 24 for the average apparent density, test weight, and moisture content for each variety

Although each size fraction passed through the same sieve, the dimensions of 1863 kernels were always larger than those of KanMark. This happened because the kernels that were retained on each sieve had a size range. The sieve on which kernels were retained dictated the lower limit of the size range, while the sieve that the kernels passed through dictated the upper limit of the size range. The size distribution for 1863 included more kernels with sizes closer to the upper end of each size fraction, which caused 1863 kernels to have larger dimensions than KanMark kernels for each size fraction, even if all the kernels passed through the same sieve.

The average kernel apparent density of 1863 was higher than that of KanMark. However, the kernel apparent density was the same across all size fractions within the same variety. This indicates that the kernel apparent density varied significantly between varieties, but not across size fractions of the same variety. This agrees with the observation by Chang (1988) that different varieties can have slightly different apparent densities even if they belong to the same wheat class.

Test weight generally decreased with decreasing kernel size. In general, the test weight of 1863 was higher than that of KanMark, except for sizes #7 and #10, where there were no significant differences between the two varieties. The average test weight of each variety in Table 2-3 is lower than the values shown in Table 2-2 because the former is the average test weight of each size fraction for each variety, while the latter is the test weight of each variety with the size fraction distribution shown in Table 2-1 and having some shrunken and broken kernels. Thus, test weight is affected by the size and size distribution of kernel fractions, including shrunken and broken kernels.

The moisture content variation across size fractions did not show a clear trend. Combining the two varieties for the analysis of moisture content showed that the effect of size on moisture content was not significant ($p > 0.05$). The moisture content of 1863 remained higher than that of KanMark even after exposing both varieties to the same environmental conditions. Thus, the moisture contents were not equal because the two varieties had different equilibrium moisture contents for these conditions.

2.3.2 Effect of size and shape factors

The shape factors are summarized in Table 2-4. For both sphericity values, the effect of size was statistically significant for both varieties; that is, it increased as size increased. In general, both sphericity values were greater for KanMark than for 1863. However, the Wadell sphericity was higher than the Mohsenin sphericity. The reason is that the Mohsenin equation is based on the geometric mean diameter for a particle that resembles a sphere, while the Wadell equation computes the sphericity, assuming a perfect ellipsoid, as the ratio of the surface area of a sphere having the same volume as the particle to the actual surface area of the particle. Because

sphericity is not easy to determine accurately due to the difficulty in measuring the surface area of a particle, both estimates of sphericity were used in this study.

The flatness increased as the kernel size increased. Generally, this indicates that the kernel cross-section became flatter or less round as the kernel size increased. However, the flatness values for kernel sizes #6 and #7 were not significantly different from each other. Flatness values ranged from 0.96 to 1.14, which suggests that the wheat kernels had a relatively round cross-section. On average, the flatness values of the two wheat varieties were not significantly different.

Elongation increased as kernel size decreased, which suggests that smaller kernels were more elongated. On average, 1863 had more elongated kernels than KanMark.

Table 2-4. Kernel shape factors for different size classes of HRW wheat varieties 1863 and KanMark.[a]

Wheat Variety	Size	*n*	Sphericity Mohsenin (φ_1)	Sphericity Wadell (φ_2)	Flatness (λ)	Elongation (ε)	Packing Ratio (Φ)[b]	Compressibility (C)[b]
1863	#6	90	0.64 (0.02) ^{aB}	0.93 (0.01) ^{aB}	1.14 (0.04) ^{aA}	2.10 (0.10) ^{dA}	0.632 (0.001) ^{aB}	0.052 (0.003) ^{cA}
	#7	90	0.62 (0.02) ^{bB}	0.92 (0.01) ^{bB}	1.11 (0.06) ^{aA}	2.17 (0.12) ^{cA}	0.631 (0.001) ^{aA}	0.055 (0.001) ^{bcA}
	#8	90	0.59 (0.03) ^{cB}	0.91 (0.02) ^{cB}	1.05 (0.10) ^{bA}	2.29 (0.17) ^{bA}	0.612 (0.002) ^{bA}	0.059 (0.001) ^{bA}
	#10	90	0.54 (0.04) ^{dA}	0.88 (0.04) ^{dA}	1.02 (0.12) ^{bA}	2.53 (0.24) ^{aA}	0.558 (0.001) ^{cA}	0.066 (0.001) ^{aA}
KanMark	#6	90	0.66 (0.03) ^{aA}	0.94 (0.01) ^{aA}	1.13 (0.10) ^{aA}	1.99 (0.12) ^{cB}	0.638 (0.001) ^{aA}	0.046 (0.003) ^{dB}
	#7	90	0.65 (0.03) ^{aA}	0.93 (0.01) ^{aA}	1.12 (0.08) ^{aA}	2.05 (0.14) ^{cB}	0.633 (0.001) ^{bA}	0.051 (0.002) ^{cB}
	#8	90	0.61 (0.03) ^{bA}	0.92 (0.02) ^{bA}	1.06 (0.09) ^{bA}	2.18 (0.15) ^{bB}	0.599 (0.001) ^{cB}	0.059 (0.001) ^{bA}
	#10	90	0.53 (0.06) ^{cA}	0.87 (0.04) ^{cB}	0.96 (0.14) ^{cB}	2.60 (0.45) ^{aA}	0.557 (0.002) ^{dA}	0.064 (0.001) ^{aA}
Combined	#6	180	0.65 (0.02) ^{a}	0.93 (0.01) ^{a}	1.14 (0.08) ^{a}	2.05 (0.12) ^{d}	0.635 (0.003) ^{a}	0.049 (0.004) ^{d}
	#7	180	0.63 (0.03) ^{b}	0.93 (0.01) ^{b}	1.11 (0.07) ^{a}	2.11 (0.14) ^{c}	0.632 (0.001) ^{a}	0.053 (0.003) ^{c}
	#8	180	0.60 (0.03) ^{c}	0.91 (0.02) ^{c}	1.06 (0.09) ^{b}	2.24 (0.17) ^{b}	0.606 (0.007) ^{b}	0.059 (0.001) ^{b}
	#10	180	0.54 (0.05) ^{d}	0.87 (0.03) ^{d}	0.99 (0.14) ^{c}	2.57 (0.36) ^{a}	0.558 (0.001) ^{c}	0.065 (0.001) ^{a}
Average								
1863		360	0.60 (0.05) ^{b}	0.91 (0.02) ^{a}	1.08 (0.10) ^{a}	2.27 (0.23) ^{a}	0.609 (0.031) ^{a}	0.058 (0.006) ^{a}
KanMark		360	0.61 (0.06) ^{a}	0.91 (0.04) ^{a}	1.07 (0.12) ^{a}	2.21 (0.34) ^{b}	0.607 (0.034) ^{a}	0.055 (0.008) ^{a}

[a] Data are means and standard deviations (in parentheses). In each column, means followed by the same lowercase letter are not significantly different at the 5% level between size fractions and variety; different uppercase letters indicate significant differences between varieties for the average.

[b] $n = 3$ for packing ratio and compressibility in each size class, and $n = 24$ for the average packing ratio and compressibility in each size class.

For both varieties, the packing ratio increased significantly with an increase in kernel size, while compressibility decreased. There were significant differences in packing ratio and

compressibility between the two varieties for the same size fraction due to the differences in kernel dimensions and shape factors for each size fraction. However, the average packing ratio and compressibility for both varieties did not vary significantly.

Figure 2-2 shows plots of the shape factors against the average equivalent spherical diameter (d_s) for each size class. The shape factors had strong linear relationships with kernel size (d_s). The two lines drawn for the shape factors for each variety have slightly different slopes, which suggests that the two varieties have slightly different shape factors. Minitab 17.0 Stat > Regression > Fit Regression Model was used to determine if there were significant differences between the coefficients of the regression equations. For each test, the shape factor was used as the response variable, d_s was the continuous predictor, and the variety was the categorical variable. In addition, the interaction term "d_s × variety" was included in the model. Tests of the difference between the regression coefficients of the two regression equations, corresponding to each variety, showed that there were no significant differences for all shape factors. Thus, for the analysis of the effect of shape on packing ratio and compressibility of wheat, the two varieties were treated as one.

The linear relationships between compressibility and packing ratio with the different shape factors are shown in Figure 2-3. All shape factors showed a linear relationship (dashed lines) with packing ratio (R^2 = 0.87 to 0.91). Sphericity and flatness had a positive linear relationship with packing ratio, while elongation had a negative linear relationship. If the kernels in each size fraction were of perfect spherical shape and of the same size, there would be no variation in packing ratio because mono-sized spherical particle assemblies are independent of particle size. However, because the kernels in each size fraction were ellipsoidal in shape and not uniform in size, the packing ratio varied depending on the different orientations of the kernels as

they filled the cylindrical container. For wheat kernels, the more spherical and flatter the kernels were, the higher the packing ratio was, while a lower packing ratio occurred with kernels that were more elongated in shape.

For compressibility (solid lines in Figure 2-3), elongation had the strongest linear relationship ($R^2 = 0.88$), followed by sphericity ($R^2 = 0.83$ and 0.85) and flatness ($R^2 = 0.79$). Sphericity and flatness had negative linear relationships with compressibility. This indicates that the more spherical or flake-like the kernels were, the less compressible they were. On the other hand, elongation had a positive linear relationship with compressibility, which indicates that the more elongated the kernels were, the more compressible they were.

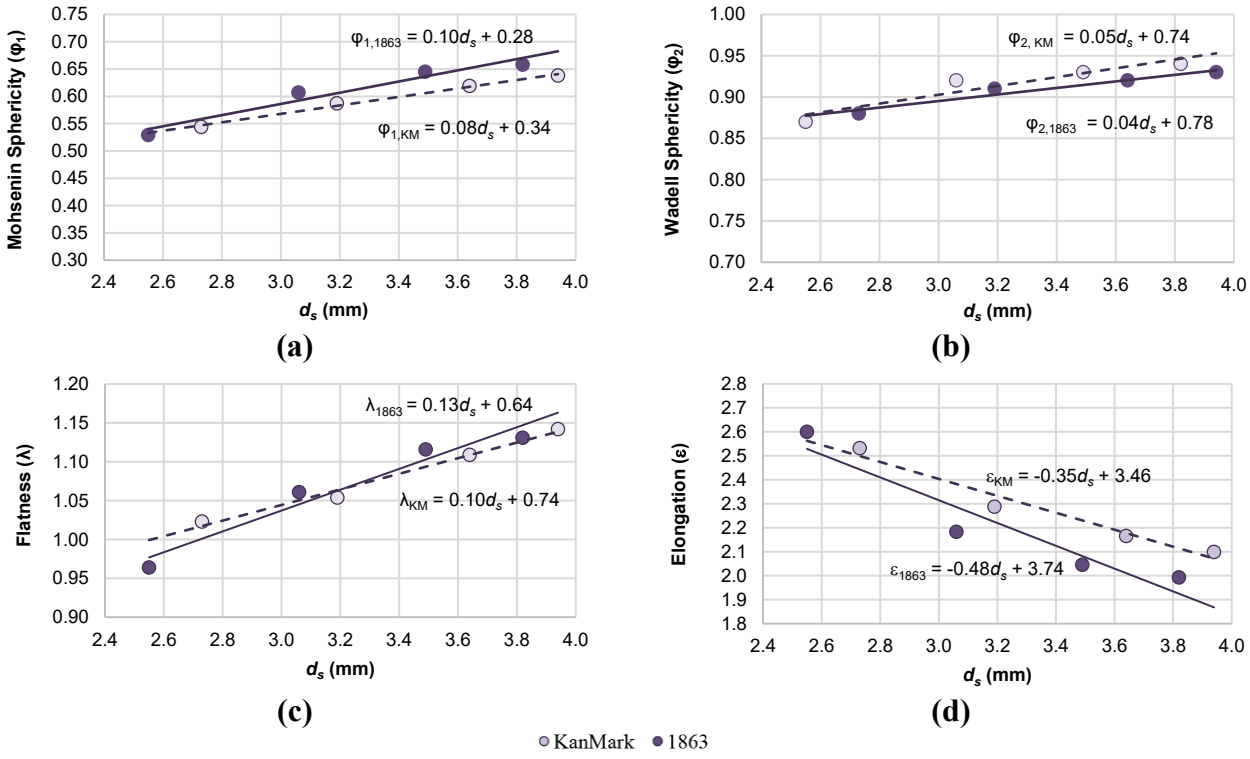

Figure 2-2. Shape factors for different size classes (equivalent spherical diameter, ds) of HRW wheat varieties KanMark and 1863: (a) Mohsenin sphericity, (b) Wadell sphericity, (c) flatness, and (d) elongation.

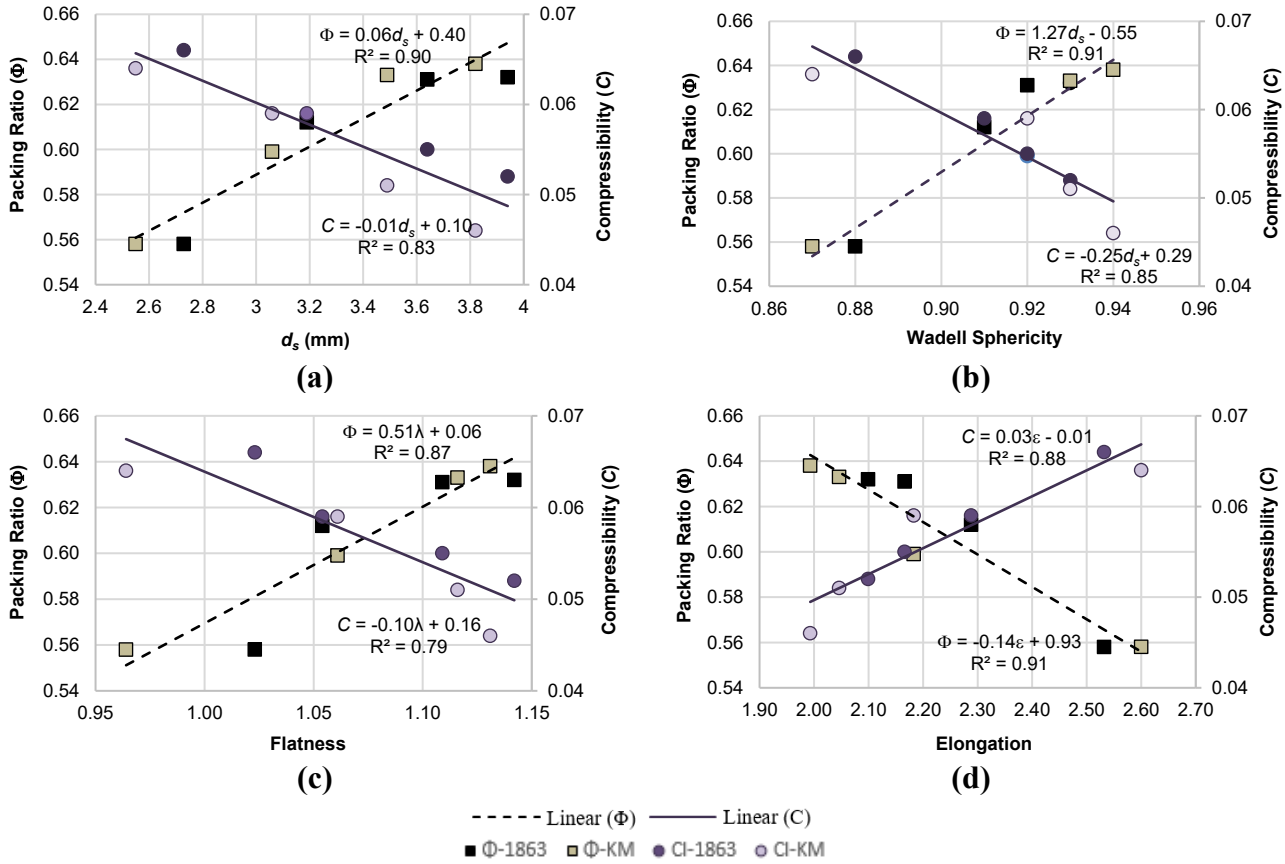

Figure 2-3. Packing ratio and compressibility of HRW wheat varieties KanMark (KM) and 1863 as affected by size and shape parameters: (a) equivalent spherical diameter (ds), (b) Wadell sphericity, (c) flatness, and (d) elongation.

In Figure 2-4, the data points can be grouped into two sets (for the two varieties) for both packing ratio and compressibility. This is because the two varieties had different bulk densities and kernel apparent densities. However, for the same size class, the kernel apparent density and compressibility were almost the same for both varieties (Table 2-4). These results all suggest that the compressibility and packing ratio were both affected by kernel shape and size and not so much by wheat variety.

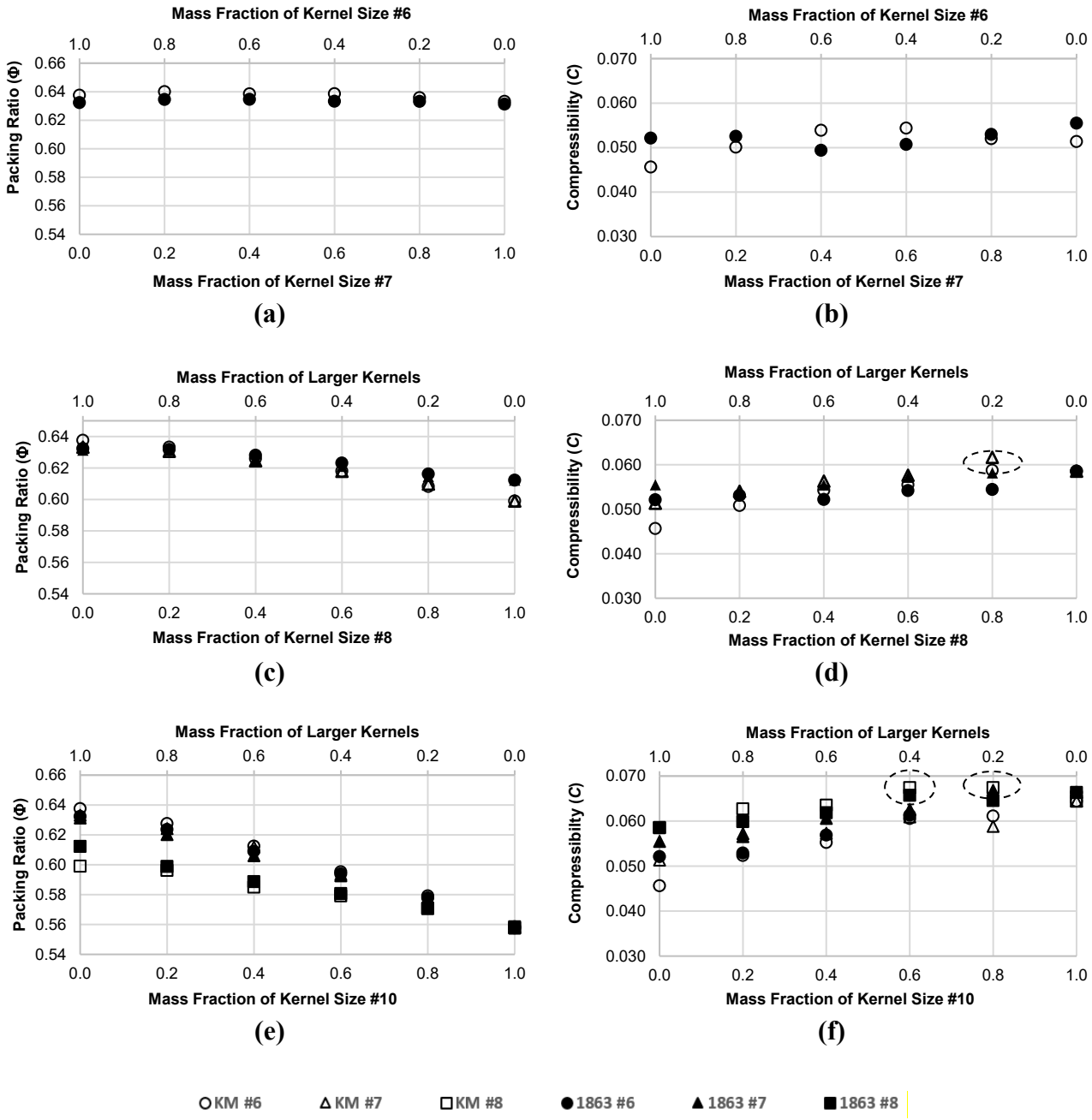

Figure 2-4. Packing ratio and compressibility of binary mixtures of different kernel sizes of HRW wheat varieties KanMark (KM) and 1863. Dashed circles indicate instances when the compressibility of the binary mixture was higher than that of the smaller single fraction.

2.3.3 Effect of size distribution

Size, shape, and variety were found to affect compressibility and packing ratio of the wheat kernels. The effect of mixing the two size fractions was also investigated to help determine how kernel size distribution affected these properties.

2.3.3.1 Binary mixtures

The experimental packing ratio and compressibility values of six binary mixtures of different kernel sizes are plotted in Figure 2-4. The primary horizontal axis (bottom) for each plot corresponds to the mass fraction of the smaller kernel size in the binary mixture, while the secondary horizontal axis (top) corresponds to the mass fraction of the larger kernel size.

The first packing ratio plot is for binary mixtures of #6 and #7 for both KanMark and 1863. The packing ratio plots for both varieties are almost a straight line with zero slope. Based on the LSD pairwise mean comparison, there was no significant difference in the packing ratios among various mass fractions of #6 and #7 for 1863 and small differences for KanMark. This is because the packing ratios of kernel sizes #6 and #7 were not significantly different for 1863 but were significantly different for KanMark (Table 2-4). This also explains why the plots of the packing ratios of binary mixtures #6-#8 and #7-#8 had the same trend and almost overlapped each other. The same is true for binary mixtures #6-#10 and #7-#10. In general, as the mass fraction of smaller kernels increased, the packing ratio of the mixture decreased.

The first compressibility plot is for the binary mixture of #6 and #7 for KanMark and 1863. Like the packing ratio, the compressibility of this combination was almost a zero-slope line. Even though the individual compressibility values of the #7 and #8 size fractions for 1863 and KanMark were significantly different (Table 2-4), the compressibility of the combinations of #7 and #8 exhibited no significant differences for varying mass fractions of 1863 and just small

differences for KanMark. Thus, the compressibility of these binary mixtures behaved differently from the compressibility of a single size fraction. This might be due to how the different kernel sizes in a mixture were arranged during measurement of loose bulk density and how they were rearranged during tapping, which affected the measured tapped bulk density.

In general, as the mass fraction of smaller kernels increased, the compressibility of the mixture increased. Smaller kernels were more elongated and less spherical than larger kernels, which could have resulted in a more random initial arrangement of the kernels. Inducing vibration by tapping disturbed this arrangement. If the kernels were spherical and of the same size, the induced vibration would have a very little effect on their arrangement because a sphere's orientation is always the same. However, because the kernels were ellipsoidal and with different sizes and shape factors, the induced vibration resulted in a different and more packed arrangement, increasing its compressibility. Similarly, the increase in the amount of smaller and more elongated kernels resulted in higher compressibility. There were also some instances in which the compressibility of the mixture was higher than the compressibility of the smaller size fraction in the mixture, i.e., $C = 0.068$ for KanMark 40% #8 and 60% #10 and for KanMark 20% #8 and 80% #10 as compared with $C = 0.064$ for KanMark #10, and $C = 0.062$ for KanMark 20% #7 and 80% #10 as compared $C = 0.059$ for KanMark #8.

Table 2-5 summarizes the packing ratio and compressibility of the different binary mixtures of kernel sizes for the two wheat varieties. The different combinations of kernel sizes forming a binary mixture had a significant effect on both the packing ratio and the compressibility. In general, mixtures of larger kernels had higher packing ratios but lower compressibility. It is well known that in binary mixtures of spherical particles, if the small particles are small enough to fill in the voids between the large particles, the mixture will have a

higher packing ratio. However, if the mixture consists of similar-sized particles (i.e., the size ratio in the binary mixture is close to one), the packing ratio will not change (Wong and Kwan, 2014). In addition, if the size ratio of small to large particles approaches zero, the packing ratio will increase due to either the occupying or filling effect depending on whether the larger or smaller particles are dominant. If the size ratio between the two particle sizes in a binary mixture is neither unity nor close to zero, the effect will be a decrease in the packing ratio due to either the loosening effect or the wall effect. Because the size ratios of the kernel fractions in this study were neither unity nor close to zero, the decrease in packing ratio was caused by the loosening effect of smaller particles when larger particles were dominant and by the wall effect of larger particles when smaller particles were dominant.

Table 2-5. Mean packing ratio and compressibility of binary mixtures of HRW wheat varieties 1863 and KanMark.[a]

Kernel Size Combination	*n*	Packing Ratio		Compressibility	
		1863	KanMark	1863	KanMark
#6 and #7	18	0.633 (0.001) ^{aA}	0.637 (0.002) ^{aB}	0.059 (0.006) ^{acA}	0.051 (0.004) ^{aB}
#6 and #8	18	0.624 (0.008) ^{bA}	0.620 (0.014) ^{bA}	0.054 (0.003) ^{abA}	0.057 (0.004) ^{bA}
#7 and #8	18	0.622 (0.008) ^{bA}	0.619 (0.012) ^{bA}	0.056 (0.002) ^{aA}	0.054 (0.005) ^{bA}
#6 and #10	18	0.599 (0.026) ^{cA}	0.602 (0.028) ^{bA}	0.052 (0.002) ^{bA}	0.057 (0.007) ^{bB}
#7 and #10	18	0.598 (0.025) ^{cA}	0.600 (0.027) ^{bA}	0.061 (0.005) ^{cA}	0.058 (0.005) ^{bA}
#8 and #10	18	0.585 (0.018) ^{cA}	0.581 (0.015) ^{bcA}	0.063 (0.003) ^{acA}	0.064 (0.003) ^{cA}
All	108	0.610 (0.024) ^{A}	0.610 (0.026) ^{A}	0.058 (0.005) ^{A}	0.057 (0.006) ^{A}

[a] Data are means and standard deviations (in parentheses). Lowercase letters compare the packing ratio (or compressibility) of different combinations within each variety. Uppercase letters compare the packing ratio (or compressibility) between the two varieties for the same combination.

The variety showed no significant effect on either packing ratio or compressibility for the same combination of kernel sizes except for the combination of sizes #6 and #7 and the combination of sizes #6 and #10. Overall, variety had no significant effect on packing ratio and compressibility. This is because the two wheat varieties had kernel apparent densities for each size fractions that were close to each other and kernel size distributions that were similar. Combining these two varieties of wheat might not significantly affect compressibility and

packing ratio. In bins and silos, different varieties of wheat are often mixed. In most grain facilities, when truckloads of wheat enter the facility and are transferred into bins, there is not as much mixing of different varieties, but there can be layering of different varieties in the same bin. More complete mixing occurs when the grain is moved, blended, and sold. However, if the range of kernel apparent densities of the wheat varieties is small, the compressibility and packing ratio might be more dependent on the proportions of different size fractions. For varieties that differ greatly in size fractions, the effect could be like the results of combining different size fractions in binary and ternary mixtures in this study.

2.3.3.2 Ternary mixtures

Ternary mixtures composed of kernel sizes #7, #8, and #10 were used to determine how different proportions of three kernel sizes in a mixture affect the packing ratio and compressibility. Table 2-6 shows the mass fractions of kernel sizes in 21 selected ternary mixtures and the results of the packing ratio and compressibility experiments. Table 2-7 shows the best-fit equations from stepwise linear regression with three independent variables and their interactions for both packing ratio and compressibility of the two wheat varieties.

Ternary plots of the packing ratios for both varieties showed similar trends (Figure 2-5). For both varieties, with 0% kernel size #10, the packing ratio did not vary much (0.61 to 0.63). With 0% kernel size #7, the packing ratio varied from 0.57 to 0.60, and with 0% kernel size #8, the largest variation in packing ratio was observed (0.57 to 0.63). This shows that the effect of the proportions of different kernel sizes on the packing ratio was more pronounced when the size difference between kernels was greater, as in the case when kernel sizes #7 and #10 were combined. In general, the increased proportion of the largest kernel size (#7) gave the highest contribution to the increase in packing ratio (Table 2-7). The best-fit equation for the KanMark packing ratio had three significant terms, while the best-fit equation for 1863 had four terms. The coefficient of the fourth term for 1863 was very small and had little effect on the packing ratio for 1863. The coefficients of the remaining three terms for the packing ratio equations of the two varieties were very similar to each other.

Table 2-6. Packing ratio and compressibility of ternary mixtures of HRW wheat varieties 1863 and KanMark.

	Mass Fraction (%)			Packing Ratio		Compressibility	
Sample Type	#7	#8	#10	1863	KanMark	1863	KanMark
Single size fraction	0	0	100	0.559	0.558	0.066	0.064
	0	100	0	0.611	0.599	0.059	0.059
	100	0	0	0.632	0.633	0.055	0.051
Binary mixture	0	20	80	0.571	0.571	0.065	0.067
(#8 and #10 with 0% #7)	0	40	60	0.581	0.579	0.066	0.067
	0	60	40	0.589	0.585	0.062	0.064
	0	80	20	0.599	0.596	0.060	0.063
Binary mixture	20	0	80	0.578	0.577	0.067	0.059
(#7 and #10 with 0% #8)	40	0	60	0.593	0.594	0.063	0.061
	60	0	40	0.606	0.612	0.061	0.057
	80	0	20	0.620	0.624	0.057	0.057
Binary mixture	20	80	0	0.615	0.610	0.058	0.062
(#7 and #8 with 0% #10)	40	60	0	0.621	0.618	0.057	0.058
	60	40	0	0.624	0.625	0.055	0.056
	80	20	0	0.631	0.631	0.053	0.054
Ternary mixture	20	20	60	0.585	0.583	0.064	0.063
(#7, #8, and #10)	20	40	40	0.594	0.588	0.062	0.061
	20	60	20	0.605	0.599	0.059	0.061
	40	20	40	0.599	0.597	0.061	0.060
	40	40	20	0.612	0.605	0.058	0.060
	60	20	20	0.612	0.612	0.059	0.058

Table 2-7. Best-fit equations for packing ratio and compressibility of ternary mixtures of HRW wheat varieties 1863 and KanMark.

	Wheat Variety	Best-Fit Equation[a]	R^2
Packing ratio	1863	$\Phi = 0.640(M_{\#7}) + 0.609(M_{\#8}) + 0.560(M_{\#10}) - 0.007(M_{\#7})^2$	1.00
	KanMark	$\Phi = 0.637(M_{\#7}) + 0.601(M_{\#8}) + 0.561(M_{\#10})$	1.00
Compressibility	1863	$C = 0.0540(M_{\#7}) + 0.0586(M_{\#8}) + 0.0673(M_{\#10}) + 0.0051(M_{\#10} \times M_{\#7})$	1.00
	KanMark	$C = 0.0531(M_{\#7}) + 0.0602(M_{\#8}) + 0.0642(M_{\#10}) + 0.01367(M_{\#8} \times M_{\#10})$	0.99

[a] $M_{\#7}$, $M_{\#10}$, $M_{\#8}$ are mass fractions of kernel sizes #7, #8 and #10, respectively.

The ternary plot of compressibility for 1863 was similar to that for KanMark. The largest increase in compressibility was with an increased proportion of kernel size #10, followed by kernel size #8. However, the shapes of the contours were different, largely because of the difference in the fourth term (the interaction term) in the equations. For KanMark, the fourth term, which is the interaction of mass fractions of #8 with #10, contributed to an increase in compressibility and resulted in a peak with a constant proportion of kernel size #7. A similar peak was shown in Figure 2-4 (dashed circle) for the binary mixture of KanMark #8 and #10.

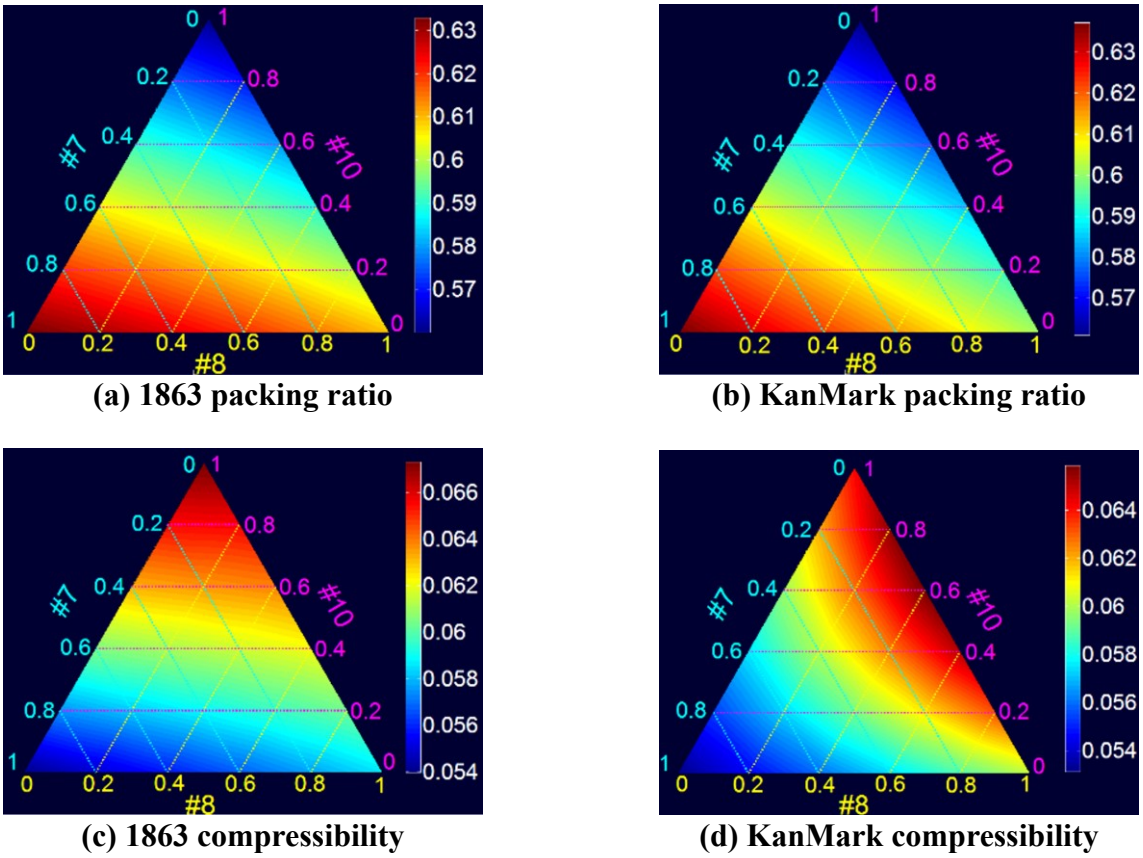

(a) 1863 packing ratio **(b) KanMark packing ratio**

(c) 1863 compressibility **(d) KanMark compressibility**

Figure 2-5. Ternary plots of packing ratio and compressibility of HRW wheat varieties 1863 and KanMark.

Similarly, the fourth term in the equation for 1863, the interaction of mass fractions of #7 with #10, contributed to an increase in the compressibility of 1863. The same effect can be seen with the interaction of #8 with #10. If there were a fifth significant term, it would be the interaction of the mass fractions of #7 and #10. These results were consistent with the compressibility of binary mixtures of 1863, with the combinations #8-#10 and #7-#10 having the highest compressibility values (Figure 2-4).

The different compressibility behavior between the two varieties may be accounted for by the variation in the size and shape of the kernels within a given size fraction between the varieties, even though the different kernels were classified in the same size fraction when sieved.

Further study is needed to understand how kernel shape and size can affect compressibility. A discrete element model simulating the loose and tapped bulk densities of wheat kernels could be used to study how different particle sizes are arranged during the packing process. In addition, x-ray topography could be used for determining the amount of interparticle voids in a wheat sample and for determining the packing ratio.

2.4 Conclusion

This research determined the effects of shape and size on the packing ratio and compressibility of two hard red winter wheat varieties (KanMark and 1863). The following conclusions were drawn:

- The packing ratio of these non-spherical particles increased with kernel size, while compressibility decreased.
- Shape factors changed with kernel size, thereby affecting compressibility and packing ratio.
- The more spherical, less elongated, and flatter the kernels, the higher the packing ratio was and the lower the compressibility was.
- Packing ratio trends were the same for single size fractions and binary mixtures of kernel fractions, while compressibility behaved differently.
- The higher the percentage of large kernels in these mixtures, the higher the packing ratio was and the lower the compressibility was.

2.5 References

ASABE. (1988). S352.2: Moisture measurement - Unground grain and seeds. St. Joseph, MI: ASABE.

ASABE. (2012). D421.4: Density, specific gravity, and mass-moisture relationships of grain for

storage. St. Joseph, MI: ASABE.

ASABE. (2010). EP413.2: Procedure for establishing volumetric capacities of cylindrical bins. St. Joseph, MI: ASABE.

Bhadra, R., Casada, M. E., Boac, J. M., Turner, A. P., Thompson, S. A., Montross, M. D., Maghirang, R. G., & McNeill, S. G. (2016). Correlating bulk density (with dockage) and test weight (without dockage) for wheat samples. *Appl. Eng. Agric., 32*(6), 925-930. https://doi.org/10.13031/aea.32.11692

Bhadra, R., Turner, A. P., Casada, M. E., Montross, M. D., Thompson, S. A., Boac, J. M., McNeill, S. G., & Maghirang, R. G. (2015). Pack factor measurements for corn in grain storage bins. *Trans. ASABE, 58*(3), 879-890. https://doi.org/10.13031/trans.58.11033

Bian, Q., Ambrose, R. P., & Subramanyam, B. (2015). Effect of chaff on bulk flow properties of wheat. *J. Stored Prod. Res., 64*(part A), 21-26. https://doi.org/10.1016/j.jspr.2015.08.004

Boac, J. M., Bhadra, R., Casada, M. E., Thompson, S. A., Turner, A. P., Montross, M. D., McNeill, S. G., & Maghirang, R. G. (2015). Stored grain pack factors for wheat: Comparison of three methods to field measurements. *Trans. ASABE, 58*(4), 1089-1101. https://doi.org/10.13031/trans.58.10898

Canadian Grain Commission. (2014). Test weight for Canadian grains. Winnipeg, Manitoba, Canada: Canadian Grain Commission. Retrieved from https://www.grainscanada.gc.ca/guides-guides/weight-poids/itwm-mrps-eng.htm

Carr, R.L. 1965. Evaluating flow properties of solids. *Chemical Engineering,* 72, 163–167

Chang, C. S. (1988). Measuring density and porosity of grain kernels using a gas pycnometer. *Cereal Chem., 65*(1), 13-15.

Dodds, J. A. (1980). The porosity and contact points in multicomponent random sphere packings

calculated by a simple statistical geometric model. *J. Colloid Interface Sci., 77*(2), 317-327. https://doi.org/10.1016/0021-9797(80)90302-1

Fang, C., & Campbell, G. M. (2000). Effect of measurement method and moisture content on wheat kernel density measurement. *Food Bioprod. Proc., 78*(4), 179-186. https://doi.org/10.1205/09603080051065278

Hosokawa Micron Powder Systems (n.d.). HMPS PT-N Carr Paper Information Brochure.

Kalkan, F., & Kara, M. (2011). Handling, frictional, and technological properties of wheat as affected by moisture content and cultivar. *Powder Tech., 213*(1), 116-122. https://doi.org/10.1016/j.powtec.2011.07.015

Klamkin, M. S. (1971). Elementary approximations to the area of *N*-dimensional ellipsoids. *American Math. Monthly, 78*(3), 280-283. https://doi.org/10.2307/2317530

Malm, J. K., & Backer, L. F. (1985). Compaction factors for six crops. *Trans. ASAE, 28*(5), 1634-1636. https://doi.org/10.13031/2013.32489

McNeill, S. G., Thompson, S. A., & Montross, M. D. (2004). Effect of moisture content and broken kernels on the bulk density and packing of corn. *Appl. Eng. Agric., 20*(4), 475-480. https://doi.org/10.13031/2013.16477

Meng, L., Lu, P., Li, S., Zhao, J., & Li, T. (2012). Shape and size effects on the packing density of binary spherocylinders. *Powder Tech., 228*, 284-294. https://doi.org/10.1016/j.powtec.2012.05.033

Mohsenin, N. N. (1986). *Physical properties of plant and animal materials: Structure, physical characteristics, and mechanical properties* (2nd ed.). New York, NY: Gordon and Breach.

Molenda, M., Horabik, J., & J. Ross, I. (1996). Effect of filling method on load distribution in model grain bins. *Trans. ASAE, 39*(1), 219-224. https://doi.org/10.13031/2013.27501

Nelson, S. O. (1980). Moisture-dependent kernel- and bulk-density relationships for wheat and corn. *Trans. ASAE, 23*(1), 139-143. https://doi.org/10.13031/2013.34540

Podczeck, F. (1997). A shape factor to assess the shape of particles using image analysis. *Powder Tech., 93*(1), 47-53. https://doi.org/10.1016/S0032-5910(97)03257-9

Ponce-Garcia, N., Ramirez-Wong, B., Escalante-Aburto, A., Torres-Chavez, P., & de Dios Figueroa-Cardenas, J. (2017). Mechanical properties in wheat (*Triticum aestivum*) kernels evaluated by compression tests: A review. In *Viscoelastic and viscoplastic materials.* Rijeka, Croatia: InTech. Retrieved from www.intechopen.com

Ross, I. J., Bridges, T. C., Loewer, O. J., & Walker, J. N. (1979). Grain bin loads as affected by grain moisture content and vertical pressure. *Trans. ASAE, 22*(3), 592-597. https://doi.org/10.13031/2013.35068

Stovall, T., de Larrard, F., & Buil, M. (1986). Linear packing density model of grain mixtures. *Powder Tech., 48*(1), 1-12. https://doi.org/10.1016/0032-5910(86)80058-4

Suzuki, M., Yagi, A., Watanabe, T., & Oshima, T. (1986). Estimation of the void fraction in a bed randomly packed with particles of three sizes. *Intl. Chem. Eng, 26*(3), 491-497.

Thompson, S. A., & Ross, I. J. (1983). Compressibility and frictional coefficients of wheat. *Trans. ASAE, 26*(4), 1171-1176. https://doi.org/10.13031/2013.34099

Thompson, S. A., McNeill, S. G., Ross, I. J., & Bridges, T. C. (1987). Packing factors of whole grains in storage structures. *Appl. Eng. Agric., 3*(2), 215-221. https://doi.org/10.13031/2013.26677

Thompson, S. A., Schwab, C. V., & Ross, I. J. (1991). Calibration of a model for packing whole grains. *Appl. Eng. Agric., 7*(4), 450-456. https://doi.org/10.13031/2013.26244

Turner, A. P., Montross, M. D., McNeill, S. G., Sama, M. P., Casada, M. E., Boac, J. M., ...

Thompson, S. A. (2016). Modeling the compressibility behavior of hard red wheat varieties. *Trans. ASABE, 59*(3), 1029-1038. https://doi.org/10.13031/trans.59.11432

USDA-FGIS. (2013). *Grain inspection handbook*. Washington, DC: USDA Federal Grain Inspection Service.

Wadell, H. (1935). Volume, shape, and roundness of quartz particles. *J. Geol., 43*(3), 250-280. https://doi.org/10.1086/624298

Wong, V., & Kwan, A. K. H. (2014). A three-parameter model for packing density prediction of ternary mixes of spherical particles. *Powder Tech., 268*, 357-367. https://doi.org/10.1016/j.powtec.2014.08.036

Xu, D., Cui, J., Bansal, R., Hao, X., Liu, J., Chen, W., & Peterson, B. S. (2009). The ellipsoidal area ratio: An alternative anisotropy index for diffusion tensor imaging. *Mag. Reson. Imaging, 27*(3), 311-323. https://doi.org/10.1016/j.mri.2008.07.018

Yu, A. B., & Standish, N. (1991). Estimation of the porosity of particle mixtures by a linear-mixture packing model. *Ind. Eng. Chem. Res., 30*(6), 1372-1385. https://doi.org/10.1021/ie00054a045

Yu, A. B., & Standish, N. (1993a). Characterisation of non-spherical particles from their packing behaviour. *Powder Tech., 74*(3), 205-213. https://doi.org/10.1016/0032-5910(93)85029-9

Yu, A. B., & Standish, N. (1993b). A study of the packing of particles with a mixture size distribution. *Powder Tech., 76*(2), 113-124. https://doi.org/10.1016/S0032-5910(05)80018-X

Yu, A. B., Standish, N., & McLean, A. (1993). Porosity calculation of binary mixtures of nonspherical particles. *J. American Ceram. Soc., 76*(11), 2813-2816. https://doi.org/10.1111/j.1151-2916.1993.tb04021.x

Yu, A. B., Zou, R. P., & Standish, N. (1992). Packing of ternary mixtures of nonspherical particles. *J. American Ceram. Soc., 75*(10), 2765-2772. https://doi.org/10.1111/j.1151-2916.1992.tb05502.x

Yu, A. B., Zou, R. P., & Standish, N. (1996). Modifying the linear packing model for predicting the porosity of nonspherical particle mixtures. *Ind. Eng. Chem. Res., 35*(10), 3730-3741. https://doi.org/10.1021/ie950616a

Zhou, R. P., & Yu, A. B. (1996). Evaluation of the packing characteristics of mono-sized non-spherical particles. *Powder Tech., 88*(1), 71-79. https://doi.org/10.1016/0032-5910(96)03106-3

Zou, R. P., Gan, M. L., & Yu, A. B. (2011). Prediction of the porosity of multi-component mixtures of cohesive and non-cohesive particles. *Chemical Engineering Science*, 66(20), 4711-4721. doi:10.1016/j.ces.2011.06.037

Chapter 3 - Influence of Particle Shape and Contact Parameters on DEM-simulated Bulk Density of Wheat[2]

3.1 Introduction

Bulk density is one of the most commonly used properties of granular material. It is used by millers in quality grading; by engineers in designing storage systems; and by federal agencies, insurance companies, and storage managers in inventory measurement and control. However, grain bulk density is an extrinsic property and is affected by several factors in a storage bin.

Stored grain bulk density is much higher than the standard bushel test weight because of the overburden pressure and effects of handling practices. Overburden pressure resulted in grain compaction caused by kernel deformation and rearrangement (Gao et al., 2018; Thompson and Ross, 1983). Higher fall height also contributed to increased bulk density as a result of a more packed arrangement of kernels (Yang and Williams, 1990; Versavel and Britton, 1984). Moreover, the use of a spreader compared to spout filling has shown a significant increase in bulk density caused by greater uniformity of fine material distribution (Chang et al., 1981 and 1983).

The widely varying details of interactions between kernels create a complex problem to analyze bulk density changes in stored grain. Several studies tried to predict the stored grain bulk density to estimate the mass of grain in bins. Some of these studies used empirical means (Bates,

[2] This chapter has been submitted as a peer-reviewed paper: Petingco, M. C., Casada, M. E., Maghirang, R. G., Fasina, O. O., Chen, Z., Ambrose, R. P. K. 2020. Influence of particle shape and contact parameters on DEM-simulated bulk density of wheat. *Transactions of the ASABE* (in press).

1925; Malm and Backer, 1985), while others combined experimental and analytical solutions (Thompson et al., 1991; Cheng et al., 2017). The problem with experimental measurement is that they are often difficult or expensive to conduct. However, analytical solutions may not be able to account for all the complexities present in the problem. Some quantities such as inter-particle forces and friction, particle orientation, and packing structure are difficult to measure and to investigate experimentally or analytically. In solving complex problems, numerical methods have proven to be an effective, less expensive alternative.

In studying the behavior of granular material numerically, two modeling approaches can be used: a continuum approach or a discrete approach. In the continuum approach, such as the finite element method, the granular material is treated as continuous substance. This approach is best suited for investigating large scale systems such as in unit operations. However, some particulate system phenomena are highly dependent on particle level behavior. In this case, a discrete approach, such as discrete element method (DEM), is more appropriate to use.

DEM is an explicit numerical scheme developed by Cundall and Strack (1979) for modeling the behavior of individual particles. In this method, each particle is represented numerically and identified with its specific properties such as shape, size, material properties, and initial velocity. It also models the overall system behavior of granular material as a result of individual interactions. Over the years, DEM has been proven to be effective in studying numerous technological processes in agriculture, engineering, and food processing as it gives the user an insight on how bulk materials will interact with equipment over a range of operation and process conditions (Kačianauskas et al., 2007; Horabik and Molenda, 2016).

Although DEM is a promising tool in understanding the behavior of granular material, it also has some disadvantages. This method requires large computational power. Moreover, the

accuracy of simulations depends highly on input parameters that include force or contact models, physical properties of particulate materials (i.e., particle shape, size distribution, solids density, Poisson's ratio, and modulus of elasticity), and contact parameters (i.e., particle-to-particle and particle-surface interaction properties). For contact model, such as Hertz-Mindlin, contact parameters include coefficient of restitution, coefficient of static friction, and coefficient of rolling friction. For DEM simulations to be effective in solving problems involving granular material, thorough understanding of how these input parameters affect simulation of the behavior of granular material is required.

Most DEM software use spheres in modeling particles. As most particles are not spherical, the sphere-clump method is commonly used to produce more accurate particles for modeling. In the sphere-clump method, several overlapping spheres can be combined to approximate the shape of the particle being modeled (Favier et al., 2001). Common sphere-clumps are of the shape of rods, spherocylinders, and ellipsoids. Automatic methods for generating sphere clump models of real particles have also been developed and employed to produce a compact representation of a particle shape that closely matches the surface of its visual hull mesh or other 3D model representation (Price et al., 2007; Li et al., 2017).

Calibration is a common practice in DEM simulation to fine tune the simulations and overcome small deficiencies in precisely capturing the true physics in these mechanistic models. This procedure involves adjusting the values of contact parameters until the experimentally determined macro-scale property (e.g. angle of repose or bulk density) of bulk material matches with that of simulated values. This process is required to ensure accurate prediction of bulk material behavior. In the study by Coetzee (2016), particle shape was considered in the calibration process. Clumps comprised of two, four, and eight spheres were calibrated

individually to obtain a unique set of contact parameters. It was shown that all three clump types, once calibrated independently, could accurately predict anchor pull-out forces and hopper discharge. However, Boac et al. (2014) reviewed DEM modeling of grain post-harvest operations and concluded that accurate shape modeling is more crucial with specific applications and grains being modeled. For example, Sarnavi et al. (2013) showed that simulation of the shear behavior of particles (i.e. pea, wheat, and rapeseeds) was strongly affected by the interparticle interactions and particle shape representation in modeling.

The objectives of this study were to determine the influence of particle shape and contact parameters on simulated wheat bulk density and to develop an effective wheat particle model for DEM simulation of filling a container using EDEM^{TM} software (DEM Solutions Ltd., 2017). Wheat particles were modeled using three different particle models to determine how particle shape affects bulk density and the six contact parameters were evaluated to determine which significantly affect the simulated wheat bulk density. Once the critical factors that affect the bulk density were identified, the remaining contact parameters were calibrated.

3.2 Materials and methods

3.2.1 Wheat samples

Wheat samples (Garrison, KanMark and Everest varieties) were cleaned by passing them through a Carter-Day dockage tester (Seedburo Equipment Co., Des Plaines, IL.USA) to remove foreign material and through a 1.63 mm × 9.53 mm (0.064 in. × 3/8 in.) oblong sieve to remove shrunken and broken kernels. The kernels were sorted with a mechanical test sieve shaker (Ro-Tap, W.S. Tyler, Mentor, OH, USA) using a series of 200 mm (8 in.) diameter sieves. The sieve sizes used were #7 (2.83 mm) and #8 (2.38 mm) to obtain three size fractions. The samples were

then conditioned for one week inside an environmental chamber to have a moisture content of about 11% wet basis.

For each size fraction, grain characteristics such as thousand kernel mass, kernel dimensions, kernel density, and bulk density were determined. The average values of the three wheat varieties were used in this study. The thousand kernel mass was used as the basis for the single kernel mass. Kernel dimensions were determined using a flatbed scanner (Epson Perfection V370, Seiko Epson America, Inc., CA) and an image processing software, GrainScan (Whan et al., 2014). The procedures for image capture and analysis as outlined by Whan et al. (2014) were followed to determine the length and width of the kernels. GrainsScan determine the best fit ellipse circumscribing the kernel. The major and minor diameters of this ellipse approximate the kernel's length and width, respectively. Since the image captured is of 2D, the kernel thickness was assumed to be equal to the kernel width. The validity of this assumption is supported by Petingco et al. (2018) wherein wheat kernel thickness is not considerably different to its width. To determine the kernel density, a gas pycnometer (AccuPyc 1330, Micromiritics, GA, USA) was employed. A laboratory setup similar to test weight determination (USDA-GIPSA, 2009) was used to determine the bulk density. This was done ten times for each size fraction.

3.2.2 Numerical modeling

DEM is a numerical modeling technique that calculates finite particle displacements and rotations and automatically performs contact detection for an assembly of particles. Using contact detection algorithms and applying suitable contact models, DEM can calculate forces acting on particles. Translational and rotational accelerations are calculated based on Newton's

second law of motion and are numerically integrated over a time step to update particle velocities and positions.

The default contact model in EDEM v2018.1 is Hertz-Mindlin no slip (DEM Solutions Ltd, 2017). This contact model is based on Hertzian contact theory in the normal and Mindlin-Deresiewicz theory in the tangential direction. Both normal and tangential forces have damping components where the damping coefficient is related to the coefficient of restitution. The tangential friction force follows the Coulomb law of friction, which is a function of coefficient of static friction. The rolling friction is implemented as the contact independent directional constant torque model which is a function of the coefficient of rolling friction.

Contact forces between particle i and particle j are illustrated in Figure 3-1. The total normal force ($F_{n,ij}$) and total tangential force ($F_{t,ij}$) between particles i and j are given by the following equations (Tsuji et al., 1992):

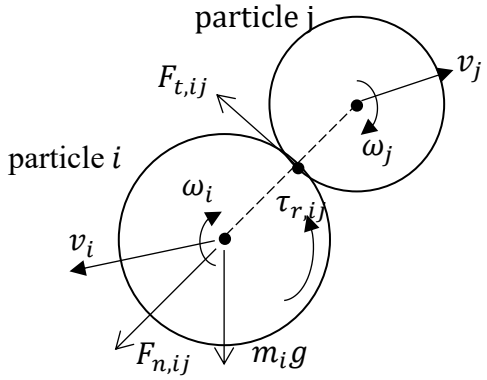

Figure 3-1. Contact forces between particle i and particle j.

$$F_{n,ij} = -\frac{4}{3}E^*\sqrt{R^*}\delta_{n,ij}{}^{\frac{3}{2}} - \frac{\ln e_{i,j}}{\sqrt{ln^2 e_{i,j}+\pi^2}}\left(\frac{20}{3}E^* m^* \sqrt{R^*\delta_{n,ij}}\right)^{\frac{1}{2}} v_{n,ij} \tag{3-1}$$

$$F_{t,ij} = min\left[-\mu_{s,ij}F_{n,ij}\,, -8G^*\delta_{t,ij}\sqrt{R^*\delta_n} - \frac{\ln e_{i,j}}{\sqrt{ln^2 e_{i,j}+\pi^2}}\left(\frac{80}{3}G^* m^* \sqrt{R^*\delta_{n,ij}}\right)^{\frac{1}{2}} v_{t,ij}\right] \tag{3-2}$$

where

$\delta_{n,ij}$, and $\delta_{t,ij}$ = normal and tangential contact overlaps, respectively;

$\mu_{s,ij}$ = coefficient of static friction between particles i and j;

$e_{i,j}$ = coefficient of restitution between particles i and j;

$v_{n,ij}$ and $v_{t,ij}$ = relative normal velocity and tangential velocity, respectively;

E^* = equivalent Young's modulus, defined as:

$$E^* = \left[\frac{(1-\upsilon_i{}^2)}{E_i} + \frac{(1-\upsilon_j{}^2)}{E_j}\right]^{-1} \tag{3-3}$$

G^*= equivalent shear modulus, defined as:

$$G^* = \left[\frac{1}{G_i} + \frac{1}{G_j}\right]^{-1} \tag{3-4}$$

R^* = equivalent radius, defined as:

$$R^* = \left[\frac{1}{R_i} + \frac{1}{R_j}\right]^{-1} \tag{3-5}$$

m^* = equivalent mass, defined as:

$$m^* = \left[\frac{1}{m_i} + \frac{1}{m_j}\right]^{-1}. \tag{3-6}$$

The terms E, υ, G, R, and m, with subscripts i and j corresponds to the Young's modulus, Poisson's ratio, shear modulus, radius, and mass of particles i and j, respectively. For simulations in which rolling friction is important, this is accounted for by applying a torque to the contacting surfaces given by:

$$\tau_{r,ij} = -\mu_{r,ij} F_{n,ij} R_i \frac{\omega_i}{|\omega_i|} \tag{3-7}$$

where $\mu_{r,ij}$ is the rolling friction coefficient between particle i and particle j; and ω_i is the angular velocity of particle i.

Contact parameters influence the behavior of bulk material as it affects the contact forces between particles. The coefficient of restitution directly affects the normal and tangential forces between particles, and indirectly affects the torque in the contacting surfaces through the normal force. The coefficient of static friction affects the tangential force between particles, while the coefficient of rolling friction affects the torque between contacting surfaces.

The time step used in integration must be sufficiently small to prevent excessive overlaps. The suitable time step is usually taken as a fraction of Rayleigh time step (T_R) given by the equation:

$$T_R = \frac{\pi \mathrm{R}\sqrt{\rho/G}}{0.01631\upsilon + 0.8766} \tag{3-8}$$

where R is the particle radius; ρ is the particle density; G is the shear modulus; and υ is the Poisson's ratio. The normal range used is 10% to 40% of the Rayleigh time step (DEM Solutions Ltd., 2017).

3.2.3 Bulk density of wheat size fractions

The bulk density of each wheat size fraction was determined using a test setup similar to a Winchester bushel test. However, a smaller hopper (stainless steel funnel) and a smaller brass test cup was used (Figure 3-2). About 325 g of wheat was prepared for each test and placed in a 250 ml glass beaker (90 mm diameter, 120 mm height). Wheat sample was poured into the funnel with the outlet cover closed. Once the grain settled, the outlet cover was opened to allow the grain to flow out of the funnel. The test cup below the funnel was filled with grain and was allowed to overflow. Afterwards, a wooden striker was used to level off the grain in the test cup. The mass of the grain remained in the test cup was determined, and the bulk density was calculated by dividing the grain mass with the volume of the test cup (275.8 cm^3). This test was replicated 10 times for each size fraction.

The usual practice in modeling particles of bulk material is to use the average size and size distribution of the particles. However, bulk materials are composed of varying shapes and sizes of particles. It is the reason that the author separated the wheat sample into three size fractions and simulated it using DEM.

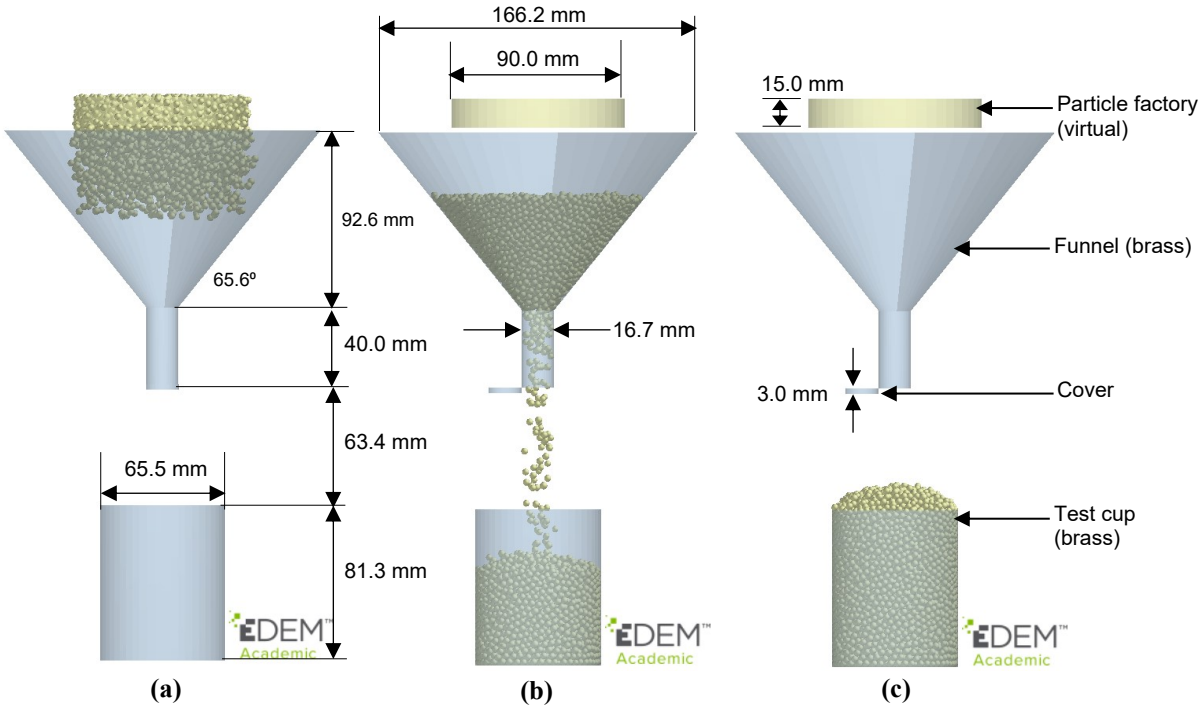

Figure 3-2. Setup for bulk density determination: (a) particle generation, (b) filling the cup, and (c) bulk density determination.

3.2.4 Simulated bulk density

The lab-scale bulk density test (Figure 3-2) was modeled using EDEM v2018.1 software (DEM Solutions Ltd., 2017) for each size fraction of wheat. To mimic the filling of the funnel, a virtual particle factory (a cylinder with diameter of 90 mm, and height of 15 mm) was created in EDEM to generate particles at a rate of 1.0 kg/s until target mass of 0.325 kg is reached. Particle generation was set to random orientation and position and fixed zero linear and angular velocities. Filling the funnel and allowing the particles to settle took 0.6 s in the experiment.

Afterward, the outlet cover below the funnel was rotated to allow grain flow into the cup. The cover was given a linear rotation with initial velocity of 7.85 rad/s and rotated 180 degrees to fully open the funnel in about 0.4 s. Once the funnel was emptied and the particles settled in the cup, the mass of particles inside the cup was determined. A cylindrical bin which coincides with the cup was created in EDEM Analysis to determine the bulk density of wheat, neglecting all the particles outside the cup. EDEM calculates the bulk density of wheat by determining the mass of the particles in the bin and dividing this mass to the volume of the bin, which is equivalent to the internal volume of the cup (275.8 cm^3).

The material properties for bulk material and equipment material used in the DEM model are summarized in Table 3-1. The EDEM solid density input for wheat should be the average kernel apparent density described by Chang (1988), and it includes the pore spaces inside the kernel. The pycnometer reading excludes the volume of pore spaces inside the individual kernels that are accessible to helium gas. To determine the kernel apparent density, the individual kernels should first be coated with paraffin prior to pycnometer measurements. In the study of Chang (1988), the kernel apparent density for wheat was 0.971 times the pycnometer reading of kernels that were not coated individually with paraffin. This relationship was used to approximate the kernel apparent density from the pycnometer-measured density (without paraffin coating) and used as input for solid density in the simulation. Other material properties for wheat and surface are based on published experimental values for wheat (at 10-12% moisture, wet basis) and brass (or steel), respectively. Published values of contact parameters used in DEM for wheat-to-wheat and wheat-to-surface are summarized in Table 3-2.

The contact model describes how elements (particle and geometry) behave when they contact each other. For both particle-to-particle and particle-to-geometry interactions, the Hertz-

Mindlin no slip contact model was used. The domain of simulation was set to auto-update from the geometry to create the smallest domain possible, producing the least possible simulation time. Gravity along z-axis of -9.81 m/s^2 was also added in the model.

Table 3-1. Material properties used in DEM simulation.

Material properties	Bulk material (wheat)	Equipment material (surface)
Poisson's ratio	0.22 [a]	0.25 [b]
Solids density (kg m^{-3})	1373	8560 [b]
Shear modulus (MPa)	22.4 [a]	37000 [b]

[a]Molenda and Horabik (2005)
[b]Mordfin (2002)

Table 3-2. Published interaction properties for wheat.

Symbol	Contact Parameters	Values
fr_{ww}	wheat-wheat coefficient of rolling friction	0.00 - 0.10[a]
fr_{ws}	wheat-surface coefficient of rolling friction	0.17[b]
fs_{ww}	wheat-wheat coefficient of static friction	0.14 - 0.40[a]
fs_{ws}	wheat-surface coefficient of static friction	0.15 - 0.27[c]
e_{ww}	wheat-wheat coefficient of restitution	0.10 - 0.90[a]
e_{ws}	wheat-surface coefficient of restitution	0.33[b]

[a]Liu and Chen (2017)
[b]Patwa (2014)
[c]Thompson and Ross (1983), Molenda and Horabik (2005), Moya et al. (2006)

For the time step in EDEM, Euler time integration was selected and a fixed time step of 20% Rayleigh time was chosen to ensure that particles will not behave erratically. For the simulation time, the total time was set at 18 seconds to allow the particles to settle upon dropping into and overflowing the cup. For the simulator grid, the grid cell was set to 2.5 times the minimum particle radius in the simulation ($2.5R_{min}$) to ensure stability.

3.2.5 Particle models

Four sets of sphere-clumps were used to model wheat kernels in each size fraction: 5-sphere pseudo-ellipsoid with different aspect ratios, 5-sphere pseudo-ellipsoid with the same aspect ratios, 7-sphere pseudo-ellipsoid, and particle models from Automatic Sphere-clump Generator (ASG) software (Cogency CC, Cape Town, South Africa), which automatically

generates a sphere-clump from a 3D image of a wheat particle. The number of spheres used in ASG-generated particles ranged between 27 and 30 spheres. The particle models used and the representative wheat kernel in each size fraction are shown in Table 3-3. For all particle models, we matched the calculated particle mass, in EDEM to the corresponding measured average kernel mass in each size fraction. The aspect ratio of each wheat size fraction was also matched in the simulation, except for set 2.

Table 3-3. Particle models for wheat size fractions used in DEM simulations.

Particle Models	Large	Medium	Small
Set 1 5-sphere pseudo-ellipsoid aspect ratio: 2.0, 2.2, 2.4			
Set 2 5-sphere pseudo-ellipsoid aspect ratio: 2.0, 2.0, 2.0	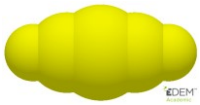		
Set 3 7-sphere pseudo-ellipsoid aspect ratio: 2.0, 2.2, 2.4	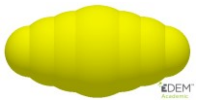		
Set 4 ASG generated particles aspect ratio: 2.0, 2.2, 2.4		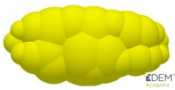	
Representative wheat kernel	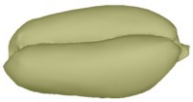		
Particle Mass	0.035 g	0.024 g	0.016 g

For sets 1 and 3, the average major and minor diameters in each size fraction were based on the average GrainScan-measured values of 200 kernels from three varieties of hard red winter wheat (Table 3-4). These diameters were used to create ellipses in CAD and filled with either five or seven circles like what Liu and Chen (2017) did. Since wheat particles are not exactly ellipsoidal, the computed mass of the particle model is usually higher than kernel mass. In order

to match the kernel mass, the radii of the interior spheres in the 5-sphere (set 1) and 7-sphere (set 3) models were adjusted. However, the radius of the middle and end sub-spheres were not adjusted so that the aspect ratio of the particle model remained the same. For set 2, the kernel mass in each size fraction was matched but the aspect ratios of all three size fractions were made equal to 2.0.

Table 3-4. Size characterization of the three size fractions of wheat.

Size fraction	Major Diameter (D) mm	Minor Diameter (d) mm	Aspect Ratio (D/d)
Large	6.12	3.05	2.0
Medium	5.84	2.68	2.2
Small	5.52	2.32	2.4

Set 4 was created for more accurate shape representation. Representative kernels from each size fraction were first selected and scanned using X-Ray microtomography (Bruker, model Skyscan 1072) to generate 3D digitized images. The 3D scanned images were processed using MeshMixer™ v3.5 (Autodesk Inc., San Rafael CA, USA) software to produce a 3D meshed shape. ASG was employed to generate the sphere-clump models of wheat kernels. This software uses an algorithm that involves sphere detection and sphere optimization (Li et al., 2017). The sphere-clump method starts by detecting candidate spheres and then refines the solution using non-linear least squares optimization. The sphere-clump generated can be characterized quantitatively using two parameters: volume error, and EIT error. The volume error shows the percentage error between the mesh volume and clump volume, while the EIT error shows the percentage error of mass distribution along the principal axes. The maximum number of spheres used in ASG-generated particles was set to 30 because of DEM computational cost constraints. The ASG-generated particles for small, medium and large particles were 28, 27, and 30, respectively. Volume errors ranged between 1.1% and 3.8%, while EIT errors ranged between 1.2% and 5.2%.

Appendix A shows the different sets of particles used in detail. The radius and coordinates of the spheres used for each sphere-clump were provided. In addition, EDEM computed mass and volume, as well as a picture of each sphere-clump, were also included for reference.

Each particle model was used for determining DEM-simulated bulk density based on the lower limits of the contact parameters to ensure that problems will not happen during the simulation. For instance, higher static friction and rolling friction caused clogging in the funnel outlet in the preliminary runs. Results of these simulations were used to evaluate the effect of the particle shape. The best particle model to represent wheat particles was chosen to evaluate the effect of the contact parameters. The contact parameters were also calibrated using the chosen particle model.

3.2.6 Particle shape

Shape is an infinitely variable parameter and rendering an exhaustive investigation of all particle shapes is infeasible (Roth and Jaeger, 2016). Petingco et al. (2018) conducted experiments to determine the influence of particle shapes, such as sphericity, flatness, and elongation, on packing ratio and compressibility of wheat. The three shape factors had strong linear relationship with packing ratio (or bulk density), with the elongation giving the highest value ($R^2 = 0.91$). In this study, we assumed that among the regular shapes, wheat particles closely resemble the shape of an ellipsoid. Single-sphere particle was not used in the simulation because unlike ellipsoids, spherical particles can only have one orientation and will not be able to mimic the bulk density results in the experiments without changing the rolling friction coefficients in each size fraction to compensate for the difference in shape. With this, we narrowed down the shape parameters and only considered aspect ratio which is like the

elongation. In addition, the number of spheres can also be increased to create the ellipsoidal particles. However, by increasing the number of spheres, the geometrical smoothness of the surface is improved. This geometrical smoothness is similar to the geometric friction mentioned in Roth and Jaeger (2016) which were present in particles represented by bonded spheres with corrugated surfaces, and to the geometric friction in Irazabal et al. (2017) which were observed in particles having undesired cavities between overlapping spheres. We also considered the effect of using a more defined shape of wheat rather than assuming that is of the shape of an ellipsoid.

3.2.6.1 Aspect ratio

The effect of kernel's aspect ratio on wheat bulk density was studied using two sets of 5-sphere pseudo-ellipsoidal particles (sets 1 and 2). Two sets of simulations were conducted in order to determine the effect of aspect ratio on DEM- simulated bulk density. Set 2 involved using the same aspect ratio (2.0) for the three size fraction, while Set 1 involved using the actual aspect ratios (2.0, 2.2, 2.4 for large, medium, and small size fractions, respectively) of wheat kernels.

In set 2, in order to achieve a constant aspect ratio of 2.0 for the three size fractions, the particle models used in medium and small size fractions were downscaled from that of the large size fraction in order to match the corresponding particle mass of medium and small wheat size fractions, respectively. This was done by trial and error. The sphere's radius and position for medium and small pseudo-ellipsoidal particles were found to be 0.89 and 0.76 smaller than that of the large pseudo-ellipsoidal particles, respectively. The EDEM-computed particle mass of the medium and small particles were within 5% error of the actual kernel mass.

In set 1, the actual aspect ratios of the three wheat size fractions were matched in the three pseudo-ellipsoidal particles. The EDEM-computed particle mass of the medium and small particles were within 5% error of the actual kernel mass.

The simulated bulk densities of using either set 1 or set 2 particles were compared to the experimental results.

3.2.6.2 Smoothness

Increasing the number of spheres to generate the pseudo-ellipsoidal particles increases the smoothness of the surface. In fact, using an infinite number of spheres will make the sphere-clump of the shape of a perfect ellipsoid. However, increasing the number of spheres will greatly increase the computational cost. In the study by Markauskas et al. (2010), the use of three sub-spheres for an ellipsoidal particle increased the CPU time by a factor of 3.3, while in the case of 17 sub-spheres, the increase of the CPU time was by a factor of 22 when both compared to the case of single-sphere particles.

To determine the effect of geometrical smoothness of the particles on bulk density, results of the simulations using 5-sphere (set 1) and 7-sphere (set 3) pseudo-ellipsoidal particles were compared to that of the experiments.

3.2.6.3 Number of spheres

The results of the simulation of the 5-sphere (set 1), 7-sphere (set 3) and ASG-generated (set 4) particle models were all compared to that of the experiments. In this case, we want to know if it is practical to use a more defined shape and increasing further the number of spheres.

3.2.7 Contact parameters

Upon determining the most practical and appropriate particle model to be used in DEM simulations of wheat particles, the effect of contact parameters on simulated bulk density was

determined. There were six contact parameters considered in the simulations. Calibration of these contact parameters is still necessary to account for the shape discrepancy of the particles used in simulation and actual wheat particles. In order to reduce the number of factors to a critical few (before calibration) that had greatest influence on the response, Plackett-Burman design (Plackett and Burman, 1946) was implemented. MiniTab® 17.0 (Minitab Statistical Software, 2010) was used to design the test, in which the six contact parameters were considered as factors and bulk density as the response. All factors had two levels, coding as -1 and +1, for low and high levels, respectively (Table 3-5). The design estimated the linear main effects for all factors. However, interaction factors were not estimated in this design. The design has 12 runs with 80% chance of detecting effects of 1.68 standard deviations or more. The low and high values were based on published values, except that some of the high values were adjusted based on preliminary runs. For example, the high values for rolling friction coefficients and static friction coefficients were limited to 0.10 and 0.40, respectively, to ensure that clogging of the funnel will not occur during simulation. The high value for coefficient of restitution was adjusted to 0.60 because this value is more realistic than 0.90.

Table 3-5. Factors for the Plackett-Burman design.

Factors	Low Level (-1)	High Level (+1)
fr_{ww}	0.00	0.10
fr_{ws}	0.02	0.10
fs_{ww}	0.10	0.40
fs_{ws}	0.17	0.40
e_{ww}	0.30	0.60
e_{ws}	0.30	0.60

The screening design of Minitab 17.0 (Plackett-Burman) identified the critical factors using a Pareto chart of standardized effects at 0.1 level of significance. After reducing the number of contact parameters to the critical few, a modeling design was created by MiniTab 17.0

to create a predictive model for the bulk density. The factor (contact parameters) levels in the modeling design were set closer together than in the screening design to increase the chances of identifying optimal settings for the critical factors. The goal of the modeling design is to construct a model that describes the relationship between the bulk density and critical factors. If the model is adequate, it will be used to find optimal settings for the factors. The design estimated all linear main effects and two-way interactions. If a curvature is detected in the model, additional runs will be added to fit a quadratic model. The optimum settings of the critical factors were determined using the best fit model, and then validation runs were conducted of simulated bulk density for the three size fractions of wheat.

3.3 Results and discussion

3.3.1 Effect of particle shape on simulated bulk density

3.3.1.1 Aspect ratio

Simulated bulk density is affected by the shape of the particles in the model. Table 3-6, shows the simulated bulk density of the three size fractions of wheat, which were modeled using 5-sphere ellipsoidal particles of similar shape (aspect ratio of 2.0). On the other hand, Table 3-7 shows simulated results with the size fractions modeled using 5-sphere ellipsoidal particles of different aspect ratios. Results showed that the bulk density was affected by the aspect ratio of particles showing a decreasing trend with increase in aspect ratio of particles. A similar trend of decreasing bulk density with increasing aspect ratio was also reported by Bhattacharya (2013) for rice bulk density. In a similar experiment conducted by Petingco et al. (2018), the packing ratio (called packing density in some literature) of wheat increased with lower values of elongation shape factor (length /thickness) of kernels. Lower elongation shape factor suggests lower aspect ratio (length/width), and higher packing ratio suggests higher bulk density. The

results of the simulations in this study matched the trend of this experiment that particles with higher aspect ratio tend to have lower bulk density. Moreover, in the DEM simulation conducted by Zhou et al. (2011), the relationship between packing fraction and aspect ratios of ellipsoids gave an M-shaped curve, with 2 peaks of packing fraction at aspect ratio of 0.6 and 1.8. The packing fraction then followed a downward trend for aspect ratios between 1.8 to 7.0, which is also observed in the DEM simulation of this study for particles with aspect ratios between 2.0 and 2.4.

Table 3-6. Simulated bulk density of three size fractions of the same shape.

Size	Number of spheres	D mm	d mm	D/d	Mass g	Bulk Density kg m^{-3}
Large	5	6.12	3.05	2.0	0.0346	869.9
Medium	5	5.45	2.71	2.0	0.0244	869.5
Small	5	4.65	2.32	2.0	0.0152	869.2

Table 3-7. Simulated bulk density of three size fractions having different shapes.

Size	Number of spheres	D mm	d mm	D/d	Mass g	Bulk Density kg m^{-3}
Large	5	6.12	3.05	2.0	0.0346	869.9
Medium	5	5.84	2.68	2.2	0.0246	847.7
Small	5	5.52	2.32	2.4	0.0160	818.3

3.3.1.2 Smoothness

The 7-sphere ellipsoidal particles had higher simulated bulk density than 5-sphere pseudo-ellipsoidal particles (Figure 3-3). This can be explained by increased smoothness of the particle surface as a result of increasing the number of spheres from five to seven. Using larger number of spheres for the pseudo-ellipsoidal particles decreased the corrugated surfaces and improved the packing of particles by having fewer void spaces with contacting particle surfaces. A larger increase in bulk density occurred when the 5-sphere model was changed to a 7-sphere model for particles having larger aspect ratios (1.9% for aspect ratio of 2.0 and 2.8% for aspect ratio of 2.4) because of greater improvement in particle smoothness (less corrugated surface).

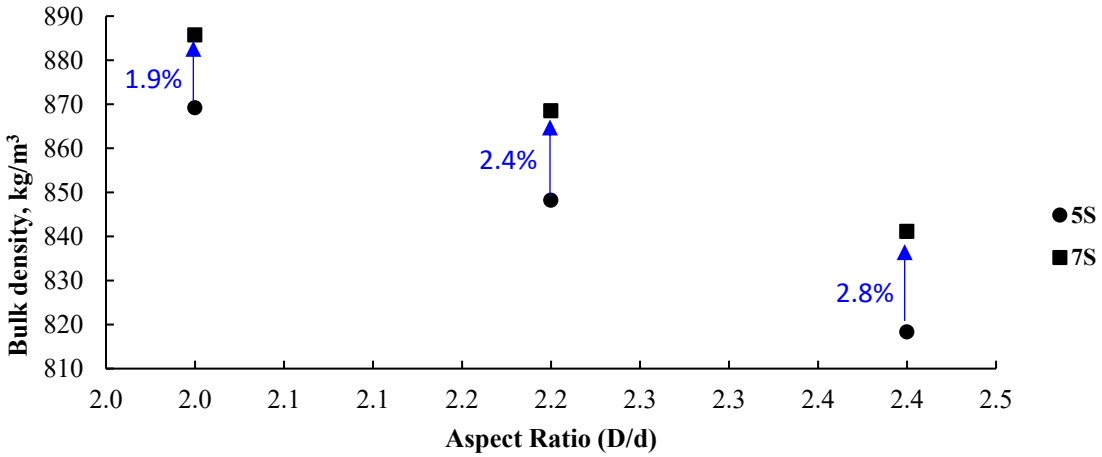

Figure 3-3. Increase in bulk density from 5-sphere (5S) to 7-sphere (7S) at different aspect ratios.

3.3.1.3 Number of spheres in particle models

The simulated bulk densities using different particle models are shown in Table 3-8. When compared with experimental results, the 5-sphere and 7-sphere pseudo-ellipsoidal models showed a similar decreasing trend with increasing aspect ratio that can be attributed to accurately capturing the aspect ratio of wheat particles in the three size fractions. However, the ASG-generated particles that used about 30 spheres to better represent the shape of wheat particles did not show this experimentally observed trend for bulk density. In the study conducted by Chung and Ooi (2006), very accurate representation of corn kernels was not necessary for the prediction of kernels under compression. They also pointed out that capturing the key linear dimensions of a particle is adequate to produce satisfactory predictions. In the case of wheat kernels, capturing the aspect ratio seemed to be adequate in simulating the bulk density of the three size fractions. Moreover, Price et al. (2007) explored the effect of the number of spheres in the sphere clump model and the extent to which realistic trajectories of diamond particles can be reproduced in DEM simulations and reported that improved shape representation by using many spheres did

not necessarily produce better simulation accuracy, unless the interacting particles exhibit highly irregular mass distributions.

Table 3-8. Effect of the number of spheres in simulated bulk density of wheat size fractions.

Size	Bulk Density, kg m^{-3}			
	5-sphere	7-sphere	ASG	Experiment
Large	869.2	885.3	863.4	826.1
Medium	847.7	868.5	860.6	798.1
Small	818.3	841.1	869.3	778.5

In simulating the behavior of wheat particles in EDEM, the 5-sphere pseudo-ellipsoidal particles seemed to be the best choice among the three particle models since it has the same decreasing bulk density trend as the experiment. Although the 7-sphere particles showed a similar decreasing trend, it will have higher computational cost than the 5-sphere model. In addition, the difference in bulk density values between the 5-sphere model and that of the experiment was much lower than with 7-sphere. Thus, higher friction coefficients would be required during calibration for the 7-sphere model to match the bulk density in experiments. Such artificially high friction coefficients will cause problems in subsequent DEM simulations such as clogging and an unrealistic angle of heap.

3.3.2 Effect of contact parameters on simulated bulk density

In determining the effects of contact parameters, the 5-sphere particle for large size fraction of wheat was used in the DEM simulations. Plackett-Burman design was used to determine which of the six contact parameters had the most significant effect on simulated bulk density. Table 3-9 shows the 12 simulations, design matrix, and results of the Plackett-Burman analysis. The main effects plots (Figure 3-4) show that four of the contact parameters had significant effects on bulk density, with fr_{ww} having the highest effect, followed by fs_{ww}, e_{ww},

and fs_{ws}. Increasing the values of fr_{ww} , fs_{ww}, and fs_{ws} resulted in a decrease in bulk density, while increasing e_{ww} resulted in a slight increase in bulk density. The effect of wheat-wheat (ww) contact parameters was greater than the effect of wheat-surface (ws) contact parameters maybe because the total contacting surface between the cup surface and wheat is much lower than the total contacting surface between individual particles.

Table 3-9. Design matrix and results of Plackett-Burman design.

StdOrder	RunOrder	fr_{ww}	fr_{ws}	fs_{ww}	fs_{ws}	e_{ww}	e_{ws}	Bulk Density (kg/ m^3)	Angle of Heap (degrees)	Time of filling (s)
7	1	-1	+1	+1	+1	-1	+1	805.7	26.5	14.6
12	2	-1	-1	-1	-1	-1	-1	870.2	38.9	12.2
11	3	-1	+1	-1	-1	-1	+1	868.7	23.4	9.8
1	4	+1	-1	+1	-1	-1	-1	773.4	23.9	16.8
8	5	-1	-1	+1	+1	+1	-1	818.5	24.8	16.4
2	6	+1	+1	-1	+1	-1	-1	830.2	26.7	11.0
10	7	+1	-1	-1	-1	+1	+1	844.1	36.9	14.9
4	8	+1	-1	+1	+1	-1	+1	769.1	40.7	12.2
5	9	+1	+1	-1	+1	+1	-1	837.2	28.6	9.6
6	10	+1	+1	+1	-1	+1	+1	778.9	21.7	17.0
9	11	-1	-1	-1	+1	+1	+1	872.3	31.1	14.8
3	12	-1	+1	+1	-1	+1	-1	820.3	22.3	10.8

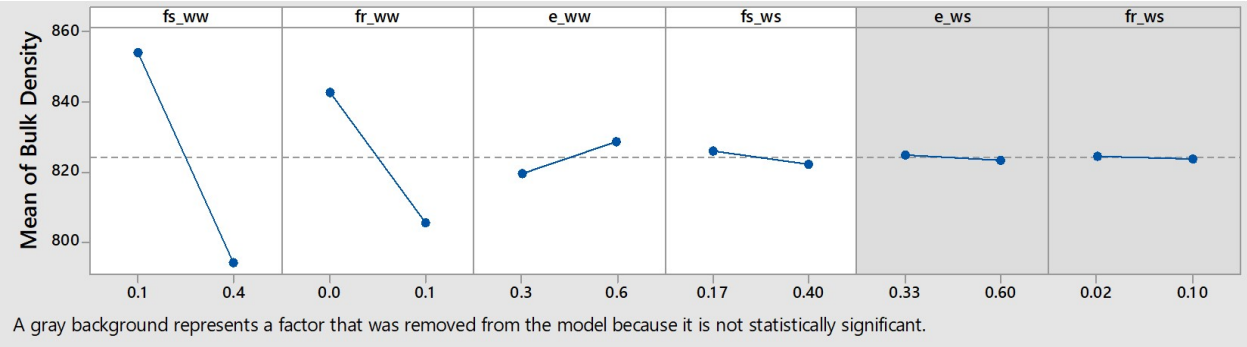

Figure 3-4. Main effects plot for bulk density showing the four significant contact parameters.

The decrease in bulk density due to increase in wheat-wheat friction coefficients can be explained by higher stability of the packing arrangement of particles. As friction coefficients increased between particles, the stability of packing increased resulting in higher angle of heap.

Most DEM studies use angle of repose tests to calibrate the contact parameters of granular materials. However, measuring the angle of heap (Figure 3-5) can be more subjective than determining the bulk density of material, which only involves mass and volume measurements. The time of filling in the simulation can be easily compared with that of the experiment; however, the simulation results were always higher than that of the experiments. In addition, the three macro-scale properties (bulk density, angle of heap, and time of filling) behaved differently with the values of contact parameters and matching the results of the simulation with that of the experiment was highly improbable. Thus, the author only focused on bulk density and how contact parameters affect this macro-scale property. Moreover, the author would like to understand the compressive behavior of wheat using DEM simulation in the future, and this study will involve bulk density changes as affected by compressive force.

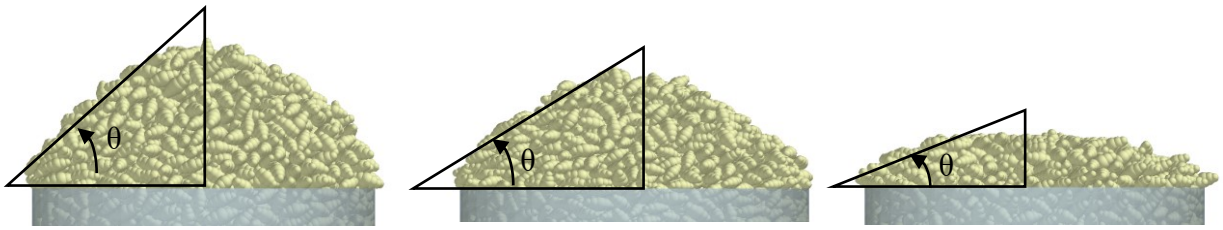

Figure 3-5. Angle of heap of selected simulation runs.

A negative correlation was observed between bulk density and angle of repose (Figure 3-6). A similar negative relationship between angle of repose and bulk density was observed by Liu (2007) with coal particles. Yan et al. (2015) and Li et al. (2017) observed that increasing the coefficient of static friction and coefficient of rolling friction in DEM simulations resulted in significant increases in the angle of repose of sand and iron ore particles, respectively. Yan et al. (2015) also observed that the coefficient of static friction had a stronger effect than the

coefficient of rolling friction and the coefficient of restitution had little influence on the angle of repose of sand. This led to higher friction coefficients producing greater heap angle and lower bulk density in simulations. This negative correlation was also observed in wheat and soybean, as the angle of repose increased and bulk density decreased with increased moisture content (Tabataefar, 2013; Kashaninejad et al., 2008).

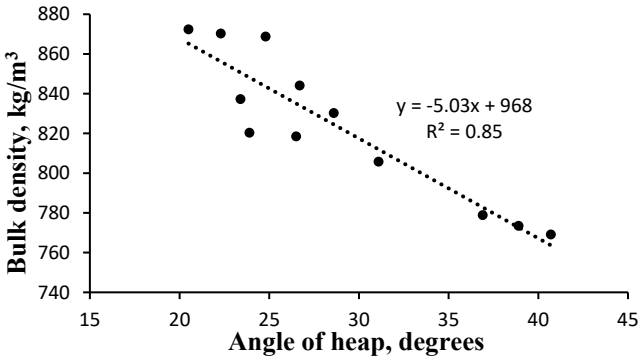

Figure 3-6. Relationship between angle of heap and bulk density.

After identifying the critical factors (fs_{ww}, fr_{ww}, e_{ww} and fs_{ws}) that affect bulk density, a modeling design consisting of 19 simulations was created in Minitab (Table 3-10). In this modeling design, the non-critical factors e_{ws} and fr_{ws} were fixed at 0.33 and 0.02, respectively. Any values of these two factors within the range used in Table 3-5 will do since the data showed that these factors were not critical. The first 19 simulations were designed to estimate the linear main effects and two-way interactions of the four contact parameters on bulk density. However, curvature in the data were detected, in which the average response at the center points is lower than the average response at the corner points (Figure 3-7), indicating that a linear model cannot adequately describe the relationship between the bulk density and the contact parameters. Thus, an additional 11 simulations were added in the design to model the curvature and fit a quadratic model.

Table 3-10. Modeling design matrix and results using the four contact parameters.

StdOrder	RunOrder	CenterPt	Blocks	fs_ww	fr_ww	e_ww	fs_ws	Bulk density (kg/m^3)	Time of filling (s)
11	1	1	1	0.170	0.100	0.200	0.400	809.6	13.2
10	2	1	1	0.400	0.010	0.200	0.400	800.5	15.0
1	3	1	1	0.170	0.010	0.200	0.170	841.6	11.2
4	4	1	1	0.400	0.100	0.200	0.170	769.0	19.2*
19	5	0	1	0.285	0.055	0.350	0.285	795.1	13.8
18	6	0	1	0.285	0.055	0.350	0.285	795.9	13.6
14	7	1	1	0.400	0.010	0.500	0.400	808.3	15.2
9	8	1	1	0.170	0.010	0.200	0.400	838.0	12.2
8	9	1	1	0.400	0.100	0.500	0.170	778.4	19.4*
7	10	1	1	0.170	0.100	0.500	0.170	819.3	12.0
2	11	1	1	0.400	0.010	0.200	0.170	802.2	14.0
6	12	1	1	0.400	0.010	0.500	0.170	811.6	13.8
16	13	1	1	0.400	0.100	0.500	0.400	771.7	23.0*
15	14	1	1	0.170	0.100	0.500	0.400	815.3	12.8
17	15	0	1	0.285	0.055	0.350	0.285	797.5	14.0
3	16	1	1	0.170	0.100	0.200	0.170	815.3	12.0
12	17	1	1	0.400	0.100	0.200	0.400	762.2	23.8*
5	18	1	1	0.170	0.010	0.500	0.170	848.9	10.8
13	19	1	1	0.170	0.010	0.500	0.400	843.9	12.2
24	20	-1	2	0.285	0.055	0.200	0.285	793.2	16.1
30	21	0	2	0.285	0.055	0.350	0.285	796.3	13.8
27	22	-1	2	0.285	0.055	0.350	0.400	794.6	14.0
23	23	-1	2	0.285	0.100	0.350	0.285	785.5	15.4
20	24	-1	2	0.170	0.055	0.350	0.285	822.3	12.0
29	25	0	2	0.285	0.055	0.350	0.285	795.6	13.6
21	26	-1	2	0.400	0.055	0.350	0.285	781.2	14.8
25	27	-1	2	0.285	0.055	0.500	0.285	801.4	13.8
28	28	0	2	0.285	0.055	0.350	0.285	796.6	13.6
26	29	-1	2	0.285	0.055	0.350	0.170	799.4	13.4
22	30	-1	2	0.285	0.010	0.350	0.285	816.9	13.2

**A little clogging occurred at these runs*

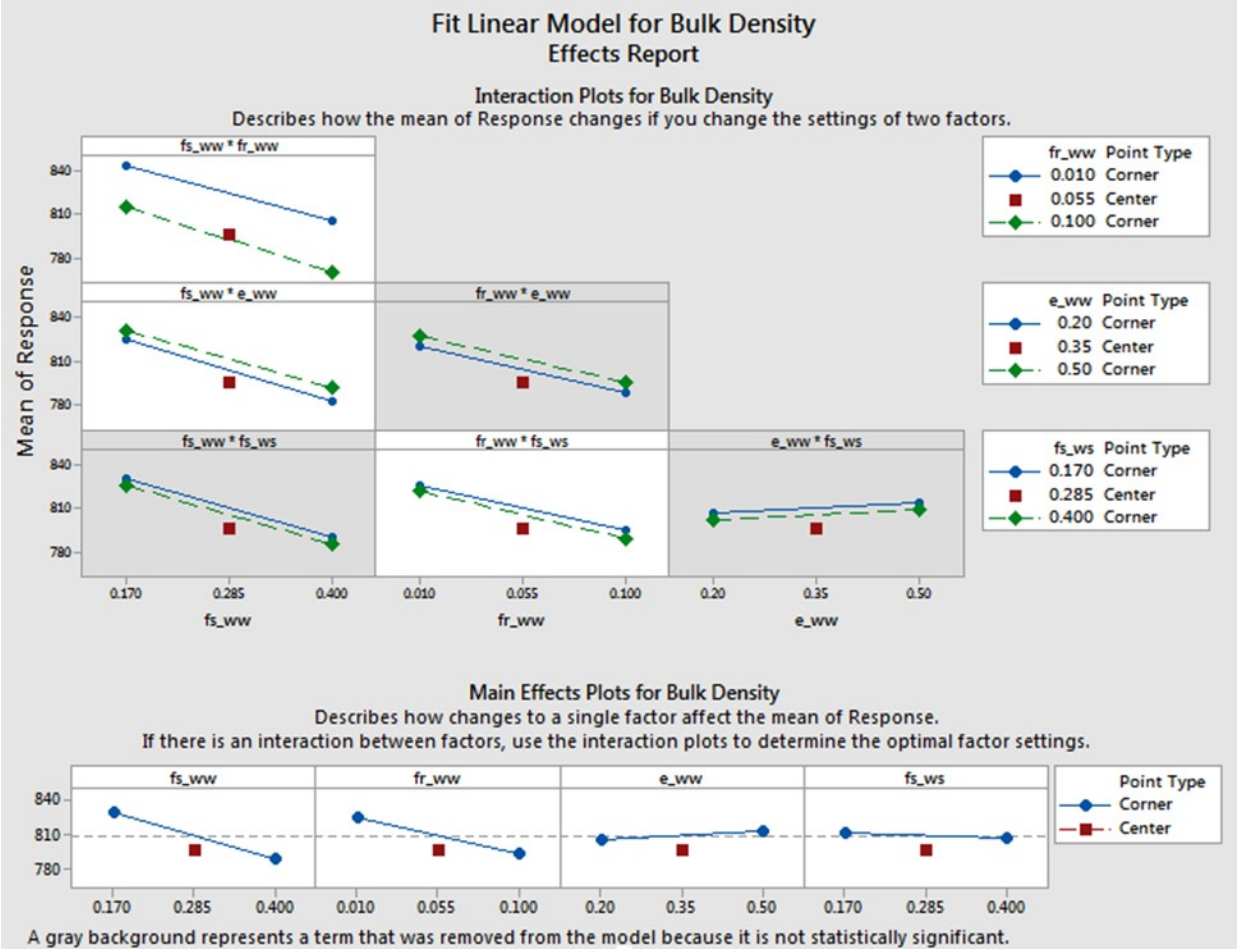

Figure 3-7. Main effects plot for bulk density showing evidence of curvature in the data for 19 runs.

A Pareto chart of standardized effects (Figure 3-8) shows which among the main effects and interaction effects of contact parameters have more influence on bulk density. The contact parameter fs_{ww} had the highest contribution to bulk density, followed by fr_{ww}, e_{ww}, and fs_{ws}. In addition to the main effects of contact parameters, some interaction effects had significant influence on bulk density at the 0.1 level of significance. Among the interaction effects, the $fs_{ww} \times fr_{ww}$ interaction had the greatest influence, followed by $fs_{ww} \times e_{ww}$, and $fr_{ww} \times fs_{ws}$.

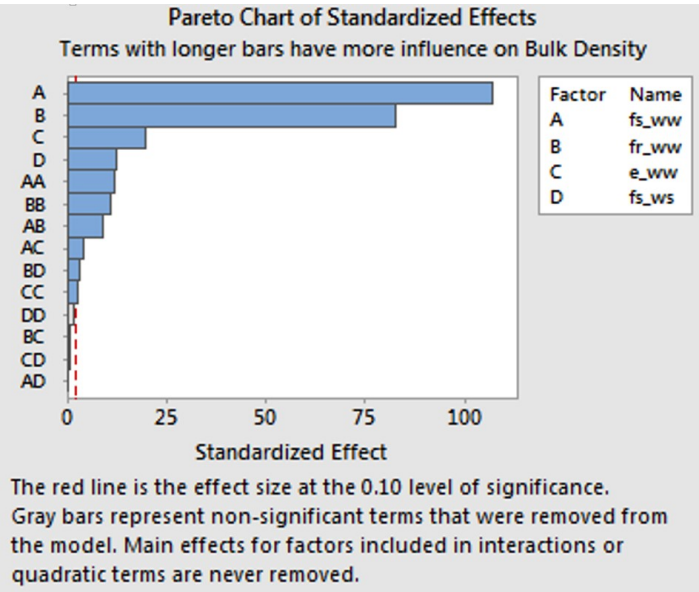

Figure 3-8. Influence of contact parameters on bulk density.

3.3.3 Optimum settings of contact parameters

The optimal settings for the four contact parameters were determined by fitting a quadratic model to the modeling design (Figure 3-9). The optimum values of these contact parameters were the result of the calibration process using the 5-sphere particle model for large size fraction of wheat (Table 3-11). Using these values for the contact parameters, bulk density was simulated in EDEM using the corresponding 5-sphere particle model in each size fraction. Results showed that the simulated bulk densities for the three size fractions were all in good agreement with that of the experiment (Table 3-12), even though calibration of the contact parameters was only done for the large size fraction. Capturing the aspect ratio in modeling the wheat size fractions using 5-sphere ellipsoidal particles eliminated any need of doing a separate calibration for the medium and small size fractions. As shown in Figure 3-10 the heap profiles (angle of heaps) were almost the same for the three size fractions, even though their bulk

densities were significantly different. This shows that the angle of repose (or heap) is not always the best macro-scale property to calibrate or fine tune the micro-properties or contact parameters.

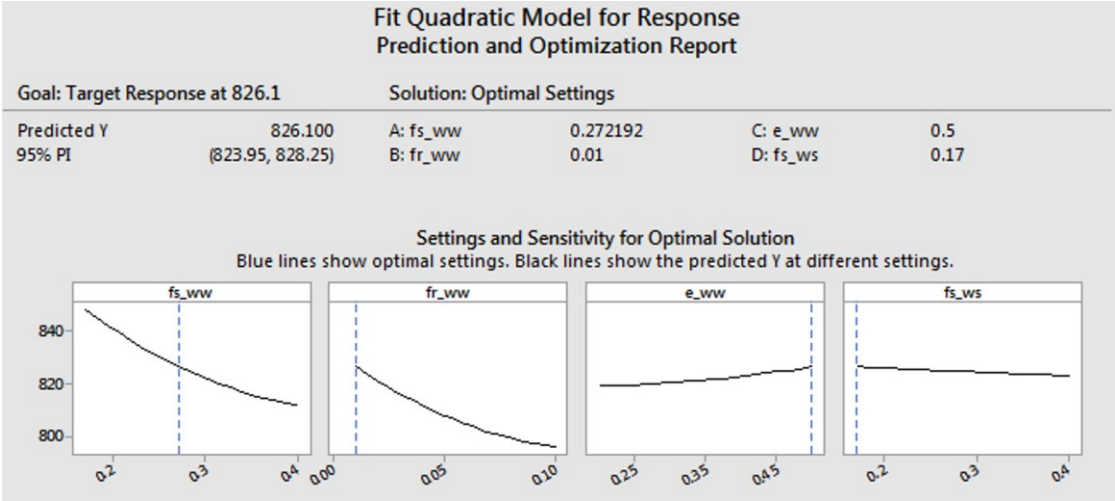

Figure 3-9. Optimal settings of contact parameters.

Table 3-11. Contact parameter values for DEM simulation of wheat bulk density.

Contact parameters	Values
fr_{ww}	0.01
fr_{ws}	0.02
fs_{ww}	0.27
fs_{ws}	0.17
e_{ww}	0.50
e_{ws}	0.33

Table 3-12. Validation of DEM model for three size fractions of wheat.

Size	Bulk Density, kg m^{-3}		
	Simulated	Experimental	% Error
Large	828.7	826.1	+0.31
Medium	806.5	798.1	+1.05
Small	775.5	778.1	-0.39

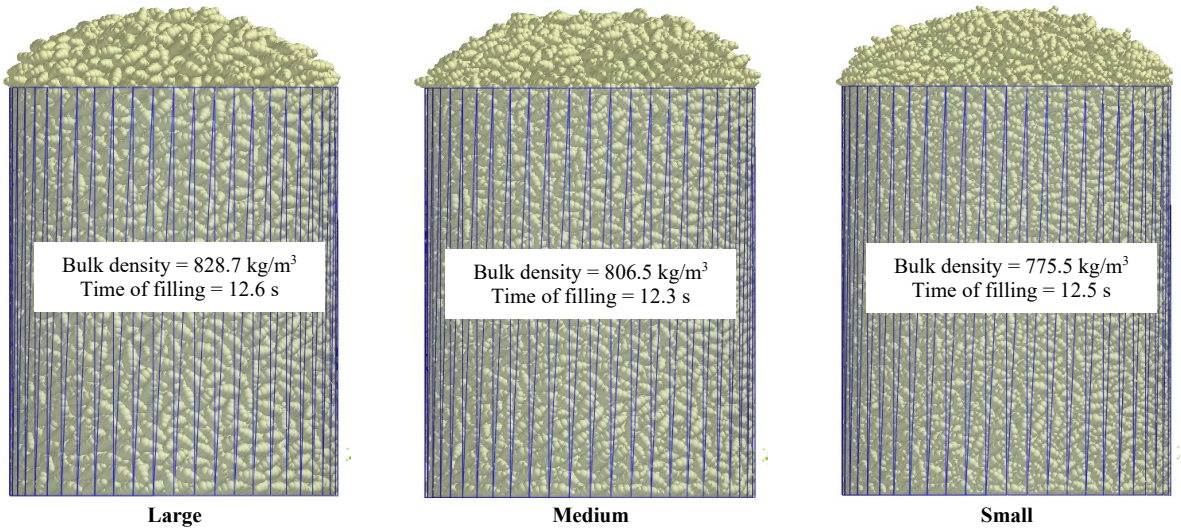

Figure 3-10. DEM output for simulation of bulk density of the three wheat size fractions.

3.4 Conclusion

In the DEM simulations, a decrease in aspect ratio and improved smoothness of particles contributed to increasing bulk density. DEM simulated bulk density of wheat using pseudo-ellipsoidal particles (5-sphere and 7-sphere) showed similar trends as the experiments with decreasing particle sizes, while ASG-generated particles did not follow the experimental trends. Thus, increasing the number of spheres for better representation of particle shape did not improve accuracy of DEM simulations for capturing bulk density changes due to particle size. Among the three particle models, the 5-sphere ellipsoidal particle model capturing the aspect ratio in each size fraction was the best option to represent wheat particles.

Regarding the contact parameters, the wheat-wheat contact parameters had stronger influence on bulk density than the wheat-surface contact parameters, with individual effects of wheat-wheat coefficient of static friction and wheat-wheat rolling friction showing the greatest influence. Increasing the wheat-wheat coefficient of static friction and the wheat-wheat rolling friction decreased the bulk density, while increasing the wheat-wheat coefficient of restitution

and wheat-surface coefficient of static friction slightly increased the bulk density. Some of the two-way interaction between these four contact parameters had significant effect on simulated bulk density, with the interaction between wheat-wheat coefficient of static friction and wheat-wheat rolling friction showing the greatest influence among the interactions.

The optimal settings of the contact parameters using 5-sphere ellipsoidal particles were determined and validation runs showed that the simulated bulk densities of the three size fractions were in good agreement with that of the experiment. This study contributes to a better understanding of the influence of particle shape and contact parameters on DEM simulated bulk density and provides a calibrated particle model for use in simulating container filling operations.

3.5 References

Bates, E. N. (1925). Estimating the quantity of grain in bins with chart reducing and the necessary computations. Misc. Circular No. 41. Washington, D.C.: USDA

Bhattacharya, K. R. (2013). Physical properties of rice. In K. R. Bhattacharya (Ed.), Rice quality: A guide to rice properties and analysis (pp. 26-60) Woodhead Publishing. doi: 10.1533/9780857092793.26

Boac, J. M., Ambrose, R. P. K., Casada, M. E., Maghirang, R. G., & Maier, D. E. (2014). Applications of discrete element method in modeling of grain postharvest operations. *Food Engineering Reviews*, 6(4), 128-149. doi:10.1007/s12393-014-9090-y

Chang, C. S., Shackelford, L. E., Lai, F. S., Martin, C. R., & Miller, B. S. (1981). Bulk properties of corn as affected by multiple-point grain spreaders. *Trans. ASAE*, 24(6), 1632-1636. doi:10.13031/2013.34504

Chang, C. S., Converse, H. H., & Martin, C. R. (1983). Bulk properties of grain as affected by self-propelled rotational type grain spreaders. *Trans. ASAE,* 26 (5): 1543-1550. doi:

10.13031/2013.34167

Cheng, X., Zhang, Q., Shi, C., & Yan, X. (2017). Model for the prediction of grain density and pressure distribution in hopper-bottom silos. *Biosystems Engineering*, 163, 159-166. doi:10.1016/j.biosystemseng.2017.09.006

Chung Y.C., & Ooi J.Y. (2006). Confined compression and rod penetration of a dense granular medium: discrete element modeling and validation. In: Wu W, Yu HS (eds) Modern trends in geomechanics. Springer, Berlin, pp 223–239

Coetzee, C. J. (2016). Calibration of the discrete element method and the effect of particle shape. *Powder Technology*, 297, 50-70. doi:10.1016/j.powtec.2016.04.003

Cundall, P. A., & Strack, O. D. (1979). A discrete element model for granular assemblies. *Geotechnique*, 29(1), 47-65.

DEM Solutions Ltd. (2017). EDEM v2018.1 Documentation. Copyright © 2017.

Favier, J., Abbaspour-Fard, M., & Kremmer, M. (2001). Modeling Nonspherical Particles Using Multisphere Discrete Elements. *Journal of Engineering Mechanics*, 127(10), 971-977.

Gao, M., Cheng, X., & Du, X. (2018). Simulation of bulk density distribution of wheat in silos by finite element analysis. *Journal of Stored Products Research*, 77, 1-8. doi:10.1016/j.jspr.2018.02.003

Horabik, J., Parafiniuk, P., & Molenda, M. (2016). Experiments and discrete element method simulations of distribution of static load of grain bedding at bottom of shallow model silo. *Biosystems Engineering*, 149, 60-71. doi:10.1016/j.biosystemseng.2016.06.012

Irazábal, J., Salazar, F., & Oñate, E. (2017). Numerical modelling of granular materials with spherical discrete particles and the bounded rolling friction model. Application to railway ballast. *Computers and Geotechnics*, 85, 220-229.

Kačianauskas R., Balevičius R., Markauskas D., & Maknickas A. (2007) Discrete Element Method in Simulation of Granular Materials. In: Eberhard P. (eds) IUTAM Symposium on Multiscale Problems in Multibody System Contacts. IUTAM Book series, vol 1. Springer, Dordrecht. https://doi.org/10.1007/978-1-4020-5981-0_7

Kashaninejad, M., Ahmadi, M., Daraei, A., & Chabra, D. (2008).Handling and frictional characteristics of soybean as a function of moisture content and variety. *Powder Tech*., 188(1), 1-8. https://doi.org/10.1016/j.powtec.2008.03.004

Li, T., Peng, Y., Zhu, Z., Zou, S., Yin, Z., & Lin, Y. (2017). Discrete element method simulations of the inter-particle contact parameters for the mono-sized iron ore particles. *Materials*, 10(5). doi:10.3390/ma10050520

Liu, C. (2007). Bulk density and angle of repose of coal (Master's thesis). University of New South Wales, Australia.

Liu, F., & Chen, J. (2017). Effect of calibration experiments on the micro-parameters of wheat required in discrete element simulations. 2017 ASABE Annual International Meeting.

Malm, J. K., & Backer, L. F. (1985). Compaction factors for six crops. *Trans. ASAE*, 28(5), 1634-1636. doi:10.13031/2013.32489

Markauskas, Kačianauskas, Džiugys, & Navakas. (2010). Investigation of adequacy of multi-sphere approximation of elliptical particles for DEM simulations. *Granular Matter*, 12(1), 107-123.

Minitab 17 Statistical Software (2010). [Computer software]. State College, PA: Minitab, Inc. (www.minitab.com)

Mordfin, L (2002). Handbook of reference data for nondestructive testing. West Conshohocken: ASTM. doi: 10.1520/DS68-EB

Moya, M., Guaita, M., Aguado, P., & Ayuga, F. (2006). Mechanical properties of granular agricultural materials, Part 2. *Trans. ASABE, 49*(2), 479-489. https://doi.org/10.13031/2013.20403

Patwa, A. (2014). Discrete element method model of the first break wheat milling process. MS thesis. Manhattan, KS: Kansas State University, Department of Grain Science and Industry.

Petingco, M. C., Casada, M. E., Maghirang, R. G., Thompson, S. A., McNeill, S. G., Montross, M. D., & Turner, A. P. (2018). Influence of kernel shape and size on the packing ratio and compressibility of hard red winter wheat. *Trans. ASABE*, 61(4), 1437-1448. doi:10.13031/trans.12648

Plackett, R.L., & Burman, J. P. (1946). The Design of Optimum Multifactorial Experiments, *Biometrika,* 33(4): 305-325.

Price, M., Murariu, V., & Morrison, G. (2007). Sphere clump generation and trajectory comparison for real particles. In: Discrete Element Methods 2007 Conference, 27--29 August, Brisbane, Australia.

Roth, L., & Jaeger, H. (2016). Optimizing packing fraction in granular media composed of overlapping spheres. *Soft Matter*, 12(4), 1107-1115.

Sarnavi H.J., Mohammadi A. N., Motlagh A.M., & Didar A. R. (2013). DEM model of wheat grains in storage considering the effect of moisture content in direct shear test. *Res J Appl Sci Eng Technol.,* 5(3):829–841

Tabatabaeefar, A. (2003). Moisture-dependent physical properties of wheat. *Intl. Agrophys., 17*(4), 207-211.

Thompson, S. A., Schwab, C. V., & Ross, I. J. (1991). Calibration of a model for packing whole grains. *Applied Engineering in Agriculture*, 7(4), 450-456. doi: 10.13031/2013.26244

Thompson, S. A., & Ross, I. J. (1983). Compressibility and frictional coefficients of wheat. *Trans. ASAE*, 26(4), 1171-1176, 1180. doi: 10.13031/2013.34099

Tsuji, Y., Tanaka, T., & Ishida. (1992). Lagrangian numerical simulation of plug flow of cohesionless particles in a horizontal pipe. *Powder Technology*, 71(3), 239-250.

USDA-GIPSA. (2009). Inspecting grain: Practical procedures for grain handlers. Washington, DC: USDA Grain Inspection, Packers and Stockyards Administration. Federal Grain Inspection Service. Retrieved from https://www.gipsa.usda.gov/fgis/publication/ref/primer.pdf.

Versavel, P. A., & Britton, M. G. (1986). Interaction of bulk wheat with bin wall configuration in model bins. *Trans. ASAE*, 29(2), 533-537.

Whan, A., Bolger, M., & Bischof, L. (2014): GrainScan - Software for analysis of grain images. v2. CSIRO. Software Collection. https://doi.org/10.4225/08/536302C43FC28

Yan, Z., Wilkinson, S., Stitt, E., & Marigo, M. (2015). Discrete element modelling (DEM) input parameters: Understanding their impact on model predictions using statistical analysis. *Computational Particle Mechanics*, 2(3), 283-299. doi:10.1007/s40571-015-0056-5

Yang, X., & Williams, D. L. (1990). Airflow resistance of grain sorghum as affected by bulk density. *Trans. ASAE*, 33(6), 1966-1970. doi:10.13031/2013.31565

Zhou, Z. Y., Zou, R. P., Yu, A. B., & Pinson, D. (2011). Dynamic simulation of the packing of ellipsoidal particles. *Industrial and Engineering Chemistry Research*, 50(16), 9787-9798

Chapter 4 - Discrete Element Method Simulation of Wheat Bulk Density as Affected by Grain Drop Height and Size Distribution

4.1 Introduction

Bulk density is an indicator of granular material compaction. It is calculated as the dry weight of material divided by its volume. The volume includes the volume of particles and the volume of the pores among solid particles.

Bulk density is an extrinsic property and is dependent on the texture of material, solid densities of particles, and particle packing. The texture of the material refers to the relative content of particles of various sizes. In wheat, the particles include different wheat kernel size fractions, dockage, and foreign material. Generally, a wheat sample with higher percentage of dockage has lower bulk density. Wheat samples composed of kernels with higher solid densities have higher bulk density. Particle packing refers to the arrangement of particles. The more packed the arrangement of kernels and other particles, the higher is the bulk density of wheat. The degree of packing depends largely on the shape of particles. Kernels with higher aspect ratio tend to have lower bulk density (Bhattacharya, 2013; Petingco et al., 2020). Smooth, rounded kernels pack more tightly than wrinkled ones (Ransom, 2017; Petingco et al., 2020).

Aside from the properties of materials mentioned above, handling practices also affect the bulk density of granular material. Bulk density of wheat in bins is affected by the manner of filling and overburden pressure. Molenda et al. (1993) showed that shower filling resulted in a higher bulk density as compared to other filling methods that produced sloping surfaces. Similar studies were done by Stephens and Foster (1978), and Chang et al. (1983) who both showed that bulk densities of wheat and sorghum were higher when bins were filled by a mechanical grain spreader than when they were filled from a spout. Higher fall height also contributed to increase

in bulk density as a result of a more packed arrangement of kernels (Yang and Williams, 1990; Versavel and Britton, 1984). Chang et al. (1983) also mentioned that when a bin is fully filled, the bulk density of grain in the bottom portion of the bin was higher than that of the grain in the top portion due to the difference in dropping height from the spreader, and the overburden pressure effect of the added grain (Thompson and Ross, 1983).

A science-based model for determining compaction factors, called WPACKING, was developed by Thompson et al. (1987) to simplify the procedure for estimating the mass of stored grain in bins. WPACKING used the differential form of Janssen's (1987) to estimate the pressure and stored grain bulk density for a given depth of grain in a bin. A mathematical expression which predicted the variation in bulk density as a function of overburden pressure and moisture content for each whole grain was developed and was of the form of:

$$D_i - D_O = a \cdot P + b \cdot P^{0.5} + c(P \cdot MC) \quad \text{(4-1)}$$

where

D_i = predicted bulk density

D_o = test weight or uncompacted bulk density

a, b, c = coefficients determined by multiple regression to model pressure-moisture-density relationship

P = pressure caused by the overbearing grain

MC = moisture content of the grain (wb).

The standard measure of bulk density in the United States is the test weight. The official procedure for determining test weight uses a standard test weight per bushel test apparatus. A dockage-free portion of a sufficient quantity of grain is allowed to discharge from a hopper and overflow to a kettle. Excess grain is removed by levelling off the top of the kettle. The test weight is determined as the ratio of the weight of the grain that fills the test cup to the volume of

the test cup and is expressed in pounds per bushel. The required distance of the hopper to the kettle (drop height) should be strictly followed, otherwise, the measured test weight is incorrect. The detailed procedure of determining test weight is outlined in FGIS Grain Inspection Handbook, Book II (USDA-FGIS, 2013).

The WPACKING model of Thompson and Ross (1987) uses the laboratory measured (standard) test weight as the uncompacted bulk density (D_o). However, the uncompacted bulk density of grain in bins is much higher than the standard test weight due to the difference in filling method and grain drop height. The particle size distribution also influenced the packing ratio (Petingco et al., 2018), thereby affecting the uncompacted bulk density of grain in bins. By using the uncompacted grain bulk density in bin to replace the standard test weight as input for D_o, the WPACKING model can be improved

The discrete element method (DEM) is an explicit numerical technique developed by Cundall and Strack (1979) for modeling the behavior of granular material. DEM is differentiated from other numerical methods, such as finite element and finite difference, with its capability of modeling the behavior of individual particles. Each particle is represented numerically and identified with its specific properties such as shape, size, material properties, and initial velocity. With this, the overall system behavior of granular material can be modeled as a result of individual particle interactions.

DEM has proven to be effective in studying numerous technological processes in agriculture, engineering, and food processing as it gives the user an insight on how bulk materials will interact with equipment over a range of operation and process conditions (Kačianauskas et al., 2007; Horabik and Molenda, 2016). However, the accuracy of the simulations depends highly on input parameters that include contact models, physical properties,

and contact parameters (or interaction properties). Physical properties include particle shape, size distribution, solids density, Poisson's ratio, and modulus of elasticity. Contact parameters include coefficient of restitution, coefficient of static friction and coefficient of rolling friction.

In any DEM simulation, particles of the granular material are modeled first. Most commercial DEM software allow the users to model the shape, size and size distribution of the particles. The simplest and most practical choice for the shape is the use of spheres due to lower computational cost. However, according to Lu et al. (2015), particle shape is one of the most important parameters to be considered in DEM simulations and has to be captured accurately for DEM to be effective as a predictive tool. For non-spherical particles, the use of clumps seems to be the most popular model amongst DEM developers. The clumps can be formed by combining two or more spheres to form one rigid particle like the shape of the particle being modeled.

Once particles are modeled, input for material physical properties and contact parameters are set in the DEM model. Published and experimentally determined values are usually used in the model otherwise, these input parameters are calibrated. In practice, contact parameters are calibrated to compensate for the difference in shape and surfaces of the particles used in the model and the real particles. In the study by Coetzee (2016), clumps comprised of different number of spheres were used to predict the anchor pull-out forces and hopper discharge. Results of his studies have shown that all three clump types, once calibrated independently, could be used for accurate predictions.

The objective of this study was to develop a DEM model to predict wheat bulk density as affected by grain drop height and size distribution. The setup for test weight per bushel test was used to determine the wheat bulk density. However, the setup was modified to have varying drop heights (5.1 cm to 163.2 cm). In the DEM simulation, two particle shapes (spherical, and pseudo-

ellipsoidal) were considered to determine how the shape of the particles in the DEM model affects the simulated wheat bulk density. For each particle shape, three different particles were used to model the three size fractions of wheat. Calibrated contact parameters were used independently for each particle model and shape for bulk density simulations. Three different particles were used to model the three size fractions that comprised a wheat sample. The percentage composition of these size fractions was varied to represent the two wheat samples having different size distributions. Bulk densities of the two wheat samples at different grain drop heights were determined numerically and were compared to experimental results.

4.2 Materials and methods

4.2.1 Wheat samples

Two wheat samples, KanMark and Garrison varieties, were cleaned by passing them through a Carter-Day dockage tester (Seedburo Equipment Co., Des Plaines, IL,USA) to remove foreign material and through a 1.63 mm × 9.53 mm (0.064 in × 3/8 in) oblong sieve to remove shrunken and broken kernels. Ten 100-g samples were set aside from each variety for size fraction analysis. Size fraction analysis was conducted by sorting the 100-g sample into three size fractions using a mechanical test sieve shaker (Ro-Tap, W.S. Tyler, Mentor, OH, USA) and a series of 200 mm (8 in) diameter sieves. The sieve sizes used were #7 (2.83 mm) and #8 (2.38 mm). This was necessary to determine the size fraction composition of the two wheat samples and use this as input in DEM modeling.

4.2.2 Laboratory experiment

Bulk density of wheat was determined using a test weight per bushel test setup. However, the set up was modified so that the filling hopper can be raised higher than the standard drop height (h) of 5.1 cm (2 in) used for filling (Figure 4-1). The hopper support columns were

replaced by longer ones to allow additional drop heights. Drop heights used were 5.1 cm, 10.2 cm, 20.4 cm, 40.8 cm, 81.6 cm, and 163.2 cm (1h, 2h, 4h, 8h, 16h, and 32h, respectively.) The falling grain stream was protected from air current disturbance with PVC pipe enclosures.

The experiment involved preparing about 1.1 kg dockage- and shrunken and broken-free work samples and following the standard method for test weight determination. The test weight per bushel apparatus was leveled and balanced. The hopper valve was closed before pouring the work sample in the hopper. The hopper was centered over the kettle. The kettle was filled by opening the hopper valve quickly. To level the grain, the kettle was struck by holding the standard wooden stroker in both hands with the flat sides in a vertical position and making a full-length zigzag motion (USDA-FGIS, 2013). The bulk density of wheat was determined by dividing the mass of the grain in the kettle by the volume of the kettle. The test was replicated three times for each drop height and variety. Analysis of variance (ANOVA) was used to determine the effects of drop height and variety on bulk density of wheat.

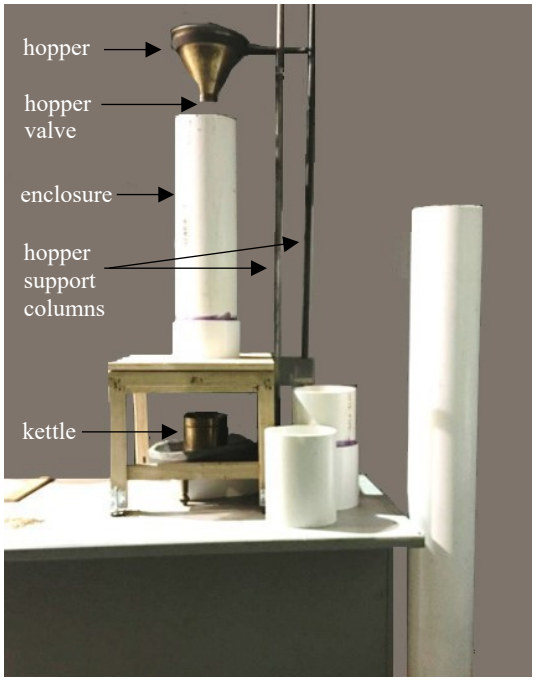

Figure 4-1. Setup for bulk density determination at different drop heights.

4.2.3 DEM simulation of bulk density determination

4.2.3.1 Particle models

The usual practice in modeling particles of bulk material is to use the average size and size distribution of the particles. However, bulk materials are composed of varying shapes and sizes of particles; thus, we separated the wheat sample into three size fractions and simulated this using EDEM v2018.1 (DEM Solutions Ltd., Edinburgh, UK).

Particles can be modeled based on shape, size, and size distribution. For DEM simulation to be effective as a predictive tool, the particles should be modeled closely to the physical shape of the wheat particles. Zhou et al. (2013) conducted a 2D DEM study that compared the effects of using irregular-shaped particle (clumps) and disc installed with coefficient of rolling resistance on the macro- and micro-mechanical behavior of granular assemblies. DEM simulation results showed that both particle models resulted in enhanced shear strength and dilatancy behavior of granular assemblies, which were attributed to the enhanced capacity of the granular assemblies to store elastic strain energy. However, the macroscopic result was achieved through a higher amount of particle rotation in a disc sample but through a higher particle interlocking effect in an irregular-shaped clump sample. Moreover, the disc samples exhibited a clear localization behavior band while the clump samples exhibited a more uniform localization pattern. These showed that the disc with rolling resistance cannot replace the particle shape effects for a simulation purpose to achieve the mor realistic and physically sound constitute behavior of granular materials due to their fundamental differences in localization behavior. However, using a realistic shape may not be practical due to higher computational cost (Coetzee, 2017). For example, Markauskas (2010) observed that using ellipsoidal particles can increase the computational cost by a factor of 4.1 over that of spherical particles. However, shape might be a

critical factor in the present study. Bulk density of wheat is affected by kernel density and the void volume between kernels. The amount of void volume depends on the spatial arrangement of particles, which is dictated by wheat kernel properties such as size, shape, and friction coefficients (Meng et al., 2012). Unlike spheres, a pseudo-ellipsoid formed by clumps of spheres can have different orientations that will greatly affect kernel arrangement. Also, it has been shown that shape and size of kernels effected compressibility and packing ratio of wheat, which are both related to bulk density (Petingco et al., 2018).

In this study, two particle models were evaluated for simulating bulk density determination. These are single-sphere particle model, and the five-sphere particle model having different aspect ratios used by Petingco et al. (2020). The single-sphere particle model was used to test the applicability of using spherical particles to model wheat particles. The five-sphere particle model was used to evaluate a more accurate shape representation of wheat kernels, in this case, a pseudo-ellipsoid.

4.2.3.2 Particle size

Wheat kernels were modeled using three different sizes of particles corresponding to the three different kernel size fractions to incorporate the size distribution in the DEM simulation. For the five-sphere particle model, set 1 particle used by Petingco et al. (2020) were used in this study. For the single-sphere particle model, equivalent sphere diameter was determined for each kernel size fraction. EDEM automatically computes the particle model mass based on the volume and solids density of the particle. The sphere diameter for each kernel size fraction was adjusted until the EDEM computed particle mass matches the single kernel mass for each size fraction in the five-sphere particle model. Figure 4-2 shows the two sets of particle models for the three kernel size fractions of wheat.

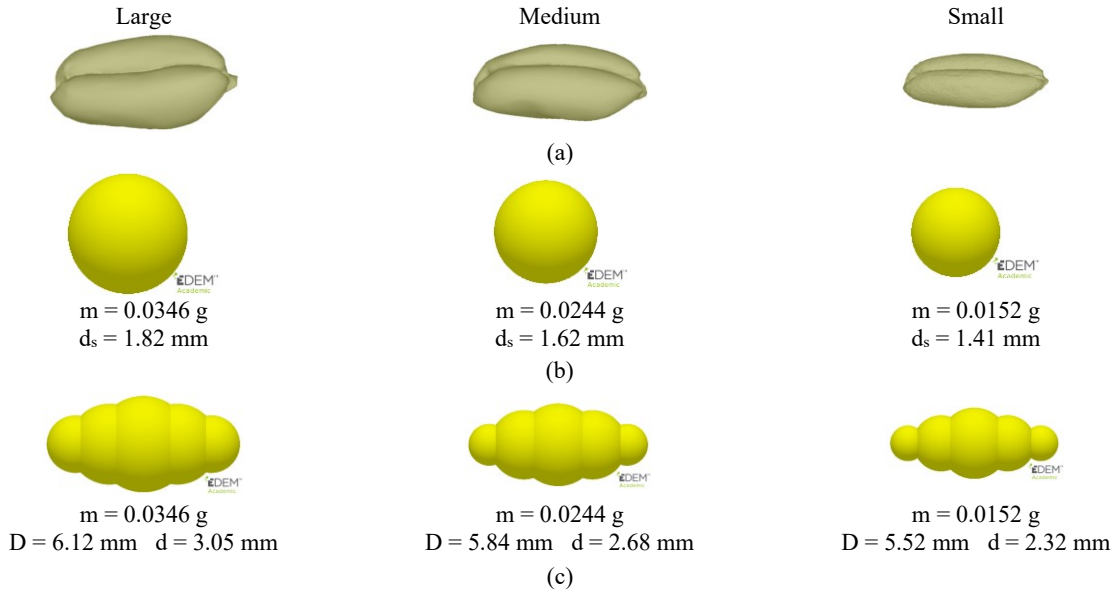

Figure 4-2. Particle models for the three wheat kernel size fractions: (a) 3D image of wheat kernels, (b) single sphere particles and their equivalent spherical diameters, and (c) five-sphere particle models and their corresponding major and minor diameters.

4.2.3.3 Calibration of contact parameters

Contact parameters were calibrated with experimentally determined bulk density using a laboratory setup similar to test weight determination (USDA-GIPSA, 2009). However, the setup (Figure 4-3) was made smaller to decrease the number of particles in the DEM simulation, decreasing the computational cost in the DEM calibration process. This setup was discussed in detail in Petingco et al. (2020).

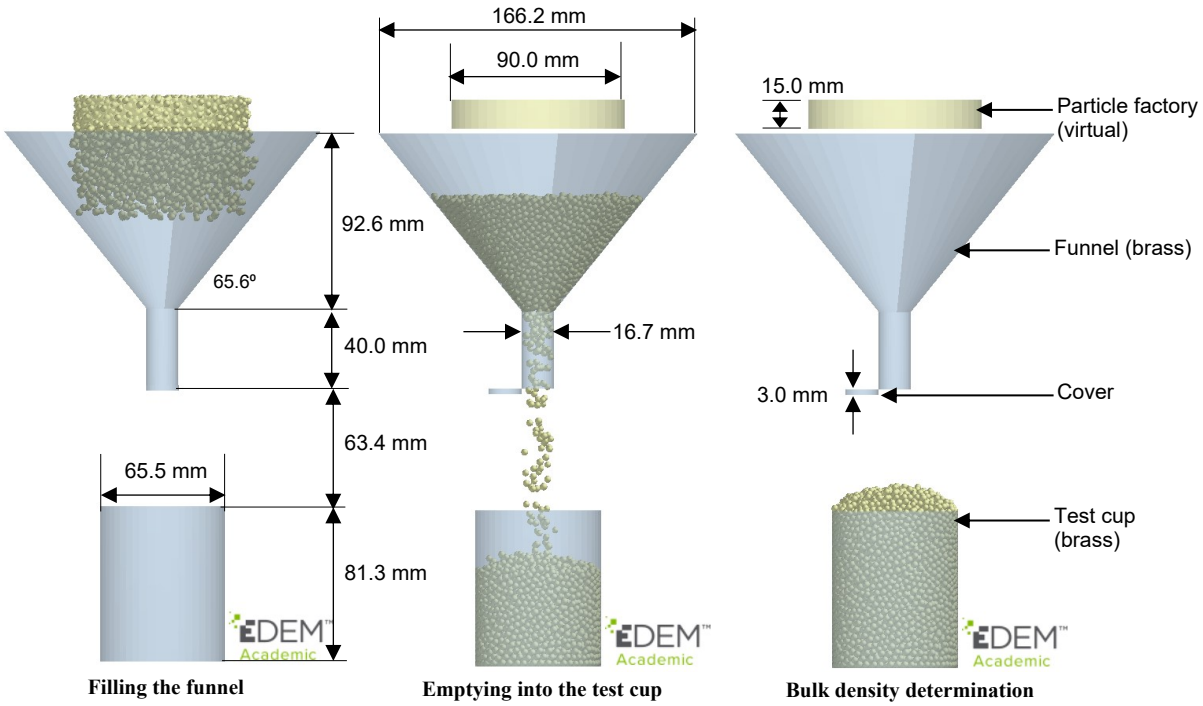

Figure 4-3. Setup for bulk density determination (Petingco et al., 2020).

4.2.3.3.1 Laboratory experiment for calibration

The laboratory experiment involved filling the funnel, with the outlet valve closed, with 0.325 kg of wheat of a single size fraction. Once the grain settled, the valve was opened to allow the grain to flow out of the funnel and into the test cup below. The grain was allowed to overflow the test cup and was leveled off using a wooden stroker. The mass of grain remained in the test cup was determined, and the bulk density was computed by dividing the grain mass by the volume of the test cup (275.8 cm^3). This test was repeated ten times for each kernel size fraction and variety.

4.2.3.1.2 DEM simulation for calibration of contact parameters

The experiment described above was modeled using EDEM v2018.1 (DEM Solutions, 2017) following the implementation of Petingco et al. (2020). The simulation started with filling the funnel through a virtual particle factory generating particles at a rate of 1.0 kg/s. Generation

of particles was set to random orientation and position, with both the initial linear and angular velocities set to zero. The particles were allowed to settle; afterwards, the outlet valve below the funnel was given a linear rotation with an initial velocity of 7.85 rad/s. The rotation stopped when the outlet cover completed a 180º rotation along the vertical, fully opening the funnel in 0.4 s. Once the funnel was emptied and the particle settled in the cup, the mass of the particles inside the cup was determined by creating a cylindrical density sensor coinciding with the internal volume of the test cup in EDEM Analyst.

The values for the Poisson's ratio and shear modulus used for wheat particles were 0.22 and 22.4 MPa, respectively (Molenda and Horabik, 2005). The value of solids density, 1373 kg/m^3, was based on the adjusted mean pycnometer reading (Petingco et al., 2020; Chang, 1988) of wheat samples. The values for the Poisson's ratio, solids density, and shear modulus used for the equipment material were 0.25, 8560 kg/m^3, and 37 GPa, respectively (Mordfin, 2002). The contact model used for particle-to-particle and particle-to-geometry interactions was Hertz-Mindlin no slip contact model. Gravity of -9.81 m s^{-2} along the *z*-axis was also added in the model. The domain of simulation was set to auto-update, the time step to Euler time integration and 20% Rayleigh time, and grid size to 2.5 times the minimum particle radius ($2.5R_{min}$) to ensure particles did not behave erratically and ensure stability. The simulation started with particle generation and ended with settling of particles into the cup. The simulated bulk density was determined by creating a density sensor (coinciding with the test cup) in EDEM Analyst.

Plackett-Burman design (Plackett and Burman, 1946) was implemented to reduce the number of factors to the critical few that had the greatest influence on the response. Minitab® 17.0 (Minitab, Inc., State College, Pa.) was used to design the screening test, in which the six contact parameters were considered as factors, and bulk density was the response. All the factors

had 2 levels, coding as -1 and +1, for low and high levels, respectively (Table 4-1). The design estimated the linear main effects for all factors. However, interaction factors were not estimated in this design. The design has 12 runs with 80% chance of detecting effects of 1.68 standard deviations or more. The low and high values were based on Petingco et al. (2020). The screening of the factors was accomplished by using only the large kernel size fraction.

Table 4-1. Factors for the Plackett-Burman design.[a]

Contact Parameters	Symbols used	Low Level (-1)	High Level (+1)
wheat-wheat coefficient of rolling friction	fr_{ww}	0.00	0.10
wheat-surface coefficient of rolling friction	fr_{ws}	0.00	0.10
wheat-wheat coefficient of static friction	fs_{ww}	0.10	0.40
wheat-surface coefficient of static friction	fs_{ws}	0.10	0.40
wheat-wheat coefficient of restitution	e_{ww}	0.10	0.60
wheat-surface coefficient of restitution	e_{ws}	0.10	0.60

[a]Petingco et al. (2020)

A Pareto chart of standardized effects at 0.1 level of significance was used to identify the critical factors in the screening design in Minitab 17.0 (Plackett-Burman). A modeling design for prediction of bulk density was created in Minitab 17.0 by using the critical factors determined in the screening design. The factor levels in the modeling design were set closer together than in the screening design to increase the chances of identifying optimal settings for the critical factors. The modeling design estimated all linear main effects and two-way interactions. If a curvature was detected in the data, additional runs were added to fit a quadratic model. The optimal settings of the critical factors were determined using the best fit model, and then validation runs were conducted.

4.2.3.4 DEM simulation of bulk density as affected by drop height and size distribution

Once the optimum contact parameter values for the three kernel size fractions were determined, the possibility of using the discrete element method in simulating bulk density as

affected by varying drop heights was investigated. Simulated bulk densities of two wheat samples (KanMark and Garrison) at different heights were determined by following the process as shown in Figure 4-4. First, the hopper was filled with 1.1 kg of wheat sample with known size distribution of wheat kernels. This was followed by opening the hopper valve to empty the funnel and allowing the kernels to fill the kettle. Once the kernels settled after overflowing in the kettle, a wooden stroker was used to level off the excess kernels in the kettle, and the bulk density was determined using a built-in density sensor (cylinder coinciding with the kettle) in EDEM.

The percentage composition of the different particles can be easily implemented in EDEM by changing the input for the particle ratios (size distribution) to the actual percentages of each kernel size fraction in a wheat sample. This feature of EDEM is very advantageous for it was shown in that percentage composition of different kernel size fractions affects the packing density and compressibility of bulk material (Petingco et al., 2018). Table 4-2 shows the mass percentage composition of the three kernel size fractions for KanMark and Garrison wheat samples. The drop height h can be easily adjusted in the simulation to determine if simulated bulk densities changes with drop heights.

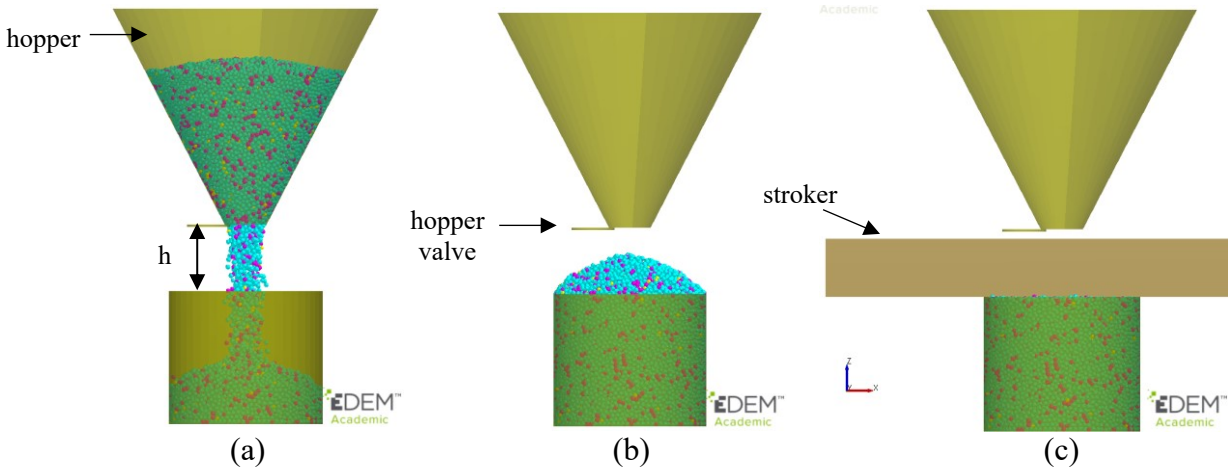

Figure 4-4. Setup for simulated bulk density determination: (a) filling the test cup with wheat having specific percentage composition of three size fractions, (b) letting the grain to settle, and (c) leveling the grain in the test cup with wooden stroker and determining bulk density.

Table 4-2. Percentage mass composition of two wheat samples.

Variety	% by Mass of Wheat Kernel Size Fraction		
	Large	Medium	Small
KanMark	81.5 (0.9)	15.5 (0.3)	3.0 (0.1)
Garrison	21.8 (0.7)	60.6 (0.8)	17.6 (0.2)

4.3 Results and discussion

4.3.1 DEM calibration of contact parameters

The Plackett-Burman design was used to determine which of the six contact parameters had the most significant effect on simulated bulk density. Since Petingco et al. (2020) already calibrated the five-sphere particle model, calibration was done only to the single-sphere particle model. Similarly, the particle model for large kernel size fraction was used for the calibration of contact parameters. Table 4-3 shows the design matrix and results of the Plackett-Burman design. The main effect plots and Pareto chart of effects are also shown in Figure 4-5. Factors with longer bars have more influence on bulk density. The red line is the effect size at the 0.10 level of significance. Gray bars represent non-significant factors that were removed from the

model. The charts show that among the six contact parameters, only three had significant effects on bulk density at the 0.1 level of significance if the single-sphere particle model is used, as compared with the five-sphere particle model, which had four significant contact parameters (critical factors).

Table 4-3. Design matrix and results of Plackett-Burman design for single-sphere particle model.

StdOrder	RunOrder	fr_{ww}	fr_{ws}	fs_{ww}	fs_{ws}	e_{ww}	e_{ws}	Bulk Density (kg m^{-3})
7	1	-1	+1	+1	+1	-1	+1	824.0
4	2	+1	-1	+1	+1	-1	+1	788.3
6	3	+1	+1	+1	-1	+1	+1	801.4
2	4	+1	+1	-1	+1	-1	-1	836.8
1	5	+1	-1	+1	-1	-1	-1	793.1
3	6	-1	+1	+1	-1	+1	-1	831.6
12	7	-1	-1	-1	-1	-1	-1	832.7
10	8	+1	-1	-1	-1	+1	+1	841.3
8	9	-1	-1	+1	+1	+1	-1	831.8
9	10	-1	-1	-1	+1	+1	+1	850.3
5	11	+1	+1	-1	+1	+1	-1	841.1
11	12	-1	+1	-1	-1	-1	+1	848.1

The critical factors for the single-sphere particle model were the three wheat-to-wheat contact parameters (fr_{ww}, fs_{ww}, and e_{ww}), with the fs_{ww} having the highest significant effect on bulk density and e_{ww} having the least significant effect. For five-sphere particle model (Petingco et al., 2020), the critical factors were the same as that of the single-sphere model with the addition of the wheat-to-surface coefficient of static friction (fs_{ws}). The main effect plots show that *i*ncreasing the values of fr_{ww}, fs_{ww}, and fs_{ws} resulted in a decrease in bulk density, while increasing e_{ww} resulted in increase in bulk density.

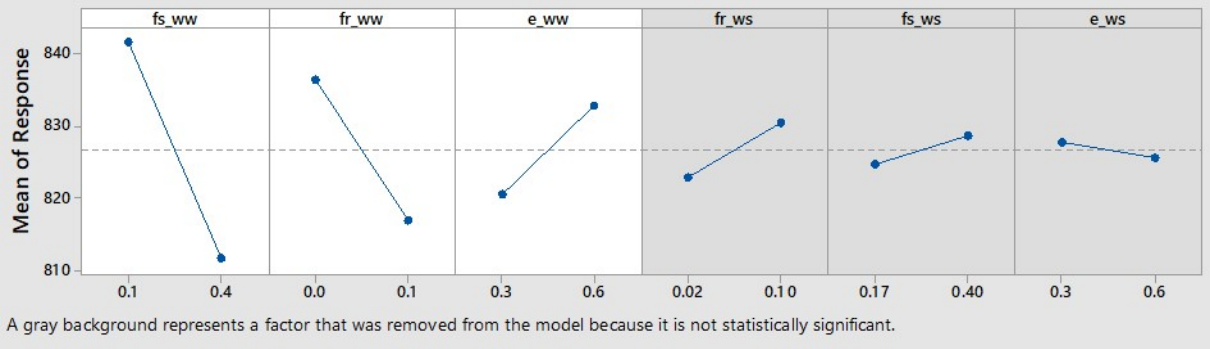

Main effect plots

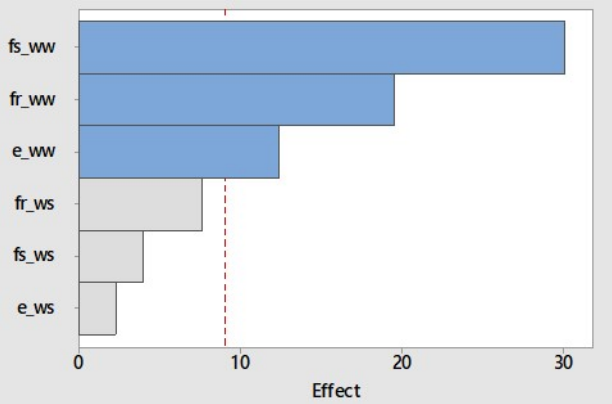

Pareto chart

Figure 4-5. Main effects plots and Pareto chart for bulk density showing the three significant contact parameters.

The modeling design (Table 4-4) for single-sphere particle model was created using Minitab 17.0 DOE > Plan and Create. Initially, the modeling design matrix for single-sphere particle had 11 runs to fit a linear model. However, Minitab detected evidence of curvatures in the data. This means that the average response at the center points is either higher or lower than the average response at the corner (cube) points. Therefore, the linear model did not adequately describe the relationship between the bulk density and the three contact parameters. Because the linear model was not adequate, we cannot determine significant factors and it is unlikely that we

will identify an optimal solution. Thus, nine additional runs were added into the modeling design to fit a quadratic model.

Table 4-4. Modeling design for determining the optimum setting of contact parameters for single-sphere.

Run	fr_{ww}	fs_{ww}	e_{ww}	Bulk density kg/m3
1	0.05	0.30	0.3	810.5
2	0.10	0.50	0.1	774.8
3	0.00	0.10	0.1	847.8
4	0.00	0.50	0.1	823.4
5	0.05	0.30	0.3	810.9
6	0.05	0.30	0.3	810.1
7	0.10	0.50	0.5	796.1
8	0.00	0.10	0.5	848.5
9	0.10	0.10	0.1	839.8
10	0.10	0.10	0.5	837.1
11	0.00	0.50	0.5	827.7
12	0.05	0.30	0.1	807.4
13	0.05	0.30	0.3	811.4
14	0.05	0.10	0.3	839.0
15	0.00	0.30	0.3	831.6
16	0.05	0.30	0.5	813.6
17	0.10	0.30	0.3	802.2
18	0.05	0.50	0.3	800.8
19	0.05	0.30	0.3	810.4
20	0.05	0.30	0.3	809.6

The optimal settings for the single-sphere large kernel size fraction were determined using Minitab 17.0 DOE > Analyze and Interpret > Fit Quadratic Model and by setting a target bulk density value of 826.1 kg/m^3 (Petingco et al., 2020), which is the experimentally determined bulk density of the large kernel size fraction. The optimum values for contact parameters for the large kernel size fraction using single-sphere were 0.05, 0.172, and 0.50, for fr_{ww}, fs_{ww}, e_{ww}, respectively (Table 4-5). The value of fs_{ws} was set to 0.17, which is the value found using the five-sphere particle model (Petingco et al., 2020). Unlike in the five-sphere model (Table 4-6), the results of the single-sphere validation indicated that the optimum setting of the contact parameters was only applicable to the large kernel size fraction. In fact, the optimum setting when used for the medium and small kernel size fractions resulted in the same bulk density as with the large kernel size fraction (about 828 kg/m^3). This was because the shape of the particles

used in all three kernel size fractions are the same, with all being spherical. Capturing the shape of the particles using the five-sphere particle model allowed us to use the same contact parameter values for the three particles used to represent the three kernel size fractions. However, using spherical particles (single-sphere) to model the three kernel size fractions required us to calibrate the contact parameters for the three kernel size fractions to achieve acceptable simulated bulk density results. The values of the three contact parameters for the medium and small kernel size fractions were also determined by using the results of the modeling design for large single-sphere and analyzing it using Minitab 17.0 DOE > Analyze and Interpret > Fit Quadratic Model, and by setting a target bulk density value of 797.7 kg/m^3 and 778.5 kg/m^3 for medium and small kernel size fractions (Petingco et al., 2020), respectively. The optimal settings for the three contact parameters for medium kernel size fraction were 0.05, 0.49, and 0.10, for fr_{ww}, fs_{ww}, and e_{ww}, respectively. For the small size fraction, the optimal settings were 0.10, 0.50, and 0.10, for fr_{ww}, fs_{ww}, and e_{ww}, respectively. The optimization for the two kernel size fractions resulted in lower restitution coefficient (e_{ww}) and/or higher coefficients of friction (fr_{ww}, fs_{ww}) to achieve lower simulated bulk densities.

These results showed that using a spherical particle to model the wheat kernels required us to calibrate the contact parameters for each kernel size fraction because of the discrepancies in shapes between spherical particle models and wheat kernels (Coetzee, 2017). Also, both the rolling and static friction coefficients using single-spheres were much higher than the optimum setting for five-sphere particles (especially for medium and small kernel size fractions), which resulted in relatively higher angle of heap. Wheat kernels are more ellipsoidal in shape than spherical. Spherical or round particles tend to slide, roll, and bounce more easily than ellipsoids and, thus, to account for the discrepancy in shape, the single-sphere (spherical) particle should

have higher friction coefficients and lower coefficient of restitution to simulate the bulk density of medium and small kernel size fractions of wheat accurately. However, this resulted in relatively higher angle of heap in simulations compared to that of the experiment. The angle of heap using five-sphere pseudo-ellipsoidal particle is close to that of the experiment.

Table 4-5. Simulated bulk densities of three size fractions using the optimum setting of contact parameters for single-sphere particle models.

Size fraction	fr_{ww}	fs_{ww}	e_{ww}	fs_{ws}	fr_{ws}	e_{ws}	Bulk density (kg/m3)			Time, s	Heap profile
							Simulated	Experiment	%Error		
Large	0.05	0.17	0.5	0.17	0.02	0.33	828.0 (0.4)	826.1 (1.2)	+0.23%	12.6	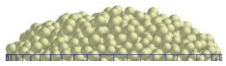
Medium	0.05	0.49	0.1	0.17	0.02	0.33	793.4 (0.7)	797.7 (1.4)	-0.59%	14.6	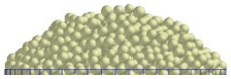
Small	0.10	0.50	0.1	0.17	0.02	0.33	780.3 (0.5)	778.5 (1.1)	+0.23%	14.1	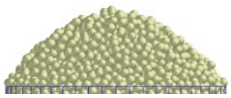

Table 4-6. Simulated bulk densities of three size fractions using the optimum setting of contact parameters for five-sphere particle models.[a]

Size fraction`	fr_{ww}	fs_{ww}	e_{ww}	fs_{ws}	fr_{ws}	e_{ws}	Bulk density (kg/m^3)			Time, s	Heap profile
							Simulated	Experiment	% Error		
Large	0.01	0.27	0.50	0.17	0.02	0.33	828.7 (0.7)	826.3 (1.2)	+0.31%	12.6	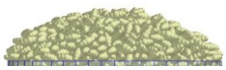
Medium	0.01	0.27	0.50	0.17	0.02	0.33	806.6 (0.8)	797.7 (1.4)	+1.07%	12.3	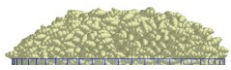
Small	0.01	0.27	0.50	0.17	0.02	0.33	775.5 (0.6)	778.5 (1.1)	-0.39%	12.5	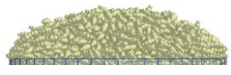

[a]Petingco et al. (2020)

4.3.2 Bulk density of two wheat samples at different drop heights

Bulk density of two wheat samples at different drop heights was determined experimentally. Figure 4-6 summarized the results and showed that the bulk density of wheat increased with increasing drop heights. The difference in bulk density between the two wheat samples can be attributed to the different percentage mass composition of the three kernel size fractions. KanMark has relatively higher bulk density than Garrison because it has a higher percentage composition of large kernel size fraction and a lower percentage composition of small kernel size fraction (Table 4-2).

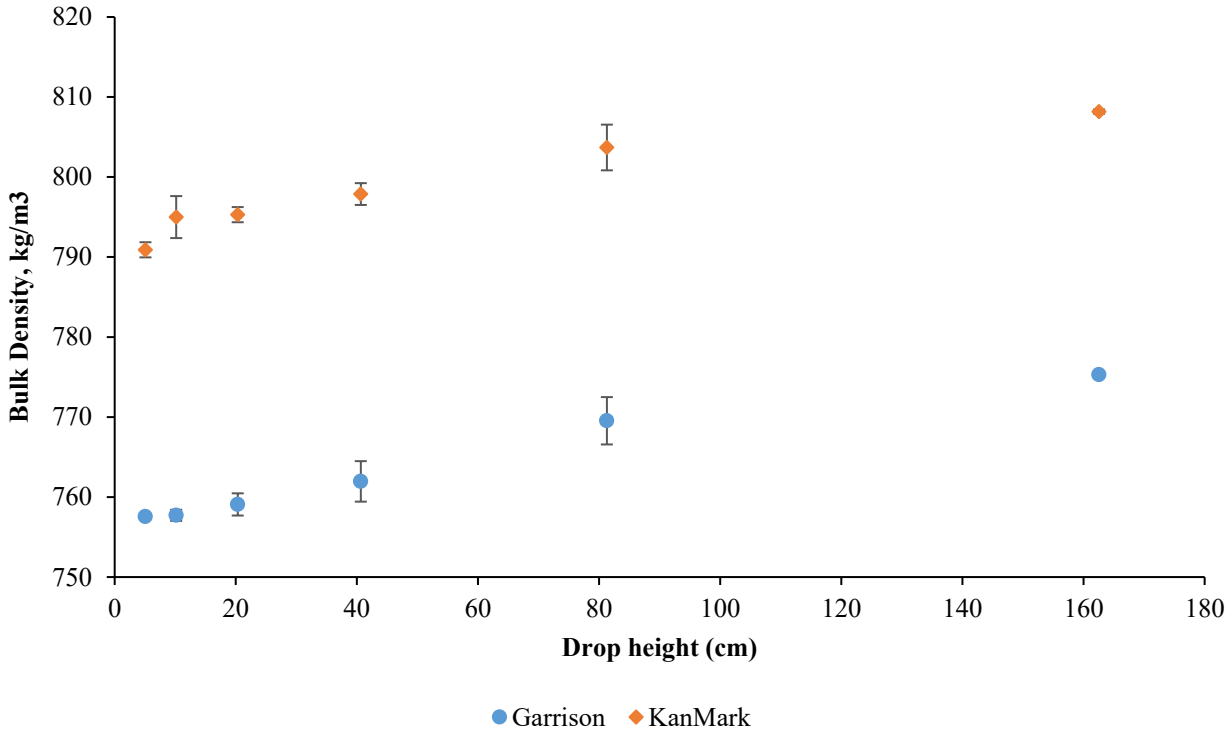

Figure 4-6. Wheat bulk density of two wheat varieties at different drop heights.

The General Linear Model (GLM) of Minitab 17.0 is used to determine whether the means of two or more groups differ. GLM is an ANOVA procedure in which calculations are performed using a least squares regression approach to describe the statistical relationship

between one or more predictors and a continuous response variable (Minitab, LLC, 2019). Because the p-values for variety and drop height are less than 0.05 level of significance, evidence exists that these two factors have significant effect on bulk density (Table 4-7). Tukey's pairwise mean comparisons were used to identify statistically significant differences between the group means of two varieties and among the different drop heights (Table 4-8). Results showed that there is a significant difference between the mean bulk densities of KanMark and Garrison. The difference in mean bulk density was due to the difference in percentage composition of three kernel size fractions (or size distribution). The effect of drop height on bulk density was significant when drop height is increased eight times (8h) from the original drop height (1h). Thus, bulk densities two wheat samples at drop heights of 1h, 8h, and 32 h were simulated in EDEM v2018.1.

Table 4-7. Analysis of variance for bulk density.

Source	df	F-value	p-value
Variety	1	3619.16	0.000
DropHeight	5	90.72	0.000
Variety*DropHeight	5	1.52	0.219

Table 4-8. Tukey's pairwise comparisons of bulk density between wheat variety and among drop heights.

Factor	n	Bulk Density[a]
Variety		
KanMark	18	798.5^{a}
Garrison	18	763.5^{b}
Drop Height		
32h	6	791.7^{A}
16h	6	786.6^{B}
8h	6	779.9^{C}
4h	6	777.2^{CD}
2h	6	776.4^{D}
1h	6	774.2^{D}

[a]Means followed by the same letter are not statistically different at the 5% level of significance

4.3.3 Simulated bulk density as affected by drop height and size distribution

Bulk density of the two wheat samples was simulated based on the percentage mass composition of the three kernel size fractions. This was easily implemented for the five-sphere model in EDEM v2018.1 because the contact parameter values were the same for all three kernel size fractions. The percentage mass composition was used to establish the particle ratios in EDEM v2018.1. However, the contact parameters were different for the three kernel size fractions when using the single-sphere model; thus, the percentage composition had to be implemented through the EDEM particle factory instead of directly from the mass composition to vary the contact parameter values for each size fraction. Three particle factories were created to generate the three kernel size fractions simultaneously. The total mass and target mass (generation rate) were varied to match the required number of particles based on the mass percentage compositions (Table 4-9). The percentage mass composition of the three size fractions in the test cup were also verified using the mass sensor tool in EDEM Analyst and results showed that the percentage composition values for both single-sphere and five-sphere models at different drop heights were close to the experiment values (Table 4-10). Paired t-test also showed that there was no significant difference in the percentage composition using single-sphere particle models (mean = 33.34, std dev = 28.69) and five-sphere particle models (mean = 33.34, std dev = 28.60); t (17) = -0.11, p-value = 0.914 (Table 4-11). Moreover, the simulated percentage mass composition of the three kernel size fractions for both KanMark and Garrison (using the two particle models) were not significantly different at the three different drop heights as indicated by the results of Tukey's pairwise mean comparison (Table 4-12). The percentage difference between the simulated values (average of three drop heights) and actual values ranged between -1.9% and 3.3%.

Table 4-9. Generation rate and total mass generated used in EDEM particle factory.

Particles		Total mass generated, kg	Generation Rate, kg/s
KanMark			
	Large	0.8965	0.815
	Medium	0.1705	0.155
	Small	0.0330	0.030
Garrison			
	Large	0.2398	0.218
	Medium	0.6666	0.606
	Small	0.1936	0.176

Table 4-10. Percentage mass composition of the three size fractions at different drop heights for the two wheat samples.

Wheat sample	Size Fraction	Percentage mass composition (%)						
		Design (actual)	Simulated 1-sphere			Simulated 5-sphere		
			1h	8h	32h	1h	8h	32h
KanMark	Large	81.5	81.4	81.0	81.0	81.2	81.3	81.3
	Medium	15.5	15.5	15.8	15.9	15.7	15.7	15.7
	Small	3.0	3.1	3.2	3.1	3.1	3.0	3.1
Garrison	Large	21.8	21.5	21.3	21.2	21.5	21.4	21.4
	Medium	60.6	60.6	60.6	60.6	60.8	60.8	60.9
	Small	17.6	17.9	18.1	18.2	17.8	17.8	17.7

Table 4-11. Paired t-test for five-sphere and single-sphere

	N	Mean	Std Deviation	SE Mean
five-sphere	18	33.34	28.69	6.76
single-sphere	18	33.34	28.60	6.74
Difference	18	-0.0056	0.2155	0.0508
95% CI for mean difference	(0.1127, 0,1016)			
T-test of mean difference	t-value = -0.11, p-value = 0.914			

Table 4-12. Tukey's pairwise mean comparison of percentage mass composition of the three size fractions at different drop heights and comparison with actual percentage mass composition.

Sample	Size	Simulated % mass composition at different drop heights[a]				Actual % mass composition	% Difference
		1h	8h	32h	Average		
KanMark	Large	81.3 (0.1)^{A}	81.3 (0.1)^{A}	81.2 (0.2)^{A}	81.2 (0.1)	81.5 (0.9)	-0.3
	Medium	15.6 (0.1)^{A}	15.8 (0.1)^{A}	15.8 (0.1)^{A}	15.7 (0.1)	15.5 (0.3)	1.4
	Small	3.1 (0.0)^{A}	3.1 (0.1)^{A}	3.1 (0.0)^{A}	3.1 (0.1)	3.0 (0.1)	3.3
Garrison	Large	21.5 (0.0)^{A}	21.4 (0.1)^{A}	21.3 (0.1)^{A}	21.4 (0.1)	21.8 (0.7)	-1.9
	Medium	60.7 (0.1)^{A}	60.7 (0.1)^{A}	60.7 (0.1)^{A}	60.7 (0.1)	60.6 (0.8)	0.2
	Small	17.9 (0.1)^{A}	18.0 (0.2)^{A}	18.0 (0.4)^{A}	17.9 (0.2)	17.6 (0.2)	1.8

[a]Means followed by the same letter are not statistically different at the 5% level of significance

The interaction or contact parameters between the three size fractions for five-sphere particle were the same for all particle-particle interactions. However, for the single-sphere particle, the interaction contact parameters between the different kernel size fractions were set as shown in Table 4-13.

Results of simulations of bulk density at different drop heights (1h, 8h, and 32h) of two wheat samples are shown in Table 4-14. The difference in percentage composition of the three kernel size fractions resulted in a different bulk density. Simulated bulk densities for KanMark was higher than that of Garrison because the former had more large size fraction and less small kernel size fraction. DEM simulations using either single-sphere or five-sphere follow the same trend as the experiment, with the simulation results slightly higher than the experiment.

Table 4-13. Particle-to-particle contact parameters for single-sphere model.

Particle-to-particle	fr_{ww}	fs_{ww}	e_{ww}
Large-Large	0.05	0.172	0.5
Medium-Large	0.05	0.486	0.1
Small-Large	0.10	0.500	0.1
Medium-Medium	0.05	0.486	0.1
Small-Medium	0.10	0.500	0.1
Small-Small	0.10	0.500	0.1

Table 4-14. Simulated bulk densities of two wheat varieties at different drop heights.

Drop height	1-sphere		5-sphere		Experiment
	without striking	with striking	without striking	with striking	(with striking)
KanMark					
1h	806.2 (0.2)	796.7 (0.4)	814.0 (0.4)	805.8 (0.6)	790.9 (0.9)
8h	811.8 (0.2)	802.2 (0.1)	819.4 (0.8)	811.2 (0.1)	797.9 (1.4)
32 h	825.9 (0.1)	814.5 (0.1)	835.0 (0.2)	825.6 (0.5)	808.2 (0.3)
Garrison					
1h	781.6 (1.8)	771.5 (1.1)	798.6 (0.2)	789.2 (0.3)	757.6 (0.3)
8h	786.7 (0.2)	777.1 (0.8)	802.9 (0.1)	794.9 (0.1)	762.0 (2.5)
32 h	799.8 (0.4)	789.2 (0.1)	815.8 (1.2)	806.5 (0.3)	775.3 (0.3)

The percentage difference of simulation results with the experiment was less for KanMark than with Garrison (Table 4-15). This might be due to the higher amount of shriveled

kernels in Garrison that makes its experimental bulk densities lower. Shriveled or wrinkled grains have lower kernel densities and irregularity in shapes than sound grains (Petingco et al., 2020; Ransom, 2017), which contribute to lower experimental bulk densities. The single-sphere model exhibited a lower percentage difference from the experiment than the five-sphere model. This might be due to a more rigorous calibration of the contact parameters in each kernel size fraction as explained in Coetzee (2016). Although the single-sphere particle model had more accurate results than the five-sphere model for predicted bulk density, it was observed in the simulation that the latter better described the different heap profiles generated at the different grain drop heights (Figure 4-7). A crater-like shape in the heap profile can be observed at higher grain fall heights. Matching the shape of the particles in the simulation using pseudo-ellipsoids made it possible to match the heap profiles of bulk material in the experiment.

Table 4-15. Percentage error of simulated bulk density results (with striking) of two particle models with reference to experiment.

	KanMark			Garrison		
Particle Model	1h	8h	32h	1h	8h	32h
1-sphere	0.7%	0.5%	0.8%	1.8%	2.0%	1.8%
5-sphere	1.9%	1.7%	2.2%	4.2%	4.3%	4.0%

4.4 Conclusion

This research developed a DEM model to predict wheat bulk density as affected by grain drop heights and size distribution. Two particle shapes were evaluated in the DEM simulation of wheat bulk density. Use of either the spherical (single-sphere) or pseudo-ellipsoidal (five-sphere) particle models resulted in simulated bulk densities following the major trend from the experiments – bulk density increased with higher grain fall heights. Accurate shape representation (using clumps) captured some features of bulk material behavior (i.e. heap profile) in the simulation better than with single-sphere particles. However, use of single-sphere particles

for modeling granular material was deemed more practical because of lower computational cost. Accuracy of DEM predictions can be improved through individual calibration of contact parameters for each size fraction and considering the size distribution of these size fractions in the model. Although the DEM model was only able to predict the bulk density of wheat in a test cup as affected by grain drop height, this model can be extended to predict uncompacted bulk density of wheat in bins. However, DEM simulations of this scale require large computational cost. With the advancement of high-performance computing technology and numerical algorithms, solving large-scale and complex problem will be feasible and faster.

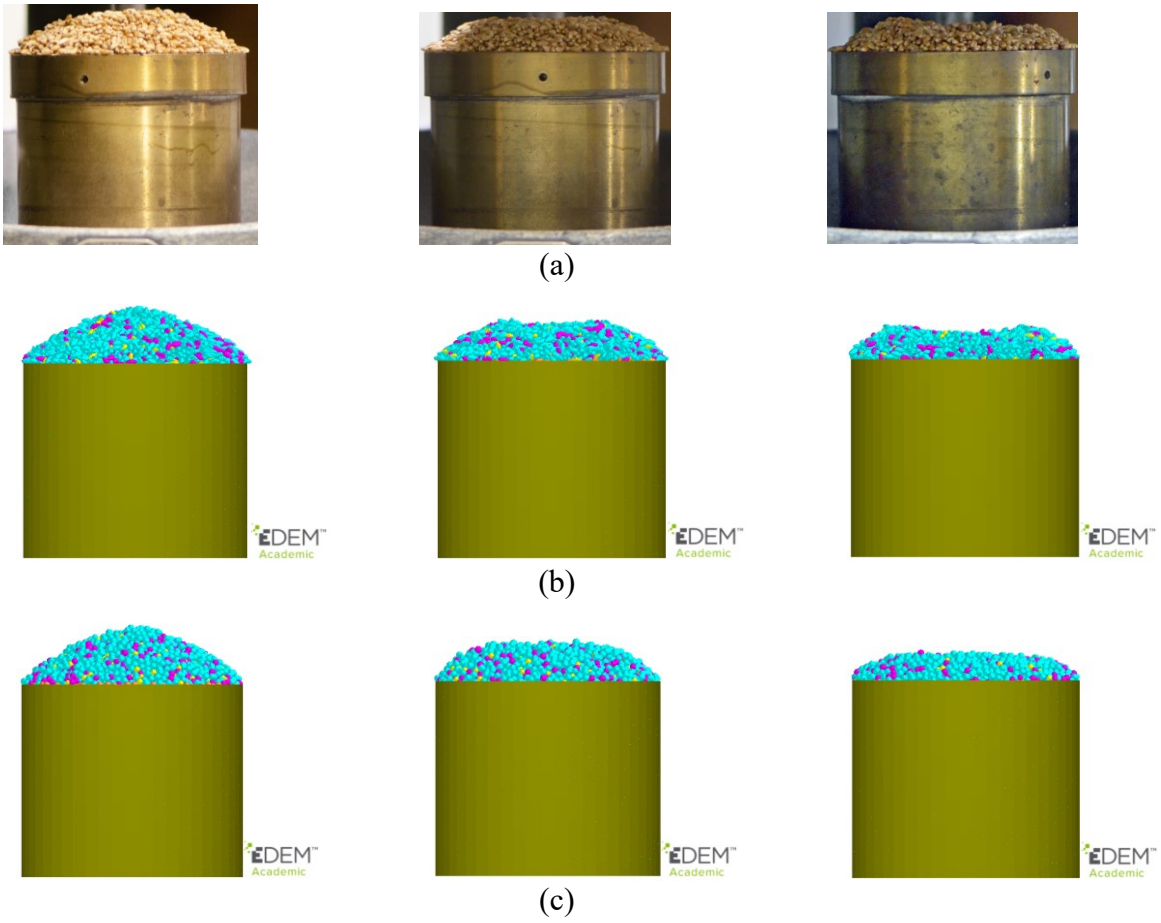

Figure 4-7. Heap profile at different drop heights: (a) experiment, (b) 5-sphere pseudo-ellipsoidal particles, and (c) 1-sphere spherical particles. From left to right: 1h, 8h and 32h.

4.5 References

Bhattacharya, K. R. (2013). Physical properties of rice. In K. R. Bhattacharya (Ed.), Rice quality: A guide to rice properties and analysis (pp. 26-60) Woodhead Publishing. doi: 10.1533/9780857092793.26

Chang, C. S., Converse, H. H., & Martin, C. R. (1983). Bulk properties of grain as affected by self-propelled rotational type grain spreaders. *Trans ASAE*, 26 (5): 1543-1550. doi: 10.13031/2013.34167

Coetzee, C.J. (2016). Calibration of the discrete element method and the effect of particle shape. *Powder Tech.*, 297. doi:10.1016/j.powtec.2016.04.003.

Coetzee, C.J. (2017). Review: Calibration of the Discrete Element Method. *Powder Tech.*, 310, 104-142. doi:10.1016/j.powtec.2017.01.015.

Cundall, P. A., & Strack, O. D. (1979). A discrete element model for granular assemblies. *Geotechnique*, 29(1), 47-65.

DEM Solutions. (2017). EDEM v2018.1 documentation. Edinburgh, UK: DEM Solutions Ltd.

Horabik, J., Parafiniuk, P., & Molenda, M. (2016). Experiments and discrete element method simulations of distribution of static load of grain bedding at bottom of shallow model silo. *Biosystems Engineering*, 149, 60-71. doi:10.1016/j.biosystemseng.2016.06.012

Janssen, H. A. (1895). Versuche über getreidedruck in silozellen. Zeitschrift d. Vereines Deutscher Ingenieure, 39(35), 1045-1049.

Kačianauskas R., Balevičius R., Markauskas D., Maknickas A. (2007). Discrete Element Method in Simulation of Granular Materials. In: Eberhard P. (eds) IUTAM Symposium on Multiscale Problems in Multibody System Contacts. IUTAM Book series, vol 1. Springer, Dordrecht. doi:10.1007/978-1-4020-5981-0_7

Lu, G., Third, J. & Müller, C.R. (2015). Discrete element models for non-spherical particle systems: From theoretical developments to applications. *Chemical Engineering Science*, 127. doi:10.1016/j.ces.2014.11.050.

Markauskas, Kačianauskas, Džiugys, & Navakas. (2010). Investigation of adequacy of multi-sphere approximation of elliptical particles for DEM simulations. *Granular Matter*, 12(1), 107-123.

Meng, L., Lu, P., Li, S., Zhao, J., & Li, T. (2012). Shape and size effects on the packing density of binary spherocylinders. *Powder Tech., 228*, 284-294. doi:10.1016/j.powtec.2012.05.033

Molenda, M., and Horabik, J. (2005). Mechanical properties of agromaterials and food powders for industrial practice: Part 1. Characterization of mechanical properties of particulate solids for storage and handling. Lublin, Poland: Polish Academy of Sciences. https://doi.org/10.13140/2.1.2810.1447

Molenda, M., Horabik, Józef & Ross, I. (1993). Loads in Model Grain Bins as Affected by Filling Methods. *Trans. ASAE*, 36(3), 915-919. doi: 10.13031/2013.28416

Molenda, M., Horabik, Józef & Ross, I. (1996). Effect of filling method on load distribution in model grain bins. *Trans. ASAE*, 39. 219-224. doi: 10.13031/2013.27501

Mordfin, L. (2002). *Handbook of reference data for nondestructive testing*. West Conshohocken, PA: ASTM. https://doi.org/10.1520/DS68-EB

Minitab, LLC (2019). Help and How-to, Modeling Statistics, ANOVA, Supporting Topics, Basics

Petingco, M. C., Casada, M. E., Maghirang, R. G., Thompson, S. A., McNeill, S. G., Montross, M. D., & Turner, A. P. (2018). Influence of kernel shape and size on the packing ratio and compressibility of hard red winter wheat. *Trans. ASABE*, 61(4), 1437-1448. doi:10.13031/trans.12648

Petingco, M. C., Casada, M. E., Maghirang, R. G., Fasina, O. O., Chen, Z., Ambrose, R. P. K. (2020). Influence of particle shape and contact parameters on DEM-simulated bulk density of wheat. *Trans. ASABE*. (in press). doi:10.13031/trans.13718

Plackett, R.L., and Burman, J. P. (1946). The Design of Optimum Multifactorial Experiments, *Biometrika*, 33(4): 305-325.

Ransom, J. (2017). Test weight in wheat (07/20/2017). North Dakota State University: Plant and Pest Report. Retrieved from https://www.ag.ndsu.edu/cpr/plant-science/test-weight-in-wheat-07-20-17.

Stephens, L.E., & Foster, G.H. (1978). Bulk properties of wheat and grain sorghum as affected by a mechanical grain spreader. *Trans. ASAE*, 21 (6): 1217-1218. doi: 10.13031/2013.35471

Thompson, S. A., & Ross, I. J. (1983). Compressibility and frictional coefficients of wheat. Trans. ASAE, 26(4), 1171-1176, 1180. doi: 10.13031/2013.34099

Thompson, S. A., McNeill, S. G., Ross, I. J., & Bridges, T. C. (1987). Packing factors of whole grains in storage structures. *Appl. Eng. Agric., 3*(2), 215-221. https://doi.org/10.13031/2013.26677

USDA-FGIS. (2013). *Grain Inspection Handbook*. Washington, DC: USDA Federal Grain Inspection Service

USDA-GIPSA. (2009). Inspecting grain: Practical procedures for grain handlers. Washington, DC: USDA Grain Inspection, Packers and Stockyards Administration. Federal Grain Inspection Service. Retrieved from https://www.gipsa.usda.gov/fgis/publication/ref/primer.pdf.

Versavel, P. A., & Britton, M. G. (1986). Interaction of bulk wheat with bin wall configuration in model bins. *Trans. ASAE*, 29(2), 533-537. doi:10.13031/2013.30186

Yang, X., & Williams, D. L. (1990). Airflow resistance of grain sorghum as affected by bulk

density. *Trans. ASAE*, 33(6), 1966-1970. doi:10.13031/2013.31565

Zhou, B. & Wang, H. & Wang, J. (2013). DEM investigation of particle anti-rotation effects on the micromechanical response of granular materials. *Granular Matter*, 15(3), 315-326. doi: 10.1007/s10035-013-0409-9

Chapter 5 - Discrete Element Method Simulation of Wheat Bulk Density under Confined Uniaxial Compression

5.1 Introduction

It is well known that grain undergoes compaction when stored in bins and other storage structures. This results in increase in grain bulk density due to compression caused by the cumulative weight of the overlying grain material. The extent of compression depends on several factors associated with the stored grain (crop type, test weight, moisture content, depth of grain in bin), bin characteristics (bin wall material, bin geometry, and dimensions), and handling practices (drop height, manner of filling the bin, aeration system, etc.).

The relatively large increase in grain bulk density (compared to its initial value) was caused by the reduction in volume of the stored grain due to compaction. This reduction in grain volume is referred as compaction factor in ASABE Standard EP413.2 (ASABE, 2010). Although grain is traded on mass basis, the majority of grain inventory and auditing assessments are based on volume measurements and use grain test weight (standard measure of bulk density) in estimating the amount of grain. Thus, there is a need for accurate compaction factors to accurately estimate the amount of grain in a storage bin. Compaction or pack factor tables for determining grain packing are used in the grain industry for inventory control, government auditing, loan and insurance purposes, and bin design. The USDA Risk Management Agency (RMA) and USDA Farm Service agency – County Offices (FSA-C) share an empirical pack factor table that provides pack factors for seven types of grain. However, these tables do not consider effects of moisture content, bin wall type, and grain height for determining pack factors (Boac et al., 2015).

The inaccuracy of the current methods prompted Thompson and Ross (1983) to develop a science-based model for determining compaction factors. A confined uniaxial test was developed and used on wheat using a device called bulk density apparatus. The device used a steel box with a chamber that contained grain during testing. The grain was subjected to a vertical pressure to represent the equivalent overburden pressure of the overlying grain material, and to determine how much it increased the grain bulk density. Aside from the over burden pressure, the effects of moisture content on the variation in bulk density was also determined. Bulk density increased with increasing overburden pressure and moisture content. The initial mechanism for compaction at low pressures was believed to be primarily due reduction in void space and particle rearrangement. For 8% and 12% moisture content, a steep density-pressure curve was observed at pressures up to 14 kPa as a result of rearrangement of particles in the test apparatus as pressure is applied with an overall decrease in void space between particles. As the void space decreased, higher inter-granular stresses occurred between particles, which explained the rate of compaction slows considerably between 14kPa and 138 kPa. At this point, it was believed that the small change in bulk density was mostly due to small deformation of the wheat particles.

Discrete element method (DEM) modeling has been gaining popularity in postharvest processing of grain and food products because of its close characterization of actual conditions in predicting various processes (Boac et al., 2014). This explicit numerical technique developed by Cundall and Strack (1979), allows each particle to be represented numerically and to be identified with its specific properties such as size, shape, material properties, and initial velocity and acceleration. It also models the overall system behavior of granular material as a result of individual interactions of a particle to another particle or a surface. However, the accuracy of DEM simulations depends highly on input parameters that include force or contact models,

physical properties of particulate materials (i.e., particle shape, size distribution, solids density, Poisson's ratio, and shear modulus), surface material properties, and contact parameters (i.e., particle-to-particle and particle-to-surface static friction coefficient, rolling friction coefficient, and restitution coefficient).

The objective of this study was to simulate the compressive behavior of wheat under uniaxial compression using discrete element method. Specifically, it aimed to (1) determine the appropriate grid size, time step and strain rate in the DEM simulation of confined uniaxial test; and (2) evaluate the accuracy of the DEM simulation in predicting the bulk density of wheat under confined uniaxial compression.

5.2 Materials and methods

5.2.1 Bulk density test apparatus – compressibility box

Thompson and Ross (1983) developed a bulk density test apparatus for measuring changes in bulk density as affected by internal pressure. The apparatus is comprised of a steel box with a test chamber (30 cm x 30 cm square, and 10 cm height) that contained the grain during testing. The top part of the box was a removable steel plate used to seal the test chamber. The test chamber is filled with grain using a special filling box to create a consistent initial loading condition and initial bulk density similar to that of using a test weight per bushel test setup (USDA-FGIS, 2013). The base of the test chamber was a flexible rubber diaphragm that allowed compressed air to be applied underneath the diaphragm. This allowed application of uniaxial pressure to the grain that simulated the equivalent overbearing pressure found in grain storage bins. The increase in pressure caused the grain to compact, thereby increasing grain bulk density. The changes in height due to the applied pressure were measured to determine the change in bulk density.

Turner et al. (2016) improved the instrumentation of the compressibility box by adding a computer data acquisition system to adjust the pressure and measure the displacement (change in grain height) within the chamber to replace the manual pressure regulator in Thompson and Ross (1983). Also, a linear variable differential transducer replaced the dial indicator for the displacement measurement. The pressure and displacement were monitored every second during testing, and the samples were subjected to a five-minute hold time at each pressure level before displacement and pressure were recorded to ensure that the displacement had stabilized. The pressure was increased linearly to the next level over a 30-second interval. The pressures applied were between 0 and 138 kPa (0, 7, 21, 34, 48, 69, 103, and 138 kPa,) which are the typical range of pressures found in most on-farm and commercial grain bins. Due to the non-uniform pressure step size, the loading rate was not constant over the range of pressures.

5.2.2 DEM modeling

5.2.2.1 Modeling approach

DEM simulation of the bulk density changes in the compressibility box can be simplified as shown in Figure 5-1. A small rectangular volume at the center of the box can be used to simplify the problem. By considering this volume, the friction between the side walls of the box and the granular material can be neglected and the problem can be simplified into a one-dimensional compression with no wall friction. Similarly, instead of using a rectangular volume, an equivalent cylindrical volume can also be used.

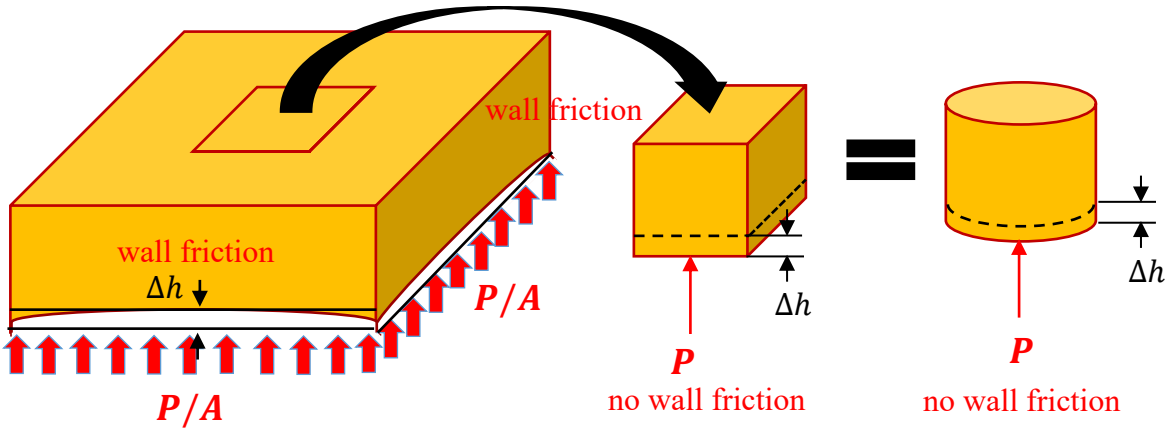

Figure 5-1. Simplification of the compressibility box problem.

The determination of the representative elementary volume (REV) is a crucial task in the study of granular material (Masson and Martinez, 2001). REV is the smallest volume over which a measurement can be made that will yield a value representative of a large volume (Wiacek et al, 2012). Determining the minimum REV is very important for it was shown that the size of the specimen have significant influence on the mechanical response of granular materials. The size of REV can be associated to the size of grain and it can be determined analytically (Bachmat and Bear, 1987), numerically (Evesque, 1991) or based on experiments (Zhang et al., 2000; Costanza-Robinson et al., 2011). According to Wiacek and Molenda (2016), the minimum REV size varies depending on the considered material and physical quantity of interest. Moreover, they said that REV is related to either the mean grain diameter or the diameter of the largest particle of the porous medium. The minimum REV size in most granular experiments and computer simulations corresponded to two or grain diameters, but may be higher in some cases (Evesque, 2001). Masson and Martinez (2000) showed that a sample size equal to 7 to 8 times the size of the largest particle was sufficient to obtain REV size for porosity and coordination number whereas 12 times the largest particle size was required for proper stress tensor evaluation.

Grain bulk density is related to the grain porosity. The more porous or void spaces present within the grain mass, the lower is the grain bulk density. For the porosity, the minimum REV size they reported for sphere packings was 15 times the particle size. This is supported by Masson and Martinez (2001) in which a value of 15 for the size ratio between the sample characteristic length and the largest particle diameter was suggested.

5.2.2.2 DEM simulation of compressive behavior of wheat

DEM simulation of the bulk density changes in the compressibility box was implemented using a smaller volume and can be broken down into three steps: (1) filling the test chamber with grain with similar bulk density as that of the test weight per bushel test, (2) applying pressure to the grain mass, and (3) measuring the change in bulk density. The simulation of filling was implemented similar to Petingco et al. (2020) in which the procedure in test weight per bushel test was simulated. This involved filling the kettle from a hopper, allowing the particles to overflow and settle, and leveling off the particles using a stroker in a zigzag fashion. The application of pressure was implemented using a moving lid similar to that of Wiacek et al. (2012) until the normal lid pressure reached the desired pressure. After filling the kettle (diameter = 58.74 mm, height = 101.6 mm), the bottom part of the cylinder that represents the kettle was set to "open" and another cylinder with diameter slightly smaller than the kettle diameter was created at the bottom of the lid. The small clearance (0.5 mm) between the kettle and the bottom lid allowed the latter to move freely once an upward velocity was introduced into it in the simulation. Another cylinder was created to cover the top part of the kettle. The top lid, kettle, and bottom lid material properties were set to steel (Table 5-1). However, the kettle rolling and static friction coefficients were set to almost zero (0.01) to make the cylinder wall somewhat frictionless. Table 5-2 summarized the input contact parameters between particle and

surfaces, and between different sizes of particles. The upward movement of the bottom lid resulted in compression of the bulk material in the cylinder. The pressure applied on the bulk material is equivalent to the pressure applied by the material to the bottom lid. The pressure acting on the bottom lid was determined by plotting in the EDEM Analyst the total vertical force (Primary Attribute: Total Force; Component: Z and Total) acting on the bottom lid and plotting it against time. This vertical force (N) was converted to pressure (Pa) by dividing it to the area (m^2) of the lid in contact with the bulk material.

Table 5-1. Input parameters in EDEM.

Geometry material properties (steel)	
Shear modulus, MPa	3.7 x 104
Poisson's ratio	0.25
Solids density, kg m-3	8490
Particle material properties (wheat)	
Shear Modulus, MPa	22.4
Poisson's ratio	0.22
Solids density, kg m-3	1373
Particle % composition	
Large, %	81.5
Medium, %	15.5
Small, %	3.0
Contact model	Hertz- Mindlin
Time integration	Euler
Time step, s	7.21 x 10-6 s (20 % Rayleigh time)
Grid size, mm	2.9mm (2.5 R_{min})
Lid displacement velocity, mm/s	1.0

Table 5-2. Input contact parameters.

Interaction Properties	*fr*	*fs*	*e*
Particle-surface			
Particle-cylinder	0.01	0.01	0.33
Particle-top lid	0.02	0.17	0.33
Particle –bottom lid	0.20	0.60	0.70
Particle-particle			
Large-Large	0.05	0.172	0.5
Medium-Large	0.05	0.486	0.1
Small-Large	0.10	0.500	0.1
Medium-Medium	0.05	0.486	0.1
Small-Medium	0.10	0.500	0.1
Small-Small	0.10	0.500	0.1

Figure 5-2 shows the results of a preliminary simulation run using a moving lid to apply pressure on the bulk material. At time = 0 second, the simulated force acting on the bottom lid is

8.7 N, and the simulated force acting on the top lid is almost zero. Because it is static and the cylinder is frictionless, it is expected that the bottom lid will carry all the weight of the bulk wheat which explained the value of the vertical force acting on it. The top lid, on the other hand, has a negligible vertical force because few wheat particles were touching the top lid. After the bottom lid moved a distance Δd over time T, the force acting on the bottom and top lid increased while maintaining the force difference equivalent to the weight of the bulk wheat.

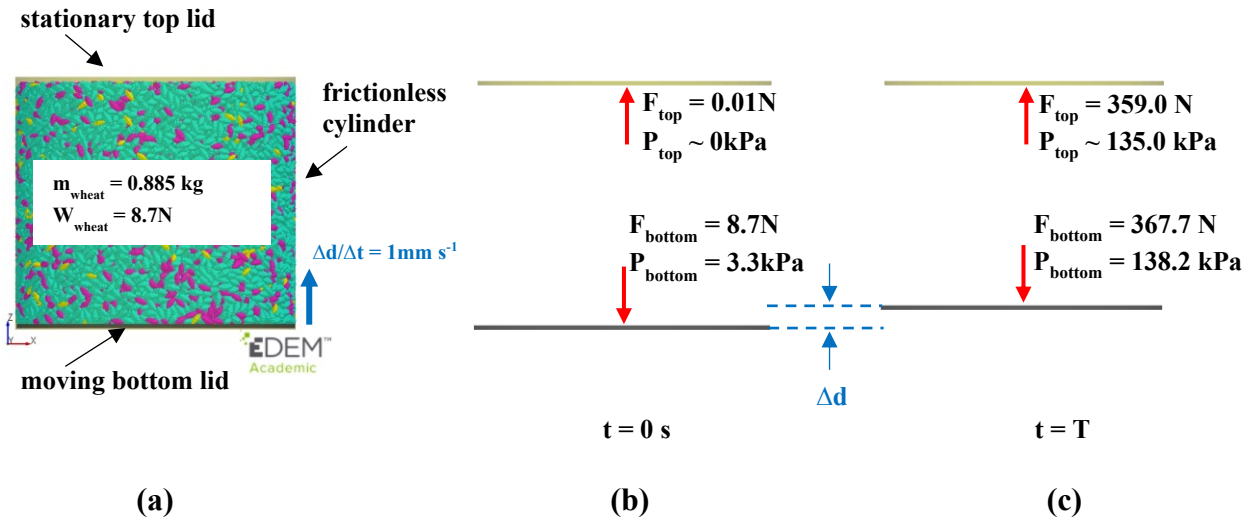

Figure 5-2. Simulation of applied pressure using a moving lid: (a) frictionless cylinder with wheat particles with stationary top lid and bottom lid moving at a constant rate upward, (b) force balance at time 0 second, and (c) force balance at time T.

In the compressibility box experiment, a holding time of 5 minutes was implemented after reaching the desired pressure level before displacement were recorded to ensure that the displacement has stabilized. However, because a moving lid was used to apply a pressure in the DEM simulation, stabilization of the lid displacement was no longer the issue, rather, it is the stabilization of the pressure once lid stop moving. Figure 5-3 shows the plot of the simulated pressure versus time. Results of simulations showed that after moving the lid at a

constant rate of 1 mm/s for about 6 seconds, the pressure reached 100 kPa, and the pressure decreased indefinitely with the hold time after the lid stop moving which shows instability in the numerical solution.

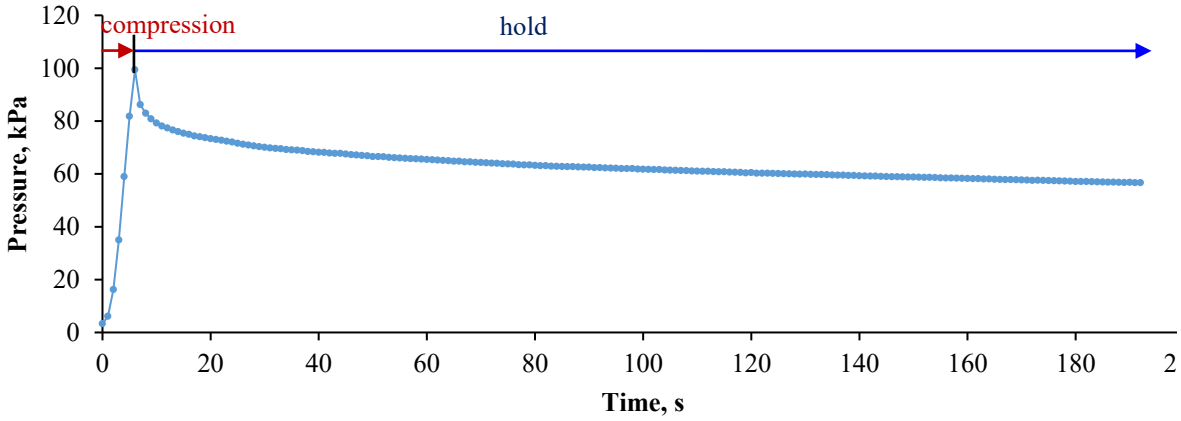

Figure 5-3. Pressure decreased indefinitely with hold time.

According to Liu et al. (2019), a numerical method is stable if: (1) there is limited oscillation in the solution such that the numerical error does not build up whereby the solution stays close to the truth; and (2) it guarantees a bounded solution irrespective of time step size. Because the simulated pressure decreased indefinitely, it is very clear that the DEM model implemented shows instability in the solution. To ensure stability, smaller time steps (2%, 5%, and 10% of Rayleigh time) were tried in the simulations. Moreover, varying grid sizes ($2R_{min}$, $3R_{min}$, and $5R_{min}$) were also considered in the simulations. Another parameter that might cause the instability is the speed of the bottom lid during compression. Similar DEM simulation of uniaxial compression of particles used different speeds of lid during compression. Parafiniuk et al. (2014) used 2 mm/s lid speed at 3% Rayleigh time step, while Wiacek et al. (2012) used 50 mm/s lid speed with no mentioned time step in simulating uniaxial compression test of particles (height of 60 mm and 75 mm, respectively) with a lid moving at 0.35 mm/min or 0.006 mm/s in

the experiment. Gong and Liu (2017) used 2 mm/s for top wall velocity in simulating triaxial test compression of ellipsoidal particles (cube having 22.32 mm side lengths). They reported that at this top wall velocity of compression, the experiential parameter *I* (ratio of unbalanced force to the mean contact force) was equal to 10^{-5} for the entire test, which according to Masson and Martinez (2001) maintain a quasi-static state. Both Parafiniuk et al. (2014) and Gong and Liu (2017) used smaller strain rate values (3.3×10^{-2} s^{-1} and 9.0×10^{-2} s^{-1}, respectively) than Wiacek et al. (2012) (6.7×10^{-1} s^{-1}). In this study, three lid displacement velocities were used: 1.0 mm/s, 0.1 mm/s, and 0.01 mm/s which have equivalent strain rates of 9.8×10^{-3} s^{-1}, 9.8×10^{-4} s^{-1}, and 9.84×10^{-5} s^{-1}, respectively.

Once the appropriate grid size, time step and strain rate (lid displacement velocity) were determined, uniaxial compression of bulk material having different initial bulk densities were simulated at each pressure level (0 to 138 kPa). The corresponding bulk densities were also determined at each pressure level. Results of simulations were analyzed and were compared to the experiment.

5.3. Results and discussion

5.3.1 Grid size, time step, and strain rate

In determining the appropriate grid size, time step, and strain rate for this compressibility problem, a smaller cylinder having the same height as the kettle was used to reduce the computational time. The cylinder diameter (65.5 mm) was still greater than the minimum REV (15d = 54.6 mm) to ensure that the sample size is still a representative of the original problem.

Figure 5-4 shows the predicted pressure on the lid over time. The bottom lid was allowed to move upward until it reached maximum pressure of about 12 kPa, after which its position was held for a minute. For these three grid sizes, the results of simulations were not substantially

different. Thus, any grid size between $2R_{min}$ and $4R_{min}$ can be used in the DEM simulation; however, a larger grid size is preferred for greater computational speed. In EDEM, the modeler can choose auto grid size setting or set a fixed grid size value. EDEM has a built-in grid size estimator that will compute the appropriate grid size for the simulation. For simulations with a narrow size distribution the ideal value is between $2R_{min}$ and $3R_{min}$, but for wider size distributions, this value could increase. The estimated grid size by EDEM for this problem was 3.5 R_{min} which is within our proven grid size range.

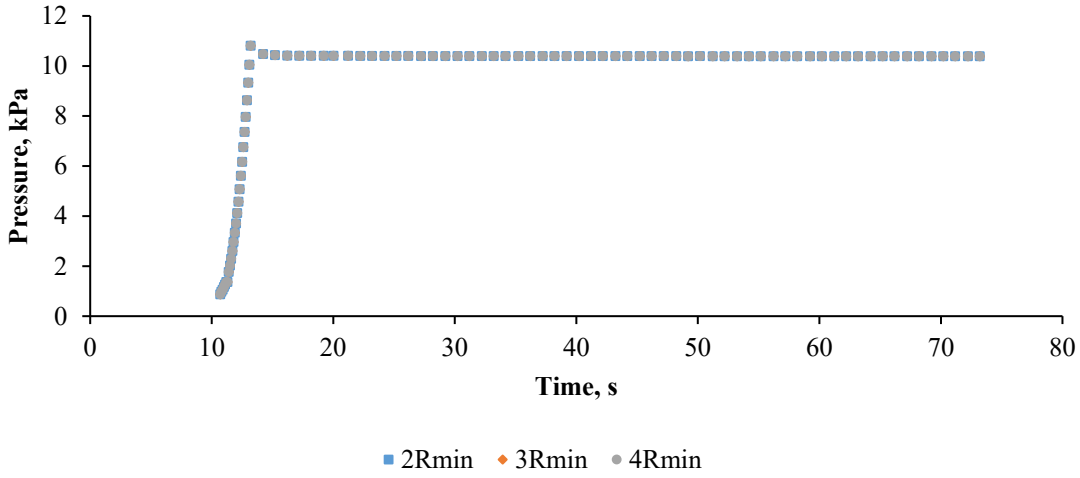

Figure 5-4. Simulated pressure values at different grid sizes.

In determining the appropriate strain rate, a grid size of 3.5 R_{min} was used for all combinations of time step and lid displacement velocity (Figure 5-5). As lid displacement velocity decreased, the simulated pressure values for different time steps moved closer to each other.

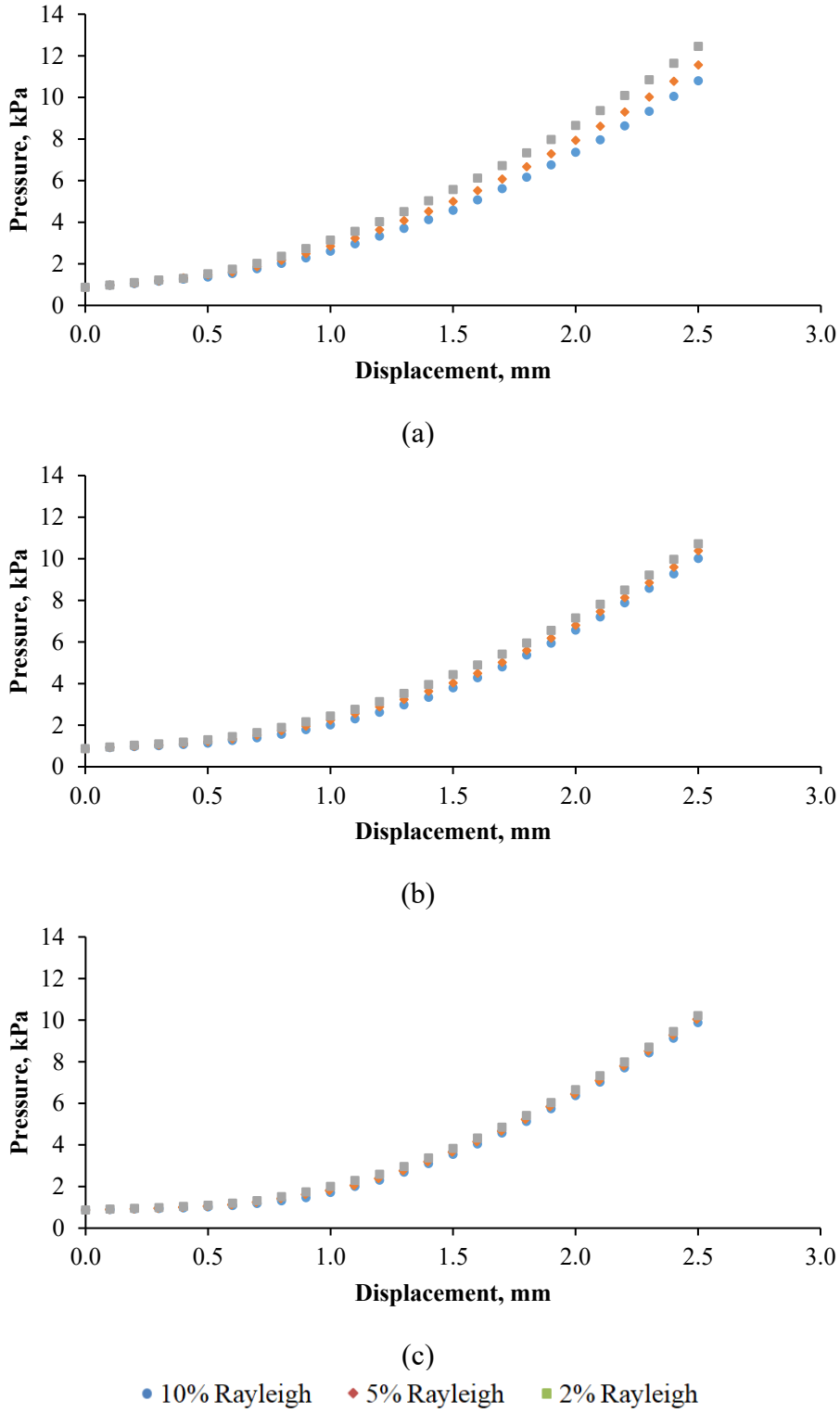

Figure 5-5. Simulated pressure values at different time steps and lid displacement velocity: (a) 1 mm/s, (b) 0.1 mm/s, and (c) 0.01 mm/s.

Table 5-3 summarizes the peak pressure values at different time step and velocity combinations, as well as the pressure after one-minute hold time of the bottom lid once peak value is reached. The inconsistent results for different timesteps at the higher lid velocities indicate those solutions were not stable. Table 5-4 shows that among the three lid velocities, 0.01 mm/s had the least variation (standard deviation = 0.16 kPa) of predicted pressure values between the three time steps and smallest percentage difference between the peak pressure and the pressure after one-minute hold time (0.8%).

Table 5-3. Peak pressure and pressure after one-minute hold time for different time steps compressed at different lid displacement velocity.

Settings	Peak Pressure (kPa)	Pressure after 1 minute (kPa)	% Change
1.00 mm/s			
10% Rayleigh time	10.65	10.38	2.5
5% Rayleigh time	11.36	10.48	7.7
2% Rayleigh time	12.24	10.49	14.3
0.10 mm/s			
10% Rayleigh time	10.04	9.91	1.3
5% Rayleigh time	10.41	10.32	0.9
2% Rayleigh time	10.74	10.48	2.4
0.01 mm/s			
10% Rayleigh time	9.93	9.91	0.2
5% Rayleigh time	10.08	10.07	0.1
2% Rayleigh time	10.25	10.04	2.0

Table 5-4. Variation of predicted pressure (among the three time steps) and stability of predicted pressure at different lid velocities.

Lid velocity (mm/s)	Standard deviation (kPa)[a]	Average % change from peak after 1 minute[b]
1.00	0.80	8.2
0.10	0.35	1.5
0.01	0.16	0.8

[a]Standard deviation of peak pressure of the three time steps
[b]Mean percentage change of pressure (after one-minute hold time) of the three time steps

Extending the hold time to five minutes also showed that the pressure had already stabilized after 1 minute for both 2% and 5% Rayleigh time steps (Table 5-5). Because smaller time steps require longer computational times, 5% Rayleigh time step is the better choice.

Table 5-5. DEM-predicted bulk density after five-minute hold time.

Time step	Pressure, kPa					
	Peak	After 1 min	After 2 mins	After 3 mins	After 4 mins	After 5 mins
10% Rayleigh	9.93	9.91	9.91	9.89	9.88	9.87
5% Rayleigh	10.08	10.07	10.07	10.07	10.07	10.07
2% Rayleigh	10.25	10.04	10.04	10.04	10.04	10.04

5.3.2 Bulk density at different overburden pressure

DEM simulation of wheat bulk density under confined uniaxial compression was implemented at $3R_{min}$ (3.5 mm) grid size, 5% Rayleigh time step (1.57×10^{-6} s), lid velocity of 0.01 mm/s (9.84×10^{-5} s^{-1} strain rate), and 1-minute hold time after reaching the desired pressure level. Predicted bulk density of wheat was determined for each pressure level using EDEM Analyst. A cylindrical density sensor, with diameter the same as the test cup and height that starts with the top lid and ends with the bottom lid, was created. The cylindrical density sensor height decreased as the bottom lid moved upward and compressing the bulk material, which caused the increased wheat bulk density. Figure 5-6 shows the DEM predicted bulk density of wheat, with initial bulk density of about 796 kg/m^3, at the different pressure levels. The properties of wheat (such as shear modulus and contact parameters) used for this simulation were representative of hard red winter wheat at 11% - 12% moisture content (wet basis). Comparing this with observed bulk densities of two tested hard red winter wheat samples (varieties TAM111 and Yellowstone) at three moisture levels (10%, 12%, and 14% wet basis), we expect the

predicted bulk density to have a similar shaped curve as the 12% MC sample with the same initial bulk density.

For a direct comparison, plots of the increase in bulk density from the sample's initial bulk density were plotted against each pressure level (Figure 5-7). The increases in bulk density from the DEM simulations were in agreement below 48 kPa. The experimental and predicted bulk densities started to deviate above 48 kPa and DEM simulations always overpredicted.

The results of the DEM simulation of uniaxial compression of hard red winter wheat (11% – 12% MC wb) were also compared with that of Thompson and Ross (1983) which used soft red wheat samples at different moisture contents (Figure 5-8). For the soft red wheat samples, the largest change in the bulk density occurred at pressure levels below 40 kPa, where a rapid increase in bulk density occurred for all moisture levels. The increase in bulk density was the result of the decrease in void space between particles due to particle rearrangement. As the pressure continue to increase(> 40 kPa), the rate at which the bulk density increased was greater for wheat samples with higher moisture contents (20% to 24%) due to higher elasticity of wheat kernels. At these pressure levels, the increase in bulk density was mainly due to kernel deformation which is further magnified in wheat samples having 24% moisture, being wet and elastic.

For a direct comparison, plots of the increase in bulk density from the sample's initial bulk density were plotted against each pressure level (Figure 5-9). The increases in bulk density from the DEM simulations tend to follow a trend of the soft red wheat between 12% and 16% moisture contents, thus overpredicting the bulk density.

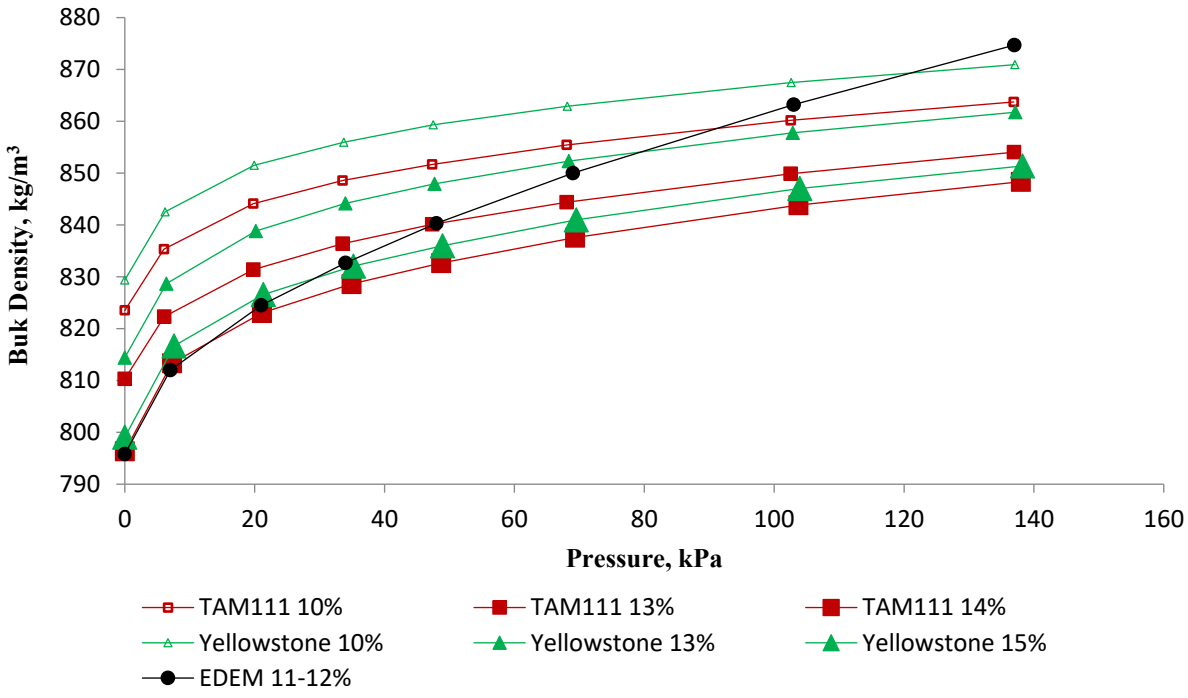

Figure 5-6. DEM predicted bulk density of wheat compared to the results of uniaxial compression tests of two hard red winter wheat samples at three moisture levels.

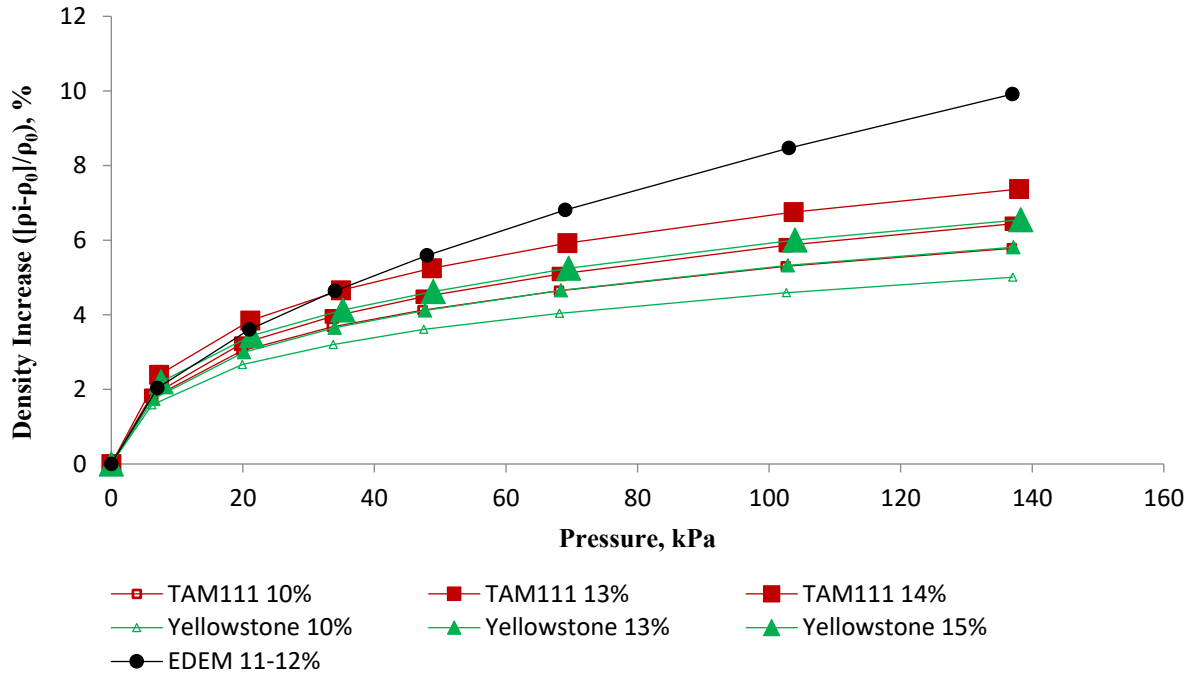

Figure 5-7. DEM predicted density increase (%) of wheat compared to actual density increase (%) of two hard red winter wheat samples at three moisture levels.

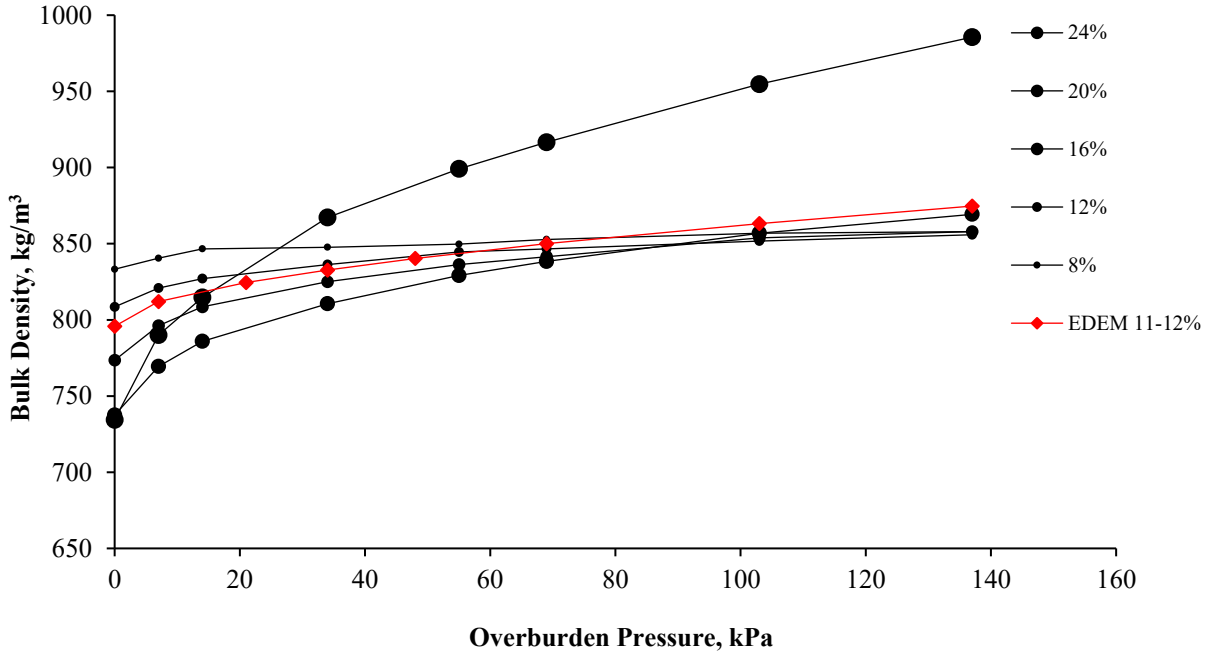

Figure 5-8. DEM predicted bulk density of hard red winter wheat compared to the results of Thompson and Ross (1983) - soft red wheat at different moisture levels.

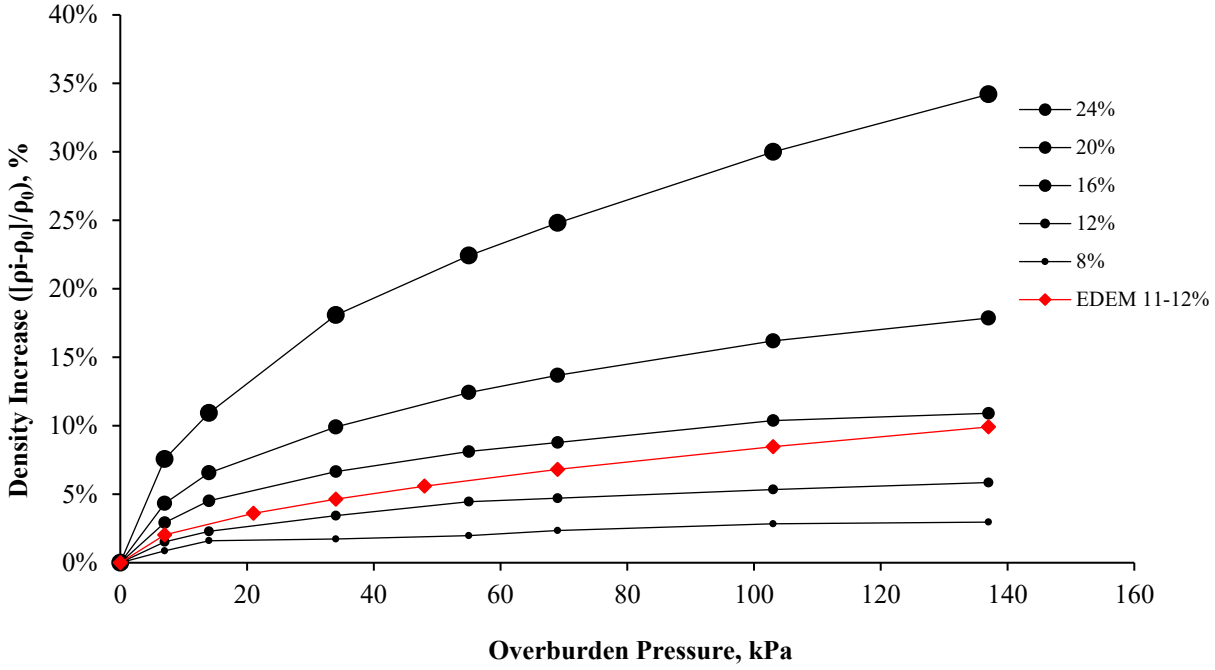

Figure 5-9. DEM predicted density increase (%) of wheat compared to actual density increase (%) of Thompson and Ross (1983) - soft red wheat at different moisture levels.

The deviation of the simulation results from the experimental results can be attributed in the particle shape used in modeling the wheat kernels and how it influenced the initial packing of the particles. Zhou et al. (2013) showed using DEM simulations how particle shape affected the packing characteristics significantly. The packing fractions (or packing ratios) of ellipsoidal particles with varying aspect ratios were determined under poured conditions. Prolate spheroids are ellipsoids with two radii equal and with another radius larger than the two ($a = b > c$) while a sphere is an ellipsoid with three equal radii ($a = b = c$). Wheat kernels can be best represented as prolate spheroids with aspect ratio (c/a or c/b) between 2.0 (large kernel fraction) and 2.4 (small kernel fraction), rather than a sphere with aspect ratio of 1.0. Based form the results of DEM simulations of Zhou et al. (2013), prolate spheroidal particles with this range of aspect ratios (2.0 – 2.4) resulted in higher packing ratio (~0.69 to ~ 0.68) in DEM simulations than the spherical particles (~0.64). This means that by using spherical particles to model wheat kernels in DEM simulation resulted in a less packed arrangement (lower packing ratio or higher inter-particle porosity) than when a prolate spheroidal particles were used. From our previous study (Petingco et al., 2018), it was also shown that samples with lower packing ratio tend to be more compressible as affected by tapping.

In a similar study conducted by Liu et al. (2019) simulating triaxial shear tests on ballast aggregates, the dilation behavior of the ballast specimen was generally overpredicted by DEM simulations due to discrepancies in the detailed mechanical behaviors (e.g., particle rearrangement and particle rotation) that could not be accurately captured in DEM simulations. This may have been due to excessive overlapping of particles during compression. It was also mentioned that the difference in shape between clumped particles using spherical particles in DEM and the angular ballast particles in reality may have affected the volumetric strain.

Another source of error in DEM simulation is the distribution of particle rotation at the different layers of the ballast specimen. DEM simulated the behavior of particle rotation the same for all layers when the particles at the bottom should have experienced significantly less rotation than the upper layers, which is reasonable for the fixed bottom boundary condition. To solve this issue, they suggested a SMART computing algorithm that can enhance DEM simulations using a wireless device called "SmartRock". This device is capable of recording real-time particle translation and rotation if embedded in granular assembly.

To correct the overprediction in bulk density at higher pressure levels, input parameter such as Young's modulus that affect the elasticity of the material can also be calibrated in the DEM model. Stasiak (2003) reported values of modulus of elasticity (Young's modulus) of wheat between 22.4 MPa and 11.1 MPa for moisture content between 10% and 20%. A stiffer material has higher modulus of elasticity, which explained why lower moisture grain has higher modulus of elasticity.

5.4 Conclusion

The uniaxial compression test was simulated with DEM using a bottom lid moving at constant velocity. The time step had to be reduced further than is normally required for applications with free flowing particles. The needed time step interacted strongly with the strain rate, which was driven by the lid displacement velocity. Errors from the time step issues interacting with load rates were largely hidden until we examined longer holding times after compression. The time step and strain rate issues have been resolved in the DEM simulations of compressibility of wheat. DEM simulations were in agreement with that of the experiment at low overburden pressure (below 48 kPa) and tend to overpredict at higher overburden pressure. Using sensor technologies to combine with DEM modeling might be able to improve the results

of DEM simulations. Using an ellipsoidal sphere-clump and reducing the Young's modulus can also correct the overprediction of bulk density due to compression in DEM simulations.

5.5 References

ASABE. (2010). EP413.2: Procedure for establishing volumetric capacities of cylindrical bins. St. Joseph, Mich.: ASABE.

Bachmat, Y., & Bear, J. (1987). On the concept and size of a representative elementary volume (REV). In Advances in transport phenomena in porous media. Dordrecht: Martinus–Nijhoff Publisher.

Boac, J. M., Ambrose, R. P., Casada, M. E., Maghirang, R. G., & Maier, D. E. (2014). Applications of discrete element method in modeling of grain postharvest operations. *Food Eng. Rev., 6*(4), 128-149. https://doi.org/10.1007/s12393-014-9090-y

Boac, J. M., Bhadra, R., Casada, M. E., Thompson, S. A., Turner, A. P., Montross, M. D., McNeill, S. G., & Maghirang, R. G. (2015). Stored grain pack factors for wheat: Comparison of three methods to field measurements. *Trans. ASABE, 58*(4), 1089-1101. https://doi.org/10.13031/trans.58.10898

Costanza-Robinson, M. S., Estabrook, B. D., & Fouhey, D. F. (2011). Representative elementary volume estimation for porosity, moisture saturation, and air–water interfacial areas in unsaturated porous media: Data quality implications. *Water Resources Research*, 47, W07513. http://dx.doi.org/10.1029/2010WR009655

Cundall, P. A., & Strack, O. D. (1979). A discrete element model for granular assemblies. *Geotechnique, 29*(1), 47-65. https://doi.org/10.1680/geot.1979.29.1.47

Evesque, P. (1991). Analysis of the statistics of sandpile avalanches using soil mechanics results and concepts. *Physical Review A*, 43, 2720–2740.

Evesque, P.(2001).Macroscopic continuous approach versus discrete approach, fluctuations, criticality and SOC: A state of the question based on articles in Powders & Grains 2001. *Powder & Grains*, 12(8), 122–150.

Liu, J. G. (2017). Effect of aspect ratio on triaxial compression of multi-sphere ellipsoid assemblies simulated using a discrete element method. *Particuology*, 32(3), 49-62.

Liu, S., Qiu, T., Qian, Y., Huang, H., Tutumluer, E., & Shen, S. (2019). Simulations of large-scale triaxial shear tests on ballast aggregates using sensing mechanism and real-time (SMART) computing. *Computers and Geotechnics*, 110, 184-198.

Markauskas, Kačianauskas, Džiugys, & Navakas. (2010). Investigation of adequacy of multi-sphere approximation of elliptical particles for DEM simulations. Granular Matter, 12(1), 107-123.

Masson, S., & Martinez, J. (2000). Effect of particle mechanical properties on silo flow and stresses from distinct element simulations. *Powder Tech*, 109, 164–178.

Masson, S, & Martinez, J. (2001). Micromechanical Analysis of the Shear Behavior of a Granular Material. *Journal of Engineering Mechanics*, 127(10), 1007-1016.

Parafiniuk, P., Molenda, M., & Horabik, J. (2014). Influence of particle shape and sample width on uniaxial compression of assembly of prolate spheroids examined by discrete element method. *Physica A*, 416, 279-289.

Stasiak, M. (2003). Determination of elastic parameters of grain with oedometric and acoustic methods. Research in Agricultural Engineering. 49. 10.17221/4953-RAE.

Thompson, S. A., & Ross, I. J. (1983). Compressibility and frictional coefficients of wheat. *Trans. ASAE, 26*(4), 1171-1176. https://doi.org/10.13031/2013.34099

Turner, A. P., Montross, M. D., McNeill, S. G., Sama, M. P., Casada, M. E., Boac, J. M., ...

Thompson, S. A. (2016). Modeling the compressibility behavior of hard red wheat varieties. *Trans. ASABE, 59*(3), 1029-1038. https://doi.org/10.13031/trans.59.11432

USDA-FGIS. (2013). *Grain inspection handbook*. Washington, DC: USDA Federal Grain Inspection Service

Wiącek, J., Molenda, M., Ooi, J.Y., & Favier, J. (2012). Experimental and numerical determination of representative elementary volume for granular plant materials. *Granular Matter,* 14(4), 449-456.

Wiacek, J. & Molenda, M. (2016). Representative elementary volume analysis of polydisperse granular packings using discrete element method. *Particuology*, 27(4), 88-94.

Zhang, D., Zhang, R., Chen, S., & Soll, W. E. (2000). Pore scale study of flow in porous media: Scale dependency, REV, and statistical REV. *Geophysical Research Letters*, 27, 1195–1198.

Zhou, Z., Zou, R., Pinson, D., & Yu, A. (2013). Discrete modelling of the packing of ellipsoidal particles. AIP Conference Proceedings 1542, 357-360. https://doi/10.1063/1.4811941

Chapter 6 - Conclusions and Recommendations for Future Work

6.1 Conclusions

Experiments and DEM simulations were conducted at USDA-ARS Center for Grain and Animal Health Research and Kansas State University to understand the effects of particle shape, size distribution, drop height, and overburden pressure on wheat bulk density. The following conclusions were drawn from the research:

- The packing ratio of these non-spherical particles increased with kernel size, while compressibility decreased.
- Shape factors changed with kernel size, thereby affecting compressibility and packing ratio.
- More spherical, less elongated, and flatter kernels produced higher packing ratio and lower compressibility.
- Packing ratio trends were the same for single size fractions and binary mixtures of kernel fractions, while compressibility behaved differently for those cases.
- Higher frcations of large kernels in these mixtures produced higher packing ratio and lower compressibility values.
- Decreased aspect ratio and improved geometrical smoothness of particles increased bulk density of wheat.
- Among the three particle models, the 5-sphere ellipsoidal particle was the best option to represent wheat particles as indicated by the simulated bulk densities that best agreed with the experiments.

- Among the contact parameters, the wheat-to-wheat coefficient of static friction and wheat-surface coefficient of rolling friction had the greatest influence on simulated bulk density.
- Bulk density as affected by drop heights and size distribution were successfully simulated using DEM.
- Accurate particle shape representation simulated the heap profile better than simpler shapes but required longer computational times.
- Prediction of simulated bulk density was improved when contact parameters were calibrated separately for each size fraction
- Use of single-sphere models is often more practical due to lower computational cost.
- The needed time step interacted strongly with the strain rate and lid displacement velocity.
- DEM simulations of wheat bulk density agreed with experimental results at low overburden pressure (below 48 kPa), but overpredicted bulk density at higher overburden pressures.

6.2 Limitations of the study

The following are the limitations of this study:

- The DEM models were limited to simulating bulk density of hard red winter wheat with moisture content between 11% to 12% wet basis and did not include presence of foreign material such as chaff and dockage.
- The percentage increase of bulk density due to increase in grain drop height were applicable only for small scale laboratory set up. The compression was due to the impact of material at higher drop heights (causing the kernel to packed closely

together) and did not include compression due to the weight of the overlying material just like in bins.

6.3 Recommendations for future work

The following are recommended for future studies:

- Use other technologies such as X-ray topography for determining the amount of interparticle voids in a container filled with wheat sample, and compare the results with that of DEM-predicted interparticle voids;
- Conduct larger scale of experiment, such as bigger test cup and hopper, on the effect of grain drop height on wheat bulk density;
- Determine experimentally the effects of size distribution on wheat compressive behavior;
- Incorporate in the DEM model the effect of moisture on wheat compressibility by calibrating the modulus of elasticity (Young's modulus) to different moisture content of wheat.
- Use the application programming interface (API) in EDEM (or use open source DEM software) for more flexibility and adaptability in simulating specific processes that can improve accuracy of DEM predicted behavior. Higher moisture wheat are more susceptible to breakage during compression. The breakage of wheat particles can also be simulated using the EDEM API by replacing a particle with its daughter particles to address fragmentation.

Appendix A - Supporting Data

Supplemental data for Chapter 4

Table A.1. Set 1 particles.

	Position X (mm)	Position Y (mm)	Position Z (mm)	Physical Radius (mm)	Image
Large – 5S (Mass = 0.0346 g, Volume = 2.52 x10^{-8} m^3, D = 6.12 mm, d = 3.05 mm, Aspect Ratio = 2.0)					
Sphere0	-2.149	0	0	0.911	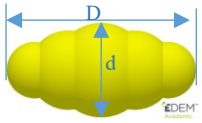
Sphere1	-1.074	0	0	1.279	
Sphere2	0	0	0	1.525	
Sphere3	1.074	0	0	1.279	
Sphere4	2.149	0	0	0.911	
Medium – 5S (Mass = 0.0246 g, Volume = 1.79 x10^{-8} m^3, D = 5.84 mm, d = 2.68 mm, Aspect Ratio = 2.2)					
Sphere0	-2.241	0	0	0.679	
Sphere1	-1.120	0	0	1.123	
Sphere2	0	0	0	1.340	
Sphere3	1.120	0	0	1.123	
Sphere4	2.241	0	0	0.679	
Small – 5S (Mass = 0.0160 g, Volume = 1.17 x10^{-8} m^3, D = 5.52 mm, d = 2.32 mm, Aspect Ratio = 2.4)					
Sphere0	-2.179	0	0	0.581	
Sphere1	-1.090	0	0	0.914	
Sphere2	0	0	0	1.160	
Sphere3	1.090	0	0	0.914	
Sphere4	2.179	0	0	0.581	

Table A.2. Set 2 particles.

Sphere No.	Position X (mm)	Position Y (mm)	Position Z (mm)	Physical Radius (mm)	Image
Large – 5S (Mass = 0.0346 g, Volume = 2.52 x10-8 m3, D = 6.12 mm, d = 3.05 mm, Aspect Ratio = 2.0)					
Sphere0	-2.149	0	0	0.911	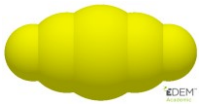
Sphere1	-1.074	0	0	1.279	
Sphere2	0	0	0	1.525	
Sphere3	1.074	0	0	1.279	
Sphere4	2.149	0	0	0.911	
Medium – 5S (Mass = 0.0244 g, Volume = 1.77 x10-8 m3, D = 5.45 mm, d = 2.71 mm, Aspect Ratio = 2.0)					
Sphere0	-1.913	0	0	0.811	
Sphere1	-0.956	0	0	1.138	
Sphere2	0	0	0	1.357	
Sphere3	0.956	0	0	1.138	
Sphere4	1.913	0	0	0.811	
Small – 5S (Mass = 0.0152 g, Volume = 1.11 x10-8 m3, D = 4.65 mm, d = 2.32 mm, Aspect Ratio = 2.0)					
Sphere0	-1.633	0	0	0.692	
Sphere1	-0.816	0	0	0.972	
Sphere2	0	0	0	1.159	
Sphere3	0.816	0	0	0.972	
Sphere4	1.633	0	0	0.692	

Table A.3. Set 3 particles.

Sphere No.	Position X (mm)	Position Y (mm)	Position Z (mm)	Physical Radius (mm)	Image
Large – 5S (Mass = 0.0346 g, Volume = 2.52 x10-8 m3, D = 6.12 mm, d = 3.05 mm, Aspect Ratio = 2.0)					
Sphere0	-2.209	0	0	0.851	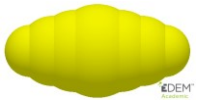
Sphere1	-1.472	0	0	1.145	
Sphere2	-0.736	0	0	1.341	
Sphere3	0.000	0	0	1.525	
Sphere4	0.736	0	0	1.341	
Sphere5	1.472	0	0	1.145	
Sphere6	2.209	0	0	0.851	
Medium – 5S (Mass = 0.0246 g, Volume = 1.79 x10^{-8} m^3, D = 5.84 mm, d = 2.68 mm, Aspect Ratio = 2.2)					
Sphere0	-2.196	0	0	0.724	
Sphere1	-1.464	0	0	0.947	
Sphere2	-0.732	0	0	1.173	
Sphere3	0.000	0	0	1.340	
Sphere4	0.732	0	0	1.173	
Sphere5	1.464	0	0	0.947	
Sphere6	2.196	0	0	0.724	
Small – 5S (Mass = 0.0161 g, Volume = 1.17 x10^{-8} m^3, D = 5.52 mm, d = 2.32 mm, Aspect Ratio = 2.4)					
Sphere0	-2.165	0	0	0.595	
Sphere1	-1.444	0	0	0.780	
Sphere2	-0.722	0	0	0.943	
Sphere3	0.000	0	0	1.160	
Sphere4	0.722	0	0	0.943	
Sphere5	1.444	0	0	0.780	
Sphere6	2.165	0	0	0.595	

Table A.4. Set 4 large particle (28 spheres).

Large – ASG (Mass = 0.0363 g, Volume = 2.64 x10^{-8} m^3, D = 6.12 mm, d = 3.05 mm, Aspect Ratio = 2.0)					
Sphere No.	Position X (mm)	Position Y (mm)	Position Z (mm)	Physical Radius (mm)	Image
Sphere0	0.352926	-1.687610	0.725768	0.891675	
Sphere1	0.838000	-2.124580	1.633570	0.401323	
Sphere2	0.540258	-1.376270	0.433642	0.898382	
Sphere3	-0.902415	1.889850	-0.859902	0.648588	
Sphere4	0.060045	1.058260	-0.792709	0.950841	
Sphere5	-0.351037	-0.138090	-0.767938	0.853340	
Sphere6	-0.273239	-0.032069	0.948462	0.818565	
Sphere7	-0.783175	1.791360	-1.829890	0.400271	
Sphere8	0.397164	-1.411770	1.660840	0.694498	
Sphere9	0.432509	-2.158390	1.150330	0.569952	
Sphere10	-0.921184	1.546050	-0.443173	0.696457	
Sphere11	-0.221058	1.748940	-1.348130	0.712593	
Sphere12	0.281069	-0.974150	1.360440	0.916666	
Sphere13	-0.722546	0.824915	-1.356730	0.749923	
Sphere14	0.521337	0.658410	-0.638267	0.705129	
Sphere15	-0.465119	0.454273	-1.055040	0.879133	
Sphere16	-0.804806	1.238790	-1.589310	0.683551	
Sphere17	0.408434	-0.551196	0.959687	0.988462	
Sphere18	0.603730	-0.142966	-0.184392	0.895608	
Sphere19	0.188797	-0.517679	0.961214	1.109220	
Sphere20	-0.016842	-0.012982	0.419431	1.213630	
Sphere21	-0.076968	-0.785471	-0.293355	0.855298	
Sphere22	-0.410218	0.546110	0.485529	0.854380	
Sphere23	0.015519	-1.436690	0.219919	0.792712	
Sphere24	0.872993	-0.833561	0.188052	0.816498	
Sphere25	-0.055711	-0.579342	1.281030	0.819093	
Sphere26	-0.025548	1.440440	-1.100590	0.823354	
Sphere27	-0.535608	0.956205	0.124424	0.838323	

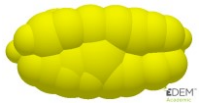

Table A.5. Set 4 medium particle (27 spheres).

Medium – 5S (Mass = 0.0241 g, Volume = 1.75 x10^{-8} m^3, D = 5.84 mm, d = 2.68 mm, Aspect Ratio = 2.2)					
Sphere No.	Position X (mm)	Position Y (mm)	Position Z (mm)	Physical Radius (mm)	Image
Sphere0	-1.108520	-0.295001	-0.265115	0.553999	
Sphere1	-1.115270	0.642836	0.027424	0.782371	
Sphere2	1.805790	0.135927	-0.492253	0.641415	
Sphere3	1.654950	-0.703099	-0.575759	0.619037	
Sphere4	0.111115	-0.218685	-0.074611	1.150350	
Sphere5	-0.876596	0.068009	0.861351	0.623894	
Sphere6	-1.931880	0.838521	0.482628	0.432572	
Sphere7	-2.141910	0.670263	0.859209	0.333767	
Sphere8	1.057870	-0.721839	-0.326674	0.793236	
Sphere9	-1.583380	-0.069043	0.043724	0.626623	
Sphere10	-0.054836	0.457291	-0.203769	0.896803	
Sphere11	0.612209	0.461415	-0.374093	0.787038	
Sphere12	-0.648299	0.741073	-0.305703	0.611541	
Sphere13	1.214200	0.167392	-0.314792	0.901931	
Sphere14	-0.466785	-0.139526	-0.045553	1.031840	
Sphere15	1.251390	-0.525414	-0.345445	0.861952	
Sphere16	-2.075570	0.373674	0.920685	0.446959	
Sphere17	-1.553750	0.256195	0.697706	0.763476	
Sphere18	2.317010	0.020793	-0.651074	0.351017	
Sphere19	2.450700	-0.392643	-0.468931	0.391401	
Sphere20	-1.524970	0.686663	0.205987	0.703273	
Sphere21	-2.301540	0.214966	0.629429	0.321667	
Sphere22	-1.943610	0.043643	0.261332	0.518028	
Sphere23	2.109940	-0.730394	-0.691953	0.382487	
Sphere24	0.394685	-0.141272	0.140214	1.049440	
Sphere25	-0.376980	-0.035022	0.592133	0.813795	
Sphere26	-0.201736	-0.526298	-0.212701	0.795853	

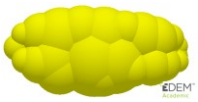

Table A.6. Set 4 small particle (30 spheres).

Small – ASG (Mass = 0.0150 g, Volume = 1.10 x10^{-8} m^3, D = 5.52 mm, d = 2.32 mm, Aspect Ratio = 2.4)					
Sphere No.	Position X (mm)	Position Y (mm)	Position Z (mm)	Physical Radius (mm)	Image
Sphere0	-0.666896	0.920480	0.528765	0.686838	
Sphere1	-0.957387	1.130900	-0.145400	0.470540	
Sphere2	-0.311273	-0.410119	0.011865	0.643939	
Sphere3	0.696505	-0.963235	-0.009342	0.663241	
Sphere4	-1.121140	1.406600	0.295846	0.423882	
Sphere5	-1.359020	1.113430	0.593097	0.391747	
Sphere6	-0.595764	0.800324	-0.372326	0.539272	
Sphere7	1.066150	-1.482060	-0.255289	0.393956	
Sphere8	-0.944580	0.212367	0.267717	0.618680	
Sphere9	-0.277264	0.468249	-0.477059	0.581540	
Sphere10	-1.364850	0.681701	0.377353	0.468175	
Sphere11	-1.061050	0.438039	0.299548	0.622229	
Sphere12	-0.409310	0.028870	0.105279	0.873093	
Sphere13	0.250788	-0.062457	-0.679200	0.556986	
Sphere14	0.053863	-0.308465	-0.000975	0.940353	
Sphere15	0.424476	-0.829825	-0.020271	0.736076	
Sphere16	-0.716857	-0.112820	0.074259	0.566791	
Sphere17	0.760428	-1.209880	-0.121923	0.562014	
Sphere18	0.924362	-0.603219	-0.741897	0.498905	
Sphere19	0.046136	-0.740398	-0.073971	0.620239	
Sphere20	1.410240	-1.112890	-0.636840	0.380277	
Sphere21	1.241450	-0.839110	-0.690324	0.463704	
Sphere22	1.417110	-1.140360	-0.383191	0.352127	
Sphere23	0.598555	-0.176444	-0.682898	0.623201	
Sphere24	-0.540655	0.634297	0.327888	0.841165	
Sphere25	-0.928755	1.008011	0.529028	0.604713	
Sphere26	0.921453	-0.444704	-0.457120	0.688966	
Sphere27	0.499795	-0.355892	0.078307	0.876539	
Sphere28	0.025207	0.157343	0.210605	0.873684	
Sphere29	0.071507	0.325437	-0.519357	0.670696	